Fractal Diffusion Coefficients in Simple Dynamical Systems

Georgie Samuel Knight

School of Mathematical Sciences

Queen Mary University of London

A thesis submitted in partial fulfilment
of the requirements for the degree of

Doctor of Philosophy

21/02/2012

Declaration

The work presented in this thesis is my own. Chapters 2 and 3 consist of collaborative work with Dr Rainer Klages[1]. Chapter 4 consists of collaborative work with Dr Orestis Georgiou[2], Dr Carl Dettmann[3] and Dr Rainer Klages.

[1] r.klages@qmul.ac.uk
[2] orestis@pks.mpg.de
[3] carl.dettmann@bristol.ac.uk

This work is dedicated to my loving parents.

Acknowledgements

I would like to acknowledge the financial support of the E.P.S.R.C.

I would like to thank all of the members of the School of Mathematical Sciences at Queen Mary University of London for making my stay as a postgraduate and as a research student such an enjoyable one.

I would like to thank Prof. Roberto Artuso, Dr Oscar Bandtlow, Prof. Leonid Bunimovich, Dr. Giampaolo Cristadoro, Dr Phil Howard, Prof. Oliver Jenkinson, Prof. Gerhard Keller, Freidrich Lenz, Prof. Jens Marklof, Prof. Yuzuru Sato, Prof. Franco Vivaldi and Prof. Lai-Sang Young for helpful and inspiring discussions at one time or another.

I would like to thank Prof. Christian Beck and Dr. Rosemary Harris for the time spent and the support they have given me as supervisors.

I would like to thank Dr. Carl Dettmann and Dr. Orestis Georgiou for many interesting and helpful discussions and for the work we have collaborated on together.

Last but of course not least, I would like to thank my supervisor Dr. Rainer Klages, whose support, help and inspiration has made this project possible.

Abstract

Deterministic diffusion is studied in simple, parameter-dependent dynamical systems. The diffusion coefficient is often a fractal function of the control parameter, exhibiting regions of scaling and self-similarity. Firstly, the concepts of chaos and deterministic diffusion are introduced in the context of dynamical systems. The link between deterministic diffusion and physical diffusion is made via random walk theory. Secondly, parameter-dependent diffusion coefficients are analytically derived by solving the Taylor-Green-Kubo formula. This is done via a recursion relation solution of fractal 'generalised Takagi functions'. This method is applied to simple one-dimensional maps and for the first time worked out fully analytically. The fractal parameter dependence of the diffusion coefficient is explained via Markov partitions. Linear parameter dependence is observed which in some cases is due to ergodicity breaking. However, other cases are due to a previously unobserved phenomenon called the 'dominating-branch' effect. A numerical investigation of the two-dimensional 'sawtooth map' yields evidence for a possible fractal structure. Thirdly, a study of different techniques for approximating the diffusion coefficient of a parameter-dependent dynamical system is then performed. The practicability of these methods, as well as their capability in exposing a fractal structure is compared. Fourthly, an analytical investigation into the dependence of the diffusion coefficient on the size and position of the escape holes is then undertaken. It is shown that varying the position has a strong effect on diffusion, whilst the asymptotic regime of small-hole size is dependent on the limiting behaviour of the escape holes. Finally, an exploration of a method which involves evaluating the zeros of a system's dynamical zeta function via the

weighted Milnor-Thurston kneading determinant is performed. It is shown how to relate the diffusion coefficient to a zero of the dynamical zeta function before analytically deriving the diffusion coefficient via the kneading determinant.

Contents

List of Figures

Chapter 1

Introduction

'For want of a nail the shoe was lost; for want of a shoe the horse was lost; and for want of a horse the man was lost.'

Old English proverb discussing S.D.I.C.[1]

The work presented in this thesis is a product of the interaction between non-equilibrium statistical mechanics and dynamical systems theory. The goal of statistical mechanics is to understand the macroscopic properties of complicated systems with many degrees of freedom such as gases, whilst taking into account the microscopic behaviour of the constituent elements. Typically, such systems have a huge number of elements, rendering standard mathematical tools used to treat physical, mechanical problems like differential equations ineffective, even if one had a thorough understanding of the equations of motion of each element. Naturally therefore, probabilistic or statistical (hence 'statistical mechanics') methods were developed to answer questions about systems with many particles in the pioneering work of the founders of statistical mechanics (Boltzmann [1964]; Gibbs [1960]; Maxwell [1965a,b]). An alternative approach to building a full understanding of statistical mechanics uses the mathematics of dynamical systems theory to take into account the microscopic complexity (see

[1] *The Oxford Dictionary of English Proverbs.* O.U.P.

for example Ruelle [1977, 2004]). In this setting, the assumption of stochasticity is replaced by the chaotic properties of a deterministic dynamical system and concepts borne out of statistical mechanics like ergodicity, can be studied in a rigorous mathematical setting (see for example Khinchin [1949]).

At the heart of this interaction between statistical mechanics and dynamical systems theory lies the study of transport processes (Cvitanović et al. [2010]; Dorfman [1999]; Gaspard [1998]; Klages [2007]). Transport processes can include the study of viscous flow in which momentum transport occurs. This process being described by Newton's law of viscosity. Radiation, heat conduction and convection give rise to the transport of energy, which is described by Fourier's law of heat conduction. We also have diffusion which involves mass transport and is governed by Fick's law of diffusion. What these laws have in common is transport from a region of high concentration to a region of low concentration controlled by transport coefficients. In momentum transport this coefficient is called viscosity, in energy transport we have thermal conductivity whilst in mass transport we have simply the diffusion coefficient. See Bird et al. [2007] for an in-depth discussion of transport processes.

Diffusion and the diffusion coefficient form the focus of the work in this thesis. In the framework of statistical mechanics, the source of diffusion is often modelled as the microscopic random movement of the individual molecules, caused by the presence of thermal energy. We will abstract the physical process of diffusion from statistical mechanics and place it in the setting of dynamical systems. This abstraction involves simplifying the physical setting as far as possible by restricting the dimension of a system under study and considering simple equations of motion. This simplification allows us to study 'toy models' based upon simple dynamical systems. This setting allows us to analytically study diffusion without any statistical assumptions. The ultimate goal of such a project is to learn something in this simplified, abstracted setting that can then be transferred back into the physical world in the form of predictions or suggestions of possible lines of research. Before describing how this is achieved in detail, we will look at the object of our investigation.

1.1 Deterministic diffusion

Here we will briefly introduce the concept of diffusion and show how it can be related to dynamical systems.

1.1.1 Diffusion as a physical phenomenon

One common setting for diffusion is the movement of particles from a region of high concentration to a region of low concentration. One can imagine placing a drop of ink into a clear glass of water and observing that, over time, the ink has managed to colour the entire glass of water uniformly, without the need to stir or introduce turbulence into the glass. Restricting this set up to one-dimension, this process is described by the diffusion equation (Reif [2008]),

$$\frac{\partial \rho_t(x)}{\partial t} = D\frac{\partial^2 \rho_t(x)}{\partial x^2}, \tag{1.1}$$

where $\rho_t(x)$ describes the concentration of points (or the drop of ink) at time t and x is the one-dimensional coordinate. D is the diffusion coefficient which measures the rate of diffusion. Eq.(1.1) can be derived by combining the simple concept of continuity of matter, which states that any rise or fall in concentration is caused by the current density F_x, that is the movement of particles into or out of a region,

$$\frac{\partial \rho_t(x)}{\partial t} = -\frac{\partial F_x}{\partial x}, \tag{1.2}$$

with Fick's first law of diffusion, dating back to 1855, which states that the current density is proportional to the concentration gradient,

$$F_x = -D\frac{\partial \rho_t(x)}{\partial x}. \tag{1.3}$$

When one solves the diffusion equation in Eq.(1.1) with the assumption that the initial distribution is given by a Dirac delta function at the point $x_0 = 0$,

$$\rho_0(x) = \delta(x - x_0), \tag{1.4}$$

one finds that the Green's function is given by a Gaussian distribution,

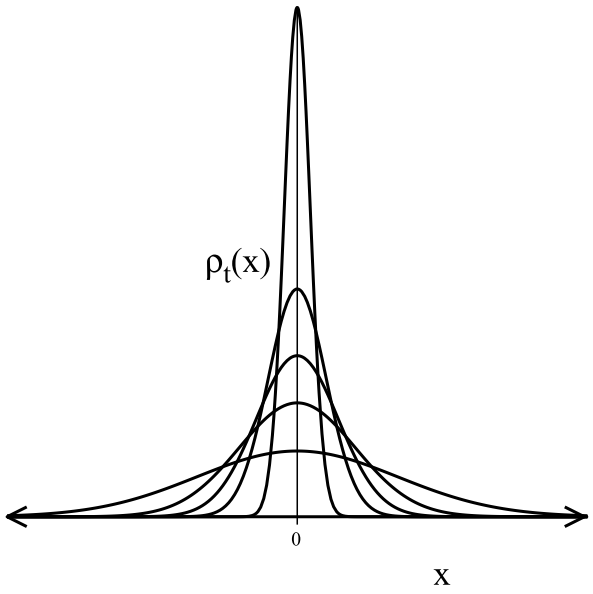

Figure 1.1: *Evolution of a density of points under the diffusion equation.* In this figure we see the evolution of a density of points under the diffusion equation taking a Gaussian form. Illustrated is the distribution at time t_1 given by the sharpest peaked distribution and the distribution at later times $t_2 < t_3 < t_4 < t_5$ which are given by the less sharp peaks respectively. The initial Dirac delta distribution at 0 spreads out as the time t increases and the distribution moves towards an equilibrium state. The rate of this spreading process is controlled by the diffusion coefficient.

$$\rho_t(x) = \frac{e^{-\frac{(x-x_0)^2}{4Dt}}}{\sqrt{4\pi Dt}}. \tag{1.5}$$

The variance, or second moment is then given by

$$\int \rho_t(x)(x-x_0)^2 dx = 2Dt. \tag{1.6}$$

See figure 1.1 for an illustration of the evolution of a density under Eq.(1.1). In order to show how we can study Eq.(1.1) within dynamical systems theory, and in particular the diffusion coefficient D, we will first need to take a random walk.

1.1.2 A random walk

In 1905, Karl Pearson described the following 'problem of considerable interest' in Nature (Pearson [1905]),

> *'...A man starts from a point O and walks l yards in a straight line; he then turns through any angle whatever and walks another l yards in a second straight line. He repeats this process n times. I require the probability that after these n stretches he is at a distance between r and $r + \delta r$ from his starting point, O...'*

From a reply of Lord Rayleigh (Strutt [1905]), Pearson concluded that

> *'...The lesson of Lord Rayleigh's solution is that in open country the most probable place to find a drunken man who is at all capable of keeping on his feet is somewhere near his starting point! '*

The process that Pearson was describing is that of a random walk (see for example Weiss [1994]). In one-dimension we can think of the man in Pearson's problem as taking steps of length Δ to the left or right with equal probability at discrete time intervals of length τ. The common analogy is that of the 'drunken sailor' attempting to return home after a heavy night (see for example Klages [2007]; Reif [2008]). The drunkenness means that the steps are 'uncorrelated' in that the sailor retains no memory of the direction of his previous step.. This equates to randomly choosing the direction of each step at each time interval τ. Hence 'random walk'.

Following Pearson, we let our man start at the point 0 and ask what the probability is of being found at a distance $k = r\Delta$ at a time $n\tau$, where $r \in \mathbb{Z}$ and $n \in \mathbb{N}$, written as $P_{n\tau}(r\Delta)$. Using the conservation of probabilities we can derive a simple solution to this problem as (Wax [1954]),

$$P_{n\tau}(k) = \frac{1}{2}\left[P_{(n-1)\tau}(k-\Delta) + P_{(n-1)\tau}(k+\Delta)\right], \tag{1.7}$$

which simply states that the probability $P_{n\tau}(k)$ is equal to the sum of the probabilities of arriving from the nearby points $k-\Delta$ and $k+\Delta$. Subtracting $P_{(n-1)\tau}(k)$ from each side, dividing by τ and multiplying the right hand side by Δ^2/Δ^2 we can rewrite Eq.(1.7) as,

$$\frac{P_{n\tau}(k) - P_{(n-1)\tau}(k)}{\tau} = \frac{\Delta^2}{2\tau}\frac{\left[P_{(n-1)\tau}(k-\Delta) + P_{(n-1)\tau}(k+\Delta) - 2P_{(n-1)\tau}(k)\right]}{\Delta^2}. \tag{1.8}$$

In the continuous time limit, that is letting Δ and τ go to zero, Eq.(1.8) reduces to the familiar partial differential equation given by Eq.(1.1) (Wax [1954]). That is, this drunken sailor taking a random walk is undergoing a diffusion process. Therefore if we were to take a crew of drunken sailors and start them from the same point, we would expect them to spread out according to the Gaussian distribution given by Eq.(1.5). Karl Pearson's response to Lord Rayleigh's solution can now be interpreted by examining the form of Eq.(1.5) and noting that the peak centres on the starting point 0, see figure 1.1. This continuous time limit of the random walk is a process known as 'Brownian motion' after the botanist Robert Brown who in 1827 observed pollen particles moving randomly whilst suspended in water (Brown [1866]). Einstein placed this process into the realm of physics in one of his 1905 papers (Einstein [1905]) by using Brownian motion to give empirical evidence for the atomic theory of matter, the theory which had previously formed the basis of statistical mechanics. From this work we obtain Einstein's formula for the diffusion coefficient D,

$$D = \lim_{n\to\infty} \frac{\langle (x_n - x_0)^2 \rangle}{2n}, \tag{1.9}$$

where the angular brackets represent an average taken over an ensemble of initial conditions x_0. In this case the mean-square displacement of an ensemble of points grows linearly with time and the diffusion coefficient is a measure of the rate of this growth. Of course we could consider more general situations like including a bias into the random walk, for example it may take place on a hill. This will introduce a current into the diffusion process and the centre of the Gaussian distribution will move accordingly. For a review of this material see for example Wax [1954]; Weiss [1994]. We can now introduce the idea of diffusion taking place in a deterministic dynamical system. In this setting we have a deterministic generalisation of the random walk.

1.1.3 Chaotic dynamical systems

Dynamical systems theory began with Newton's paradigmatic 1687 work on the laws of motion that form the basis of classical mechanics. Newton's laws equipped scientists with the philosophy that *if* they knew the current state of a system, they could then, in principle, work out the state at any future time. However, this is a big 'if' as in order to ascertain the current state of a system, one must take measurements, and inherent in any physical measurement will be some level of inaccuracy, even if only very small. This inaccuracy was famously discovered to have drastic consequences by Poincaré in his work on the 'Three-body problem' of celestial mechanics (Poincaré [1899]) and later by Edward Lorenz in his work on simple models of the weather system (Lorenz [1963]). The latter work gave rise to the term '*butterfly-effect*' which poetically captures the concept of 'sensitive dependence on initial conditions' (S.D.I.C.). This is the concept that a small change in the initial conditions of a system, eg. a flap of a butterfly's wings, could have a big effect, eg. the occurrence of a tornado. If a system exhibits the property of sensitive dependence on initial conditions, then the errors in one's measurements grow as the system evolves in time. This is, for example, why current weather forecasts only yield around five days worth of useful information. Dynamical systems theory is essentially the study of such systems. For good accounts of the history and development of chaos theory and the underlying ideas see for example Gleick [1988] or Ruelle [1993]. For comprehensive, mathematical introductions to the ideas of chaos and also dynamical systems theory see for example Cvitanović et al. [2010]; Devaney [1989]; Katok and Hasselblatt [1995]; Ott [1993]. A very good set of lecture notes introducing dynamical systems theory can be found in Klages and Howard [2008].

A dynamical system in a mathematical sense, basically consists of a 'phase space' X, which is a set of all the possible states of the system, a deterministic rule M which describes how the system evolves in time and a 'measure' μ which is a function that acts on the elements of X and generalises distance. The measure describes how far apart any two states of a system are which allows one to quantify the growth in the error over time. The evolution rule can either be defined in continuous time which leads to the study of nonlinear differential equations or

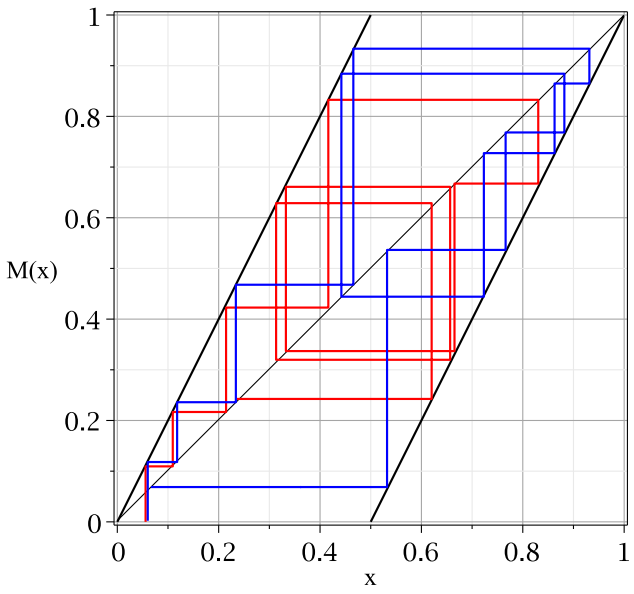

Figure 1.2: *Chaos in a simple dynamical system.* In this figure the property of sensitive dependence on initial conditions is illustrated in the doubling map modulo one. We see that two points which are initially very close, separate as they are iterated. Their orbits take completely different paths as they become uncorrelated from their starting point.

discrete time which gives rise to the study of nonlinear maps. The movement of a state under the evolution rule is called an 'orbit'. We will follow the latter route and consider discrete-time dynamical systems. As an illustrative example we can consider the doubling map modulo one or 'Bernoulli shift' map (see figure 1.2). The phase space for this dynamical system is given by the unit interval $X = [0, 1)$ with the endpoints 0 and 1 identified so that we consider the dynamics on a circle. The elements of X or possible states of the system are then given by the real numbers between 0 and 1. The measure on this system we can simply take as 'Lebesgue' measure which gives the difference between two numbers. That is the distance between two states of the system x and y is given by,

$$\mu(x, y) = |x - y| \,. \tag{1.10}$$

The equations of motion for this system are given by $M(x) : [0, 1) \to [0, 1)$,

$$M(x) = \begin{cases} 2x & 0 \leq x < \frac{1}{2} \\ 2x - 1 & \frac{1}{2} \leq x < 1 \end{cases} . \tag{1.11}$$

But in what sense can the dynamics created by Eq.(1.11) be described as chaotic? There is no universally agreed definition of chaos, (for a discussion of the various definitions of chaos and the links between them see Klages and Howard [2008]) but there are three main elements which underpin the idea. The first of these that we have discussed is sensitive dependence on initial conditions. We see that two points that are separated by an infinitesimally small amount δ are after one iteration separated by 2δ, then 4δ and after n iterations are separated by $2^n\delta = e^{n \ln 2}\delta$. Therefore the distance between points grows exponentially with n, the rate of growth in this case given by $\ln 2$. This growth rate is quantified with the local Lyapunov exponent $\lambda(x_0)$, defined by,

$$\lambda(x_0) = \lim_{k\to\infty} \frac{1}{n} \sum_{n=0}^{k-1} \ln |M'(x_n)| . \tag{1.12}$$

In Eq.(1.12), x_0 is an initial point and x_n is the n^{th} iterate of x_0 under Eq.(1.11). For $M(x)$, $M'(x)$ is equal to two for all x so we recover the result that $\lambda(x_0) = \ln 2$. This however is not enough, if we had the simple doubling map we would also have sensitive dependence on initial conditions, but we would not describe the dynamics generated by a doubling map as chaotic. We also need a system to exhibit some sort of irregular behaviour, not simply have all orbits diverge off to infinity. This is captured by the concept of topological transitivity which implies that there exists a point in your phase space whose orbit is dense. This loosely means that it comes arbitrarily close to any other point in phase space. This implies that there is an element of recurrence in the dynamics which is provided by the modulo one action in Eq.(1.11) which folds the space back onto itself after stretching. The third property is an element of regularity in the dynamics. This is provided by the periodic orbits of $M(x)$. These are the points which get iterated back onto themselves or onto another point in their orbit. The periodic orbits are dense in Eq.(1.11) which means you can find them anywhere you look. This dense set provides a skeleton of regular behaviour mixed in with the irregular behaviour of topological transitivity and exponential separation of points. It is

this mixture which we call chaotic.

1.1.4 Diffusion in dynamical systems

In the early 1980s, simple, discrete-time, chaotic dynamical systems were constructed which exhibited random walks (Geisel and Nierwetberg [1982]; Grossmann and Fujisaka [1982]; Schell et al. [1982]). That is, although the dynamics are controlled by deterministic equations of motion, the orbits of the individual points in phase space can be mapped onto random walks. This leads to the study of an evolution of a density of points in a dynamical system rather than individual orbits and leads to the concept of 'deterministic diffusion'. What sets deterministic (or chaotic) diffusion apart from the simple random walk process is that the dynamics is fully correlated, meaning the diffusion coefficient is dependent on all the higher-order correlations in the system.

The ratio between the uncorrelated random walk solution for diffusion and the actual diffusion coefficient due to higher order correlations is known as the 'correlation factor' in the physics literature, (Beijeren and Kehr [1986]; Chen and Dunham [2011]; Kaisermayr et al. [2001]; Kärger and Ruthven [1992]) and can be linked to 'persistence effects' in diffusion. This is for instance where particles diffusing in lattice structures such as metals Bardeen and Herring [1952] leave a lattice space vacant behind them when they 'jump' between sites. The particles are then more likely to jump back into these spaces leading to low order correlations between the jumps. This physically motivated effect called 'persistence', was first studied in the context of Brownian motion (Fürth [1920]) and hydrodynamics (Taylor [1922]). See Weiss [1994] and Haus and Kehr [1987] for reviews of this material.

Studying transport in the fully-correlated setting of deterministic dynamical systems became a very important topic (Wiggins [1992]). In particular, the parameter-dependence of the diffusion coefficient attracted much interest as the higher-order correlations are often very sensitive to variation of a control parameter in even simple systems, in some cases it was shown to introduce anomalous diffusion via intermittency (Fujisaka and Grossmann [1982]; Geisel and Thomae [1984]; Geisel et al. [1985]; Grossmann and Thomae [1983]). Anomalous diffusion

is the nonlinear growth of the mean square displacement with time, see Klages et al. [2008] for a review of this area.

A concentrated effort to fully understand the parameter-dependence of deterministic diffusion came from the area of dynamical systems. In particular, 'cycle expansion' techniques based on using the skeleton of periodic orbits to derive the diffusion coefficient were developed and applied to periodic one-dimensional dynamical systems (Artuso [1991]), Lorentz gases (Cvitanović et al. [1992]; Vance [1992]) and sawtooth maps (Artuso and Strepparava [1997]). However, these cycle expansion techniques are hampered by the very complicated structure of the periodic orbits, this being caused by the topological sensitivity of the higher order correlations under parameter variation. For a comprehensive introduction to these methods see (Cvitanović et al. [2010]). In Klages and Dorfman [1995], using techniques from the escape rate formalism developed in Gaspard [1992]; Gaspard and Nicolis [1990], which explicitly linked transport coefficients to fundamental properties of dynamical systems, the diffusion coefficient of a simple, piecewise-linear map of the real line was shown to behave very irregularly under parameter variation. It was conjectured in Klages and Dorfman [1995] that the diffusion coefficient was a 'fractal' function of the control parameter, which led to the conjecture that higher dimensional, more physically realistic systems such as the sawtooth maps (Dana et al. [1989]) may also exhibit fractal diffusion coefficients.

It is worth remarking that the term 'fractal', introduced to describe the 'rough' or 'broken' geometry of the natural world (Mandelbrot [1982]), as opposed to the smooth, regular geometry of the Euclidean world, is another concept that has no strict mathematical definition. It is used to describe objects that exhibit self-similarity and non-trivial fine scale structure. They may also have strange properties like non-integer dimensions, see Falconer [2003] for a mathematical discussion of fractals and associated concepts of generalised dimension. An attempt to understand the nature of the fractality observed in Klages and Dorfman [1995] was made in Klages and Klauß [2003] where it was conjectured that the parameter-dependent diffusion coefficient has a non-integer dimension that itself varies with the parameter. In Koza [2004], a mixture of analytical and numerical techniques led to the alternative conjecture that the parameter-dependent

diffusion coefficient has a dimension of one along with logarithmic corrections. This conjecture was made analytically rigorous in Keller et al. [2008] where it was shown that the dimension is one and that the fractality of the function is captured in the logarithmic corrections.

In Klages [1996], it was observed that the structure exhibited by the parameter-dependent diffusion coefficient in a simple, piecewise-linear, periodic map of the real line, resembled a set of fractal functions defined by functional 'de Rham' equations (de Rham [2003]), these functions previously being linked to deterministic diffusion in Tasaki and Gaspard [1994]; Tasaki et al. [1993a,b]. These observations led to the development of powerful analytic methods based upon recursion relations which derive the diffusion coefficient via fractal functional equations in Klages [1996]. In an attempt to understand the fractal structure in the parameter-dependent diffusion coefficient, these methods were applied to a simple piecewise-linear map and yielded a series of analytical and numerical approximations to the diffusion coefficient, which systematically took into account the higher order correlations in the dynamics.

This thesis represents the culmination of this line of research. By application to a set of one-dimensional, piecewise-linear, periodic maps of the real line, the methods developed in Klages [1996] are explored to their full analytical capability. This permits the analytical evaluation of the diffusion coefficient at any parameter value to (practically) any desired accuracy. This analysis leads to a full understanding of the origin of the fractal structure in these simple systems.

Of course there are still many fundamental unanswered questions in deterministic diffusion. The nature of the structure of parameter-dependent diffusion coefficients in more physically realistic, higher-dimensional dynamical systems remains an open question. In particular, area preserving Hamiltonian systems like the sawtooth maps have received a lot of attention, see for example Dana et al. [1989], and references therein or more recently Venegeroles and Saa [2008]. Again the higher order correlations are sensitive to variations in a control parameter called the 'stochasticity' parameter K. It has only been possible to analytically calculate the diffusion coefficient at integer values of K where one can show that all higher-order correlations vanish, (Cary and Meiss [1981]). This is because the map becomes a linear automorphism at integer values of K (at $K = 1$ this

is Arnold's CAT map (Arnold and Avez [1968])). Despite the development of a good knowledge of the underlying periodic orbit structure in the sawtooth maps in Percival and Vivaldi [1987a] and Percival and Vivaldi [1987b], the fractality remains an open question with some conjectures claiming it to be smooth (Sano [2002]). Parameter-dependent diffusion in Hamiltonian particle billiards such as the periodic Lorentz gas (Lorentz [1905]) also receives much interest (see Klages [2007] and references therein). The irregularity of the diffusion coefficient in this system was observed to exist only on very fine scales (Klages and Dellago [2000]), which meant that making conclusions about the fractality was very difficult. Indeed it was conjectured that the parameter-dependent diffusion coefficient may be a C^1 function but not a C^2 function, the fractality existing in the higher derivatives. This led to the deliberate construction of billiard systems which display more irregular diffusion coefficients (Harayama et al. [2002]), and also to the study of billiard systems subject to an external field where irregularities are clearer (Harayama and Gaspard [2001]), yet fully analytical answers are still far off.

1.2 Structure and summary of results

In chapter 2 we will realise the full potential of the functional recursion relation method for deriving the diffusion coefficient developed in Klages [1996]. This will involve the exploration of a family of parameter-dependent, piecewise-linear, periodic maps of the real line. We will fully analytically derive the parameter-dependent diffusion coefficient for each of the maps and observe a mixture of fractal and also linear behaviour. We will explain the fractality by associating extreme points in the diffusion coefficient to particular behaviour in the orbit of the critical points of the map. This allows us to pinpoint the extrema precisely when explaining the source of the fractality. The linear behaviour is in some cases linked to the breaking of the ergodicity of the map. Along with this full understanding also comes some new questions and observations. We observe certain parameter regions where the linearity of the diffusion coefficient can not be explained in terms of ergodicity-breaking, rather there is a microscopic 'dominating-branch' effect which causes the diffusion coefficient to withstand drastic changes in the

microscopic dynamics. How ubiquitous in dynamical systems is this newly observed phenomenon, is left as an open question. We then numerically explore the diffusion coefficient for the two-dimensional sawtooth map (Dana et al. [1989]), in an attempt to understand the parameter-dependent diffusion coefficient. We show that in analogy with parameter-dependent diffusion coefficients in other higher dimensional systems like the Lorentz gas, (Klages [2007]), the irregularities in the diffusion coefficient exist on a very fine scale making it difficult to draw concrete conclusions as to the nature of the diffusion coefficient.

Inspired by the exploration of the sawtooth map in chapter 2 and by criticism of an approximation method based on the functional recursion relation approach explored in chapter 2 (Klages and Knight [2011]), in chapter 3 we will look at three different approximation procedures for the parameter-dependent diffusion coefficient in a simple one-dimensional map. The goal is to critically explore the individual capabilities and weaknesses at exposing fractal structures of the individual methods. The results we obtain are very different for each method. The first method is based on truncating the Taylor-Green-Kubo formula for diffusion which forms the basis of the functional recursion relation approach from chapter 2. This leads to a series of converging approximations which contain points that converge in finite time. In this way one can see the fractal structure emerge as the approximations are built up. The second method is based on the 'persistent' random walk discussed above. We analytically and numerically include memory effects persistently, thereby obtaining a series of approximations. The third method is based on the escape rate theory of diffusion (Gaspard [1992]; Gaspard and Nicolis [1990]) and consists of approximating the Markov transition matrix of a system by truncating the associated 'generating orbit' (the orbit of a critical point which yields the Markov partition points). Again we analytically and numerically build up a series of approximations whose functional form points to regions of self-similarity.

In chapter 4 we are inspired by the recent surge of interest in open systems (Altmann and Endler [2010]; Altmann and Tél [2009]; Bunimovich and Yurchenko [2011]; Demers and Young [2006]; Dettmann [2011]; Keller and Liverani [2009]) to explore a novel form of parameter-dependence in deterministic diffusion. We again consider a simple, piecewise-linear, periodically copied map of the real line

but we derive the diffusion coefficient as a function of the size and the position of the 'escape holes' (regions in phase space that couple the individual copies of the map) rather than as a function of a continuous parameter. We find non-trivial dependence of the diffusion coefficient on the position of the holes in analogy with corresponding results on the escape rate (Bunimovich and Yurchenko [2011]; Keller and Liverani [2009]) and observe that the diffusion coefficient decreases non-monotonically with the size, as opposed to results for the escape rate. We also explore the small-hole asymptotic behaviour of the system which we find to be dependent on the limiting point of the hole. This result generalises the simple random walk result for small hole asymptotic behaviour (Fujisaka and Grossmann [1982]; Klages [1996]; Klages and Dorfman [1997]; Schell et al. [1982]). Conjectures are made that it should be ubiquitous in dynamical systems and also potentially observable in experiment. Lastly we calculate the escape rate in the corresponding open system in order to compare the two transport phenomena.

In chapter 5 we look at an alternative method for analytically deriving the diffusion coefficient. This method is based on a generalisation of the work in Milnor and Thurston [1988], in which the determinant of a 'kneading matrix' was related to the zeros of a topological zeta function. The entries of the kneading matrix are determined by the orbits of the critical points of the map, these orbits are called 'kneading orbits' (Devaney [1989]; Katok and Hasselblatt [1995]). The generalisation in Baladi and Ruelle [1994] extended this result to weighted dynamical zeta functions, from which the diffusion coefficient can be derived, this generalisation being used in Cristadoro [2006] to derive the parameter-dependent diffusion coefficient of a simple, piecewise-linear map of the real line. We begin by showing how the zero of a weighted dynamical zeta function can be related to the diffusion coefficient via the generating function for diffusion, in order to give some theoretical background for the method. We then fully analytically employ the method to compute the diffusion coefficient to again any (practically) desired accuracy. This leads to the observation of a set of increasingly complex step-functions which converge to the diffusion coefficient. Chapter 6 is a summary and outlook.

This thesis is largely based upon published work. In particular chapters 2, 3 and 4 follow closely papers which can be found in the publication list near

the end of this thesis. Chapter 5 contains results which will form part of a future publication. Each chapter is therefore motivated individually and contains individual conclusions. The intention is that each chapter can be read separately as a stand-alone piece. This has the side-effect that some ideas are repeated which may be noticeable to the more dedicated cover-to-cover reader. The references are given at the end of the thesis in alphabetical order along with the page numbers where they are referenced. In the colour version of this thesis the references are highlighted in red, the pdf version contains links which take you to the relevant part of the references. Objects in the text highlighted in blue link to internal sections within the thesis whilst blue text in the references are linked to external websites for the corresponding publications where available. All of the figures in this thesis were created using *Maple 15* software whilst the numerical experiments on the sawtooth map in chapter 2 were performed using *Fortran 77* software.

Chapter 2

Linear and fractal diffusion coefficients in a family of one dimensional chaotic maps

Deterministic diffusion is analysed in a family of four parameter dependent, chaotic maps of the real line. When iterated under these maps, a probability density function spreads out and one can define a diffusion coefficient. Of particular interest is how the diffusion coefficient varies across the family of maps and under parameter variation. Using a technique by which Taylor-Green-Kubo formulae are evaluated in terms of generalised Takagi functions, we derive exact, fully analytical expressions for the diffusion coefficients. Typically, for simple maps these quantities are fractal functions of control parameters. However, this family of maps exhibits both fractal and linear behaviour. This mixture is explained by looking at the topology of the Markov partitions and the ergodic properties of the maps. This analysis exposes a new phenomenon ('dominating branch effect') in dynamical systems theory in which the diffusion coefficient is very robust to changes in the microscopic dynamics.

2.1 Introduction

One of the most prominent problems in statistical physics and dynamical systems theory is to understand non-equilibrium transport from first principles, that is, starting from the nonlinear equations of motion of many-particle systems (Cvitanović et al. [2010]; Dorfman [1999]; Gaspard [1998]; Klages [2007]). Such a theory aims at explaining the origin of macroscopic transport in terms of the chaotic and fractal properties of the underlying microscopic deterministic dynamics. Unfortunately, physical many-particle systems are typically far too complex to allow for exact analytical solutions of this problem. A common strategy is therefore to first study solvable toy models, such as deterministic random walks defined by one-dimensional chaotic maps (Geisel and Nierwetberg [1982]; Grossmann and Fujisaka [1982]; Schell et al. [1982]) before applying the knowledge gained to more difficult dynamics.

An interesting and surprising result when studying a simple piecewise linear model of this type was that the diffusion coefficient was found to be a fractal function of a control parameter (Klages and Dorfman [1995]). That this result was not an artefact of the model used was confirmed by studying other transport processes, such as biased diffusion (Groeneveld and Klages [2002]) and reaction-diffusion (Gaspard and Klages [1998]) in other (nonlinear) maps (Cvitanović et al. [2010]; Korabel and Klages [2004]) and in physically more realistic systems like periodic particle billiards (Gaspard [1998]), which in turn can be linked to experiments (Klages et al. [2004]), see Klages [2007] for a review of this material and references therein.

Unfortunately, even for the simplest piecewise linear deterministic models exact solutions for transport coefficients are rare (Dorfman [1999]): for specific values of control parameters analytical results are available by cycle expansion techniques (Cvitanović et al. [2010]) or by first passage methods (Klages [1996]; Klages and Dorfman [1999]). Numerical extensions of these methods include stability ordering of periodic orbits (Dettmann and Morriss [1997]) and transition matrix methods (Gaspard and Klages [1998]; Klages [1996]; Klages and Dorfman [1995, 1999]). As methods yielding exact formulae for fractal transport coefficients, there is the 'twisted eigenstate' method based on kneading theory

described in Groeneveld and Klages [2002] and Klages [2007] whose extension to maps that have more than one 'lap' per unit interval, such as we will consider in this chapter, is currently an open question and there an alternative technique, also based on kneading theory (Cristadoro [2006]) that we will discuss in chapter 5.

In order to better understand existence and properties of fractal transport coefficients in chaotic dynamical systems, it is vital to develop both more powerful tools for calculating these quantities, and to enlarge the set of systems studied. Correspondingly, in this chapter we will introduce a new family of deterministically diffusive models which define the simplest class of systems exhibiting fractal diffusion coefficients. We then calculate these quantities using the Taylor-Green-Kubo formula (Dorfman [1999]; Gaspard [1998]; Klages [2007]) in combination with generalised Takagi functions (Gaspard and Klages [1998]; Klages [1996]). This approach is for the first time explored analytically to its full power and will allow us to obtain an accurate insight into the complicated, fractal structures we observe in the diffusion coefficient. The main results are exact analytic expressions for the parameter dependent diffusion coefficients for the whole family of maps and the discovery that there is a mixture of linearity and fractality in the diffusion coefficients. The linearity is non-trivial, because in the regions of linearity the maps are either non-ergodic or topologically unstable. The latter property typically generates fractal parameter dependencies, however, our method reveals a subtle mechanism of 'dominating branches, which can stabilise diffusion coefficients under parameter variation in maps whose microscopic symmetry is broken.

In section 2.2 we will introduce the family of parameter dependent maps and then analytically derive the diffusion coefficient as a function of the parameter for each map via a functional recursion relation. In section 2.3 we will analyse the structure of the diffusion coefficients and explain the features that we observe. Most importantly, we explain why we observe a mixture of fractality and linearity. We then employ a method based on the Markov partitions of the maps to pinpoint exactly where the local extrema will be in these fractal diffusion coefficients (Klages [1996]; Klages and Dorfman [1995, 1999]) which will lead to an explanation of the fractal structure. In addition, we will explore the fact that in certain parameter regions the diffusion coefficients are very stable

to dramatic changes in the microscopic dynamics of the maps, this property being interestingly opposed to the fact that the diffusion coefficients are extremely sensitive to parameter variation in other areas of the parameter space. This phenomenon leads to the discovery of the 'dominating branch effect'. In section 2.4 we will explore the limitations of the functional recursion relation method when we apply it to a pseudo-two-dimensional system, namely the sawtooth map (Dana et al. [1989]). We will attempt to apply the method analytically before resorting to numerical computations to explore the diffusion coefficient. This numerical exploration reveals non-trivial dependence of the diffusion coefficient on the parameter, although this non-trivial dependence appears on very fine scales. This result matching those found in other higher dimensional systems such as the Lorentz gas (Klages [2007]; Klages and Dellago [2000]). Section 2.5 forms a conclusion. This work was done in collaboration with Dr. Rainer Klages of Queen Mary University of London and was published in Knight and Klages [2011b].

2.2 A functional recursion relation

In this section we will define the family of one-dimensional maps that we will study. Then, starting from the Taylor-Green-Kubo formula we will derive the parameter dependent diffusion coefficient of these maps via the solutions of some fractal generalised Takagi functions.

2.2.1 The family of maps

For $h \geq 0$ let $M_h(x) : [0,1] \to \mathbb{R}$ be a parameter dependent variant of the well known Bernoulli shift map. The parameter lifts the first branch, and lowers the second branch i.e.

$$M_h(x) = \begin{cases} 2x + h & 0 \leq x < \frac{1}{2} \\ 2x - 1 - h & \frac{1}{2} \leq x < 1 \end{cases} . \tag{2.1}$$

In order to create an extended system for diffusion, we define $M_h(x) : \mathbb{R} \to \mathbb{R}$ by periodically copying Eq.(2.1), with a lift of degree one such that

$$M_h(x+n) = M_h(x) + n, \quad n \in \mathbb{Z}. \tag{2.2}$$

This map was first studied in Gaspard and Klages [1998] as a projection of a generalization of the diffusive-reactive multibaker map. We call it the lifted Bernoulli shift map. This process of periodically copying a map with a lift of degree one is a common way to create a diffusive map (Geisel and Nierwetberg [1982]; Grossmann and Fujisaka [1982]; Schell et al. [1982]). The use of the lift parameter h ensures that the invariant probability density function (p.d.f) remains a constant function throughout the entire parameter range. This helps simplify the derivation of the diffusion coefficient as an invariant p.d.f is an essential ingredient in the Taylor-Green-Kubo formula that is used to derive the diffusion coefficient (Dorfman [1999]; Klages [1996]). The remaining members of the family are created by changing the sign of the gradient in Eq.(2.1). Let $W_h(x) : [0,1] \to \mathbb{R}$

$$W_h(x) = \begin{cases} -2x + h + 1 & 0 \leq x < \frac{1}{2} \\ -2x + 2 - h & \frac{1}{2} \leq x < 1 \end{cases}, \tag{2.3}$$

which we call the lifted negative Bernoulli shift map. Let $V_h(x) : [0,1] \to \mathbb{R}$

$$V_h(x) = \begin{cases} -2x + 1 + h & 0 \leq x < \frac{1}{2} \\ 2x - 1 - h & \frac{1}{2} \leq x < 1 \end{cases}, \tag{2.4}$$

which we call the lifted V map. Let $\Lambda_h(x) : [0,1] \to \mathbb{R}$

$$\Lambda_h(x) = \begin{cases} 2x + h & 0 \leq x < \frac{1}{2} \\ -2x + 2 - h & \frac{1}{2} \leq x < 1 \end{cases}, \tag{2.5}$$

which we call the lifted tent map. Again we apply the lift of degree one condition of Eq.(2.2) to Eq.(2.3), Eq.(2.4) and Eq.(2.5) to create spatially extended systems defined over the real line. See figure 2.1 for an illustration.

2.2.2 The Taylor-Green-Kubo formula

We begin with the discrete version of the Taylor-Green-Kubo formula which gives the diffusion coefficient as an integral over the velocity correlations of a system.

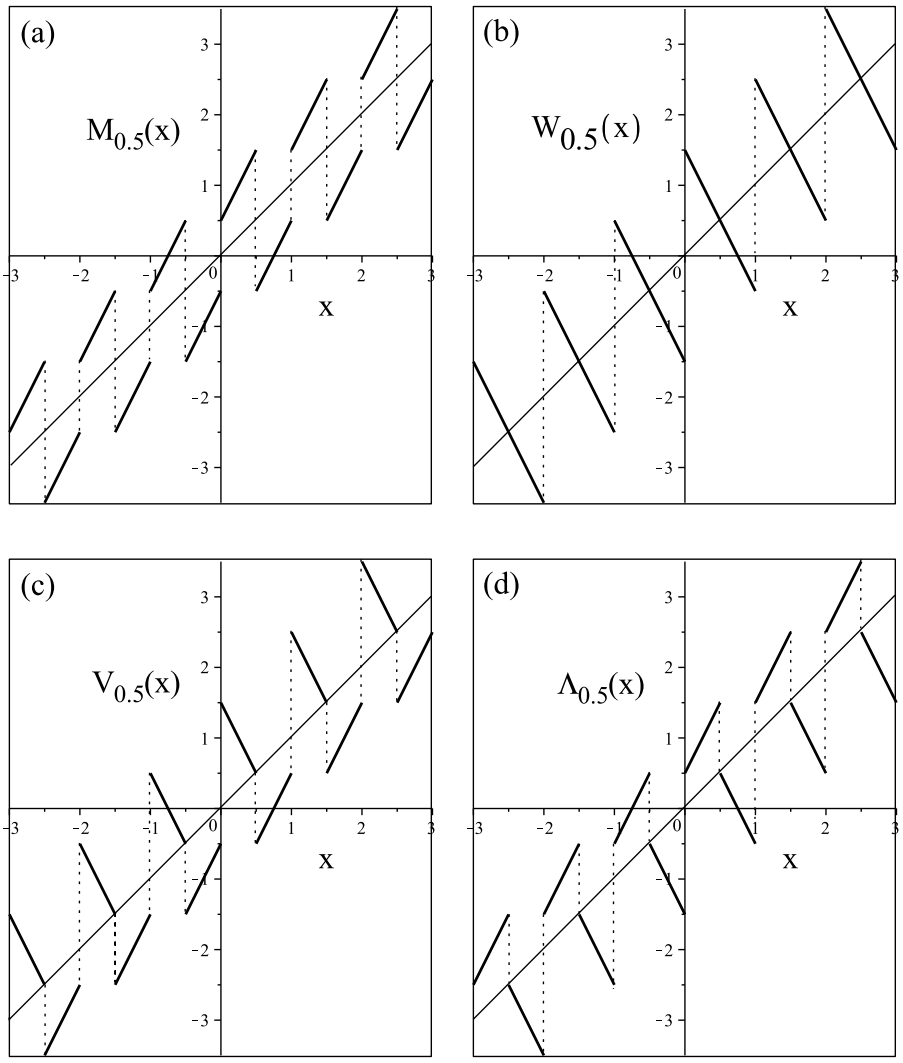

Figure 2.1: *The family of maps.* In this figure, a section of each of the four maps in our family is illustrated at a parameter value of $h = 0.5$. In **(a)** the lifted Bernoulli shift, so-called because the Bernoulli shift is recovered when $h = 0$ on the unit interval. In **(b)** the lifted negative Bernoulli shift, so-called because a version of the Bernoulli shift with a negative gradient is recovered when $h = 0$. In **(c)** the lifted V map, so-called because a V map is recovered when $h = 0$. In **(d)** the lifted tent map, so-called because a tent map is recovered when $h = 0$.

This formula is often referred to simply as the Green-Kubo formula after derivations of the continuous version in Green [1954] and Kubo [1957]. However, a derivation was already given in Taylor [1921] so 'Taylor-Green-Kubo' formula, as it is referred to in Klages [2007] seems more appropriate. In order to derive the Taylor-Green-Kubo formula (see Dorfman [1999] for a similar derivation) we begin with Einstein's formula in one-dimension which gives the diffusion coefficient D directly in terms of the mean square displacement (Einstein [1905]),

$$D(h) = \lim_{n\to\infty} \frac{\langle (x_n - x_0)^2 \rangle}{2n}, \tag{2.6}$$

where we are evaluating the diffusion coefficient as a function of the parameter h. The angular brackets $\langle ... \rangle$ represent an average taken over the invariant p.d.f, $\rho^*(x)$ where x_n is the position of a point x at time n

$$\langle ... \rangle = \int_0^1 dx \rho^*(x) ... \quad . \tag{2.7}$$

The first step to derive the Taylor-Green-Kubo formula is to telescopically expand the numerator in Eq.(2.6),

$$D(h) = \lim_{n\to\infty} \frac{1}{2n} \left\langle (x_n - x_{n-1} + x_{n-1} - x_{n-2} + x_{n-2} - x_{n-3} + ... - x_0)^2 \right\rangle . \tag{2.8}$$

We then define a 'velocity function' $\tilde{v}_k(x) : [0,1] \to \mathbb{R}$

$$\tilde{v}_k(x) = x_{k+1} - x_k, \tag{2.9}$$

which gives the displacement of a point x at time k. We substitute Eq.(2.9) into Eq.(2.8) which gives a sum,

$$D(h) = \lim_{n\to\infty} \frac{1}{2n} \left\langle \left(\sum_{k=0}^{n-1} \tilde{v}_k(x) \right)^2 \right\rangle . \tag{2.10}$$

We can simplify Eq.(2.10) by replacing Eq.(2.9) with the simpler function (Klages and Korabel [2002])

$$v_k(x) = \lfloor x_{k+1} \rfloor - \lfloor x_k \rfloor, \tag{2.11}$$

where $\lfloor ... \rfloor$ denotes the 'floor' function. Eq.(2.11) gives the integer displacement of a point x at time k. We can see that this substitution is possible if we let $\Delta x_n = x_n - x_0$ in Eq.(2.6), and further we let $\Delta x_n = \Delta X_n + \Delta \tilde{x}_n$. Where X_n is the integer part of the displacement and $\tilde{x}_n \in [0, 1)$ is the fractional part of the displacement,

$$\begin{aligned} D(h) &= \lim_{n\to\infty} \frac{\langle (\Delta X_n + \Delta \tilde{x}_n)^2 \rangle}{2n} \\ &= \lim_{n\to\infty} \frac{\langle (\Delta X_n^2 + 2\Delta X_n \Delta \tilde{x}_n + \Delta \tilde{x}_n^2) \rangle}{2n} \quad . \end{aligned} \tag{2.12}$$

The second term in the numerator of Eq.(2.12) is bounded by the 'Cauchy-Hölder inequality' (Lasota and Mackey [1994]), and the third term is also bounded, hence in the limit as n goes to infinity, only ΔX_n contributes to $D(h)$. The next step is to multiply out the square in Eq.(2.10) and collect together the diagonal terms and the off-diagonal terms,

$$D(h) = \lim_{n\to\infty} \frac{1}{2n} \left\langle \left(\sum_{k=0}^{n-1} (v_k(x))^2 + 2 \sum_{k\neq k'} v_k(x) v_{k'}(x) \right) \right\rangle . \tag{2.13}$$

As we are taking an average over an invariant density, we have translational invariance in the velocity correlation functions, that is

$$\langle v_m(x) v_n(x) \rangle = \langle v_{m-n}(x) v_0(x) \rangle \, . \tag{2.14}$$

Using this property of Eq.(2.14) in Eq.(2.13) we arrive at the Taylor-Green-Kubo formula

$$D(h) = \lim_{n\to\infty} \left(\sum_{k=0}^{n} \langle v_0(x) v_k(x) \rangle \right) - \frac{1}{2} \langle v_0(x)^2 \rangle \tag{2.15}$$

2.2.3 Deriving the diffusion coefficient

In order to evaluate Eq.(2.15) for our family of maps, we first make use of the fact that the invariant density is a simple constant function, $\rho^*(x) = 1$. This means we can rewrite Eq.(2.15) as

$$D(h) = \lim_{n\to\infty} \left(\int_0^1 v_0(x) \sum_{k=0}^{n} v_k(x) \;\; dx \right) - \frac{1}{2} \int_0^1 v_0(x)^2 dx \;\; . \tag{2.16}$$

The second integral is simple enough to evaluate as it is simply taken over a step function. For example for the lifted Bernoulli shift map $M_h(x)$ the velocity function is

$$v_0(x) = \begin{cases} \lfloor h \rfloor & 0 \leq x < \frac{1-\hat{h}}{2} \\ \lceil h \rceil & \frac{1-\hat{h}}{2} \leq x < \frac{1}{2} \\ -\lceil h \rceil & \frac{1}{2} \leq x < \frac{1+\hat{h}}{2} \\ -\lfloor h \rfloor & \frac{1+\hat{h}}{2} \leq x < 1 \end{cases} \;\; , \tag{2.17}$$

where $\lfloor ... \rfloor$ and $\lceil ... \rceil$ are the floor function and ceiling function respectively. The function $\hat{h} : \mathbb{R} \to [0, 1]$ is defined as

$$\hat{h} = \begin{cases} 1 & h \in \{\mathbb{Z}\} \\ h \;\; modulo \;\; 1 & otherwise \end{cases} \;\; . \tag{2.18}$$

Eq.(2.18) is simply a corrective function that ensures Eq.(2.11) is correct at the points of discontinuity. The first integral in Eq.(2.16) poses a greater problem. To solve it we first define a cumulative 'jump function' $J_M^n(x) : [0, 1] \to \mathbb{R}$ as

$$J_M^n(x) = \sum_{k=0}^{n} v_k(x), \tag{2.19}$$

which gives the integer displacement of a point x after n iterations. The subscript M tells us we are considering the jump function for the lifted Bernoulli shift map $M_h(x)$. We substitute Eq.(2.19) into Eq.(2.16) to obtain

$$D_M(h) = \lim_{n\to\infty} \left(\int_0^1 v_0(x) J_M^n(x) \;\; dx \right) - \frac{1}{2} \int_0^1 v_0^2(x) \;\; dx. \tag{2.20}$$

In order to extract the information we need from (2.20), we define the cumulative function $T_M(x) : [0,1] \to \mathbb{R}$,

$$T_M(x) = \lim_{n\to\infty} T_M^n(x) = \lim_{n\to\infty} \int_0^x J_M^n(y)dy. \tag{2.21}$$

Eq.(2.21) defines the 'generalised Takagi functions' discussed above and in Klages [1996]. Due to the chaotic nature of the maps, and in particular, the sensitive dependence on initial conditions, the jump function behaves very erratically for large n, see figure 2.2 for an illustration of this. This is reflected in $T_M(x)$ which becomes fractal in the limit $n \to \infty$. We call these functions 'generalised Takagi functions' because for the lifted Bernoulli shift map with parameter $h = 1$, one reproduces the function first studied in Takagi [1903]. This special case of the 'De Rham' function (de Rham [2003]), was presented as a simple example of a function that is both continuous and non-differentiable. In order to control the chaotic nature of the jump function, we derive a functional recursive relation Klages [1996]. For the lifted Bernoulli shift map

$$J_M^n(x) = v_0(x) + J_M^{n-1}\left(\tilde{M}_h(x)\right), \tag{2.22}$$

where $\tilde{M}_h(x)$ is Eq.(2.1) taken modulo one. In turn, we define a functional recursive relation for the generalised Takagi functions, by substituting Eq.(2.22) into Eq.(2.21)

$$T_M(x) = \lim_{n\to\infty}\left(t_M(x) + \frac{1}{2}T_M^{n-1}\left(\tilde{M}_h(x)\right)\right), \tag{2.23}$$

where $t_M(x) : [0,1] \to \mathbb{R}$ is an integral over $v_0(x)$,

$$t_M(x) = xv_0(x) + c_i \quad i \in \{1,2,3,4\}. \tag{2.24}$$

Where c_i is a constant of integration which we must solve on each interval in $\tilde{M}_h(x)$. Using Eq.(2.17) in Eq.(2.23) gives

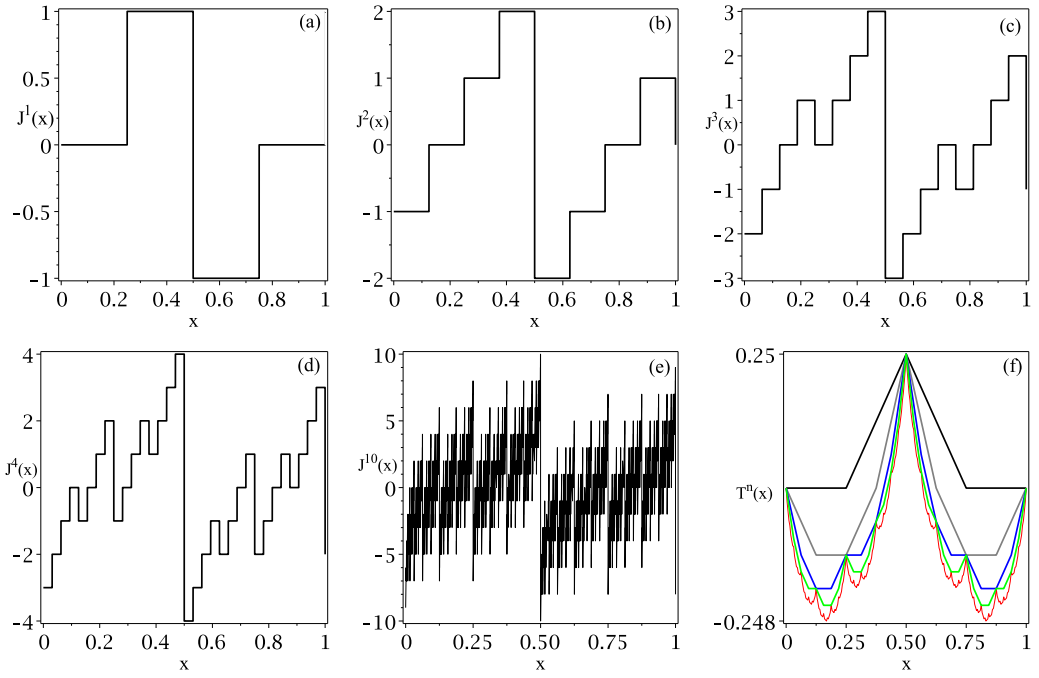

Figure 2.2: *Building the generalised Takagi functions.* In this figure the 'jump function' $J_h^n(x)$ is illustrated for the lifted Bernoulli shift map at parameter value $h = 0.5$ at time $n = 1, 2, 3, 4$ and 10 in **(a)**,**(b)**,**(c)**, **(d)** and **(e)** respectively. Due to the sensitive dependence on initial conditions in the map, the distance between points increases exponentially. This property is reflected in the increasing complexity of the step function of $J_h^n(x)$ as n increases. In figure **(f)** the corresponding cumulative integrals over $J_h^n(x)$; $T_h^n(x)$ are illustrated for $n = 1, 2, 3, 4$ and 10 in (decreasing from $x = 3/16$ respectively) black, grey, blue, green and red respectively. In the limit n to infinity the points of discontinuity become dense in $J_h^n(x)$ resulting in a 'fractal' function $T_h(x)$.

$$T_M(x) = \begin{cases} \frac{1}{2}T_M\left(2x + \hat{h}\right) + \lfloor h \rfloor x + c_1 & 0 \le x < \frac{1-\hat{h}}{2} \\ \frac{1}{2}T_M\left(2x + \hat{h} - 1\right) + \lceil h \rceil x + c_2 & \frac{1-\hat{h}}{2} \le x < \frac{1}{2} \\ \frac{1}{2}T_M\left(2x - \hat{h}\right) - \lceil h \rceil x + c_3 & \frac{1}{2} \le x < \frac{1+\hat{h}}{2} \\ \frac{1}{2}T_M\left(2x - 1 - \hat{h}\right) - \lfloor h \rfloor x + c_4 & \frac{1+\hat{h}}{2} \le x \le 1 \end{cases} , \tag{2.25}$$

The constants of integration c_i, are evaluated by using the two conditions

1. $T_M(0) = T_M(1) = 0$.

2. The Takagi functions are continuous.

Condition 1 follows from the definition of $T_M(x)$ in Eq.(2.21) combined with the fact that we have no mean drift. Condition 2 simply follows from Eq.(2.21). For example, from Eq.(2.25), using $T_M(0) = 0$ gives

$$\frac{1}{2}T_M\left(\hat{h}\right) + c_1 = 0, \tag{2.26}$$

which yields

$$c_1 = -\frac{1}{2}T_M\left(\hat{h}\right). \tag{2.27}$$

We can apply the continuity condition at the points of discontinuity of $\tilde{M}_h(x)$ to get the remaining constants. That is for example

$$\lim_{x\to((1-\hat{h})/2)^-} T_M(x) = \lim_{x\to((1-\hat{h})/2)^+} T_M(x). \tag{2.28}$$

From Eq.(2.25) and Eq.(2.27) we have

$$\lim_{x\to((1-\hat{h})/2)^-} T_M(x) = \lfloor h \rfloor \frac{1-\hat{h}}{2} - \frac{1}{2}T_M\left(\hat{h}\right), \tag{2.29}$$

and from Eq.(2.25) we have,

$$\lim_{x\to((1-\hat{h})/2)^+} T_M(x) = \lceil h \rceil \frac{1-\hat{h}}{2} + c_2. \tag{2.30}$$

Combing Eq.(2.29) with Eq.(2.30) via Eq.(2.28) we have

$$c_2 = \frac{\hat{h}-1}{2} - \frac{1}{2}T_M\left(\hat{h}\right). \tag{2.31}$$

We can similarly evaluate c_3 and c_4 to finally obtain

$$T_M(x) = \begin{cases} \frac{1}{2}T_M\left(2x+\hat{h}\right) + \lfloor h \rfloor\, x - \frac{1}{2}T_M(\hat{h}) & 0 \le x < \frac{1-\hat{h}}{2} \\ \frac{1}{2}T_M\left(2x+\hat{h}-1\right) + \lceil h \rceil\, x + \frac{\hat{h}-1}{2} - \frac{1}{2}T_M(\hat{h}) & \frac{1-\hat{h}}{2} \le x < \frac{1}{2} \\ \frac{1}{2}T_M\left(2x-\hat{h}\right) + \frac{1+\hat{h}}{2} - \lceil h \rceil\, x - \frac{1}{2}T_M(\hat{h}) & \frac{1}{2} \le x < \frac{1+\hat{h}}{2} \\ \frac{1}{2}T_M\left(2x-1-\hat{h}\right) + \lfloor h \rfloor\,(1-x) - \frac{1}{2}T_M(\hat{h}) & \frac{1+\hat{h}}{2} \le x \le 1 \end{cases} , \tag{2.32}$$

where we have taken the limit $n \to \infty$. We now have the ingredients that we need to derive the parameter dependent diffusion coefficient. Using Eq.(2.17) in Eq.(2.20)

$$\begin{aligned} D_M(h) &= \lim_{n\to\infty} \int_0^{\frac{1-\hat{h}}{2}} \lfloor h \rfloor\, J_M^n(x)\ dx + \int_{\frac{1-\hat{h}}{2}}^{\frac{1}{2}} \lceil h \rceil\, J_M^n(x)\ dx \\ &- \int_{\frac{1}{2}}^{\frac{1+\hat{h}}{2}} \lceil h \rceil\, J_M^n(x)\ dx - \int_{\frac{1+\hat{h}}{2}}^{1} \lfloor h \rfloor\, J_M^n(x)\ dx \\ &- \frac{1}{2}\left(\int_0^{\frac{1-\hat{h}}{2}} \lfloor h \rfloor^2 + \int_{\frac{1-\hat{h}}{2}}^{\frac{1}{2}} \lceil h \rceil^2 + \int_{\frac{1}{2}}^{\frac{1+\hat{h}}{2}} \lceil h \rceil^2 + \int_{\frac{1+\hat{h}}{2}}^{1} \lfloor h \rfloor^2 \right). \end{aligned} \tag{2.33}$$

Evaluating the integrals, simplifying using Eq.(2.32) and gathering relevant terms we obtain

$$\begin{aligned} D_M(h) &= (\lfloor h \rfloor - \lceil h \rceil)\left(\lfloor h \rfloor - \hat{h}\, \lfloor h \rfloor - T_M\left(\hat{h}\right)\right) + \lceil h \rceil \left(\lceil h \rceil + \hat{h} - 1 \right) \\ &- \frac{1}{2}\left(\lfloor h \rfloor^2 \left(1-\hat{h}\right) + \lceil h \rceil^2\, \hat{h} \right), \end{aligned}$$

which after some wrangling can be rewritten as

$$D_M(h) = \frac{\lceil h \rceil^2}{2} + \left(\frac{1-\hat{h}}{2}\right)(1 - 2\lceil h \rceil) + T_M\left(\hat{h}\right) \quad . \tag{2.34}$$

Eq.(2.34) is an exact analytic expression for the parameter dependent diffusion coefficient of the lifted Bernoulli shift map. The first two terms in this equation

form a piecewise linear function that is equal to $h^2/2$ for large h, which defines the asymptotic growth of the diffusion coefficient in this parameter regime. Interestingly, our shifted map thus belongs to a different universality class compared to the maps studied in Klages [1996]; Klages and Dorfman [1997] where the gradient was varied as a control parameter yielding a coefficient of 1/6 for the quadratic scaling in this regime. The last term $T_M(\hat{h})$ in Eq.(2.34) tells us about the fine structure of $D_M(h)$, which is periodic modulo one as it is a function of $\hat{h}$, see figure 2.3 for an illustration. For small h we get a different region of asymptotic behaviour where the diffusion coefficient is given by

$$D_M(h) = \frac{h}{2} + T_M(h) \quad 0 \leq h \leq 1 \,. \tag{2.35}$$

In this regime Eq.(2.32) yields $T_M(h) = \frac{1}{3} T_M(3h)$, that is, if we make h smaller by a factor of 3 the deviation from $h/2$ in the diffusion coefficient is also reduced by a factor of 3. This explains why the fine structure that we observe in the inset of figure 2.3.(a) becomes smaller and smaller in the limit of $h \to 0$. The diffusion coefficient thus behaves asymptotically like $h/2$ corresponding to the simple random walk result for diffusion in this map for small parameter values. In other words, higher order correlations of our system are negligible as $h \to 0$, in agreement with the findings in Klages [1996]; Klages and Dorfman [1997]. Such a change between two different types of asymptotic random walk behaviour for small and large parameter values was denoted as a 'crossover in deterministic diffusion' (Klages and Dorfman [1997]).

Although the calculations have been presented for the lifted Bernoulli shift, the method is essentially the same for the other three maps. If we turn our attention to the lifted negative Bernoulli shift map $W_h(x)$ the Takagi function is

$$T_W(x) = \begin{cases} -\frac{1}{2} T_W\left(-2x + \hat{h}\right) + \lceil h \rceil \, x + \frac{1}{2} T_W(\hat{h}) & 0 \leq x < \frac{\hat{h}}{2} \\ -\frac{1}{2} T_W\left(-2x + \hat{h} + 1\right) + \lfloor h \rfloor \, x + \frac{\hat{h}}{2} + \frac{1}{2} T_W(\hat{h}) & \frac{\hat{h}}{2} \leq x < \frac{1}{2} \\ -\frac{1}{2} T_W\left(-2x + 2 - \hat{h}\right) - \lfloor h \rfloor \, (x+1) + \frac{\hat{h}}{2} + \frac{1}{2} T_W(\hat{h}) & \frac{1}{2} \leq x < 1 - \frac{\hat{h}}{2} \\ -\frac{1}{2} T_W\left(-2x + 3 - \hat{h}\right) + \lceil h \rceil \, (1-x) + \frac{1}{2} T_W(\hat{h}) & 1 - \frac{\hat{h}}{2} \leq x \leq 1 \end{cases} \tag{2.36}$$

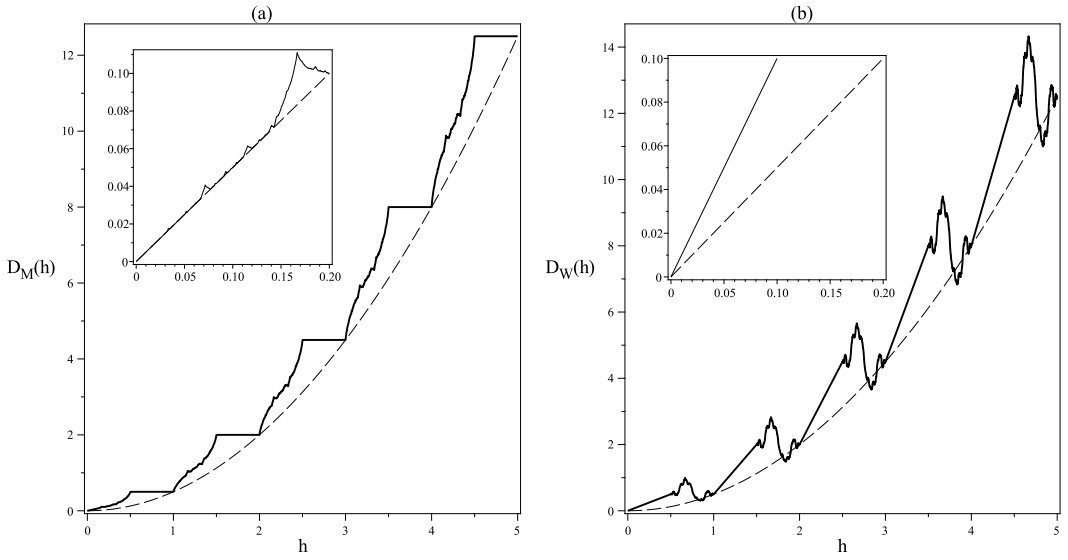

Figure 2.3: *Large scale structure and asymptotic behaviour.* In this figure, the diffusion coefficients for the lifted Bernoulli shift (a) and the lifted negative Bernoulli shift (b) are illustrated. Also included in both is $f(h) = h^2/2$ to show how the function grows for large h. Note the periodicity of the fine scale structure. Inset in both is an illustration of the asymptotic behaviour as $h \to 0$.The dashed lines are $\frac{h}{2}$ to show the different behaviour in the two maps.

and the corresponding expression for the parameter dependent diffusion coefficient is,

$$D_W(h) = \frac{\lfloor h \rfloor^2}{2} + \frac{\hat{h}}{2}\left(\lceil h \rceil^2 - \lfloor h \rfloor^2\right) + T_W(\hat{h}). \tag{2.37}$$

The first two parts of Eq.(2.37) form the same piecewise linear function found in Eq.(2.34) so as $h \to \infty$ we observe the same asymptotic behaviour found in the lifted Bernoulli shift map, see figure 2.3.

The parameter dependent Takagi functions for the lifted tent map and lifted V map are different in character to the two Bernoulli shift maps discussed above. In order to emphasise this difference we restrict the parameter to $h \in [0, 1]$. For the lifted tent map the Takagi function is

$$T_\Lambda(x) = \begin{cases} \frac{1}{2}T_\Lambda(2x+h) - \frac{1}{2}T_\Lambda(h) & 0 \le x < \frac{1-h}{2} \\ x + \frac{1}{2}T_\Lambda(2x+h-1) + \frac{h-1}{2} - \frac{1}{2}T_\Lambda(h) & \frac{1-h}{2} \le x < \frac{1}{2} \\ -\frac{1}{2}T_\Lambda(-2x+2-h) + \frac{h}{2} + \frac{1}{2}T_\Lambda(1-h) & \frac{1}{2} \le x < 1-\frac{h}{2} \\ -x - \frac{1}{2}T_\Lambda(-2x+3-h) + 1 + \frac{1}{2}T_\Lambda(1-h) & 1-\frac{h}{2} \le x < 1 \end{cases} . \tag{2.38}$$

Whilst the Takagi function for the lifted V map is

$$T_V(x) = \begin{cases} x - \frac{1}{2}T_V(-2x+h) + \frac{1}{2}T_V(h) & 0 \le x < \frac{h}{2} \\ -\frac{1}{2}T_V(-2x+1+h) + \frac{h}{2} + \frac{1}{2}T_V(h) & \frac{h}{2} \le x < \frac{1}{2} \\ -x + \frac{1}{2}T_V(2x-h) + \frac{h}{2} + \frac{1}{2} - \frac{1}{2}T_V(1-h) & \frac{1}{2} \le x < \frac{1+h}{2} \\ \frac{1}{2}T_V(2x-1-h) - \frac{1}{2}T_V(1-h) & \frac{1+h}{2} \le x < 1 \end{cases} . \tag{2.39}$$

The important difference is the inclusion of the $T(1-h)$ terms. In Eq.(2.32) and Eq.(2.36) we used the symmetry of the Takagi functions about the point $x = 0.5$ to equate $T(1-h)$ with $T(h)$. The Takagi functions for the lifted V map and lifted tent map do not have this property. We will discuss the consequences of this in subsection 2.2.4.

2.2.4 Evaluating the Takagi functions

In order to analyse the diffusion coefficient, we need to solve the functional equations of the generalised Takagi functions we have defined. We begin with the Takagi functions for the lifted Bernoulli shift map given by Eq.(2.32). The idea is to repeatedly apply the recursion relation from Eq.(2.23) in order to obtain an infinite sum

$$\begin{aligned} T_M(x) &= t_M(x) + \frac{1}{2}T_M(\tilde{M}_h(x)) - \frac{1}{2}T_M(h) \\ &= t_M(x) + \frac{1}{2}t_M(\tilde{M}_h(x)) + \frac{1}{4}T_M(\tilde{M}_h^2(x)) - \frac{1}{2}T_M(h) - \frac{1}{4}T_M(h) \\ &= \sum_{k=0}^{\infty} \frac{1}{2^k} t_M\left(\tilde{M}_h^k(x)\right) - T_M(h), \end{aligned} \tag{2.40}$$

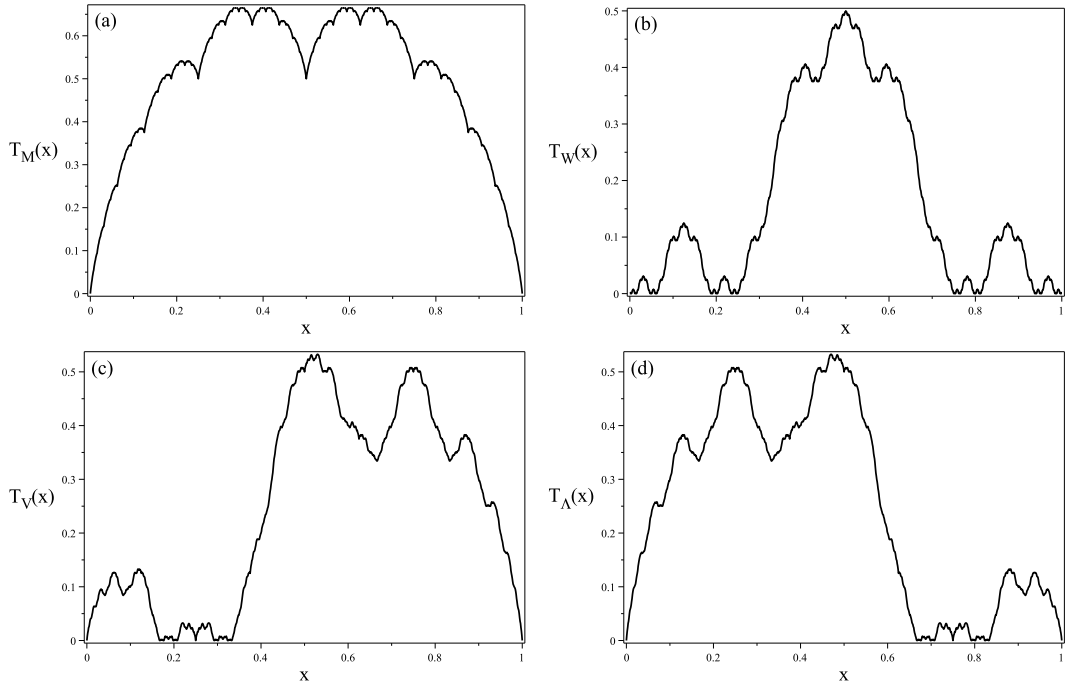

Figure 2.4: *The generalised Takagi functions.* In this figure, the generalised Takagi functions are shown for the four maps at a parameter value of $h = 1$. In **(a)**; the lifted Bernoulli shift, which one may recognise as the famous Takagi function. In **(b)**; the negative Bernoulli shift. In **(c)**; the lifted V map. In **(d)**; the lifted tent map. Note the self similarity and 'fractal' structure. Note also the asymmetry in **(c)** and **(d)** compared to **(a)** and **(b)**, this is due to the asymmetry in the evolution of the p.d.f for these maps. Also portrayed here is $T_V(x) = T_\Lambda(1-x)$, this is due to the symmetry between the two maps.

where explicitly,

$$t_M(x) = \begin{cases} \lfloor h \rfloor \, x & 0 \leq x < \frac{1-\hat{h}}{2} \\ \frac{\hat{h}-1}{2} + \lceil h \rceil \, x & \frac{1-\hat{h}}{2} \leq x < \frac{1}{2} \\ \frac{1+\hat{h}}{2} - \lceil h \rceil \, x & \frac{1}{2} \leq x < \frac{1+\hat{h}}{2} \\ \lfloor h \rfloor - \lfloor h \rfloor \, x & \frac{1+\hat{h}}{2} \leq x \leq 1 \end{cases} . \tag{2.41}$$

Eq.(2.40) can be simplified by removing the $T_M(h)$ term to obtain an infinite sum involving only Eq.(2.41). The first step is to split the $T_M(h)$ term in two

$$T_M(x) = \sum_{k=0}^{\infty} \frac{1}{2^k} t_M\left(\tilde{M}_h^k(x)\right) - \frac{1}{2}\left(T_M(h) + T_M\left(h\right)\right), \tag{2.42}$$

and reapply Eq.(2.40) to one of the halfs to give

$$T_M(x) = \sum_{k=0}^{\infty} \frac{1}{2^k} t_M\left(\tilde{M}_h^k(x)\right) - \frac{1}{2} T_M\left(h\right) - \frac{1}{2}\left(\sum_{k=0}^{\infty} \frac{1}{2^k} t_M\left(\tilde{M}_h^k(h)\right) - T_M(h)\right). \tag{2.43}$$

The $T_M(h)$ terms in Eq.(2.43) now cancel leaving us with

$$T_M(x) = \sum_{k=0}^{\infty} \frac{1}{2^k}\left(t_M\left(\tilde{M}_h^k(x)\right) - \frac{1}{2} t_M\left(\tilde{M}_h^k(h)\right)\right). \tag{2.44}$$

Eq.(2.44) allows us to solve Eq.(2.32) using only Eq.(2.41) which is simple enough to obtain from Eq.(2.17). Taking Eq.(2.34) and Eq.(2.44) into account, we see that we evaluate the diffusion coefficient as a function of the orbit of the point $x = h$. Furthermore we see that the preimages of the point $x = h$ are the critical points of the map $\tilde{M}_h(x)$. So we remark that underpinning this method is kneading theory. That is the study of the orbits of the critical points, called 'kneading orbits' (see for example Devaney [1989] or Katok and Hasselblatt [1995]). In section 2.3 we will look at how to use the kneading orbits, which we will call 'generating orbits' to understand the structure of the diffusion coefficient. In chapter 5 we will look at a method for deriving the diffusion coefficient directly from kneading theory.

The Takagi functions for the lifted negative Bernoulli shift map can be solved in a similar way. We use the same recursive definition to obtain

$$\begin{aligned} T_W(x) &= \sum_{k=0}^{\infty} \left(\frac{-1}{2}\right)^k t_W(x) + \sum_{k=0}^{\infty} \left(\frac{-1}{2}\right)^k T_W(h) \\ &= \sum_{k=0}^{\infty} \left(\frac{-1}{2}\right)^k t_W(x) + \frac{1}{3} T_W(h) \end{aligned} \tag{2.45}$$

where

$$t_W(x) = \begin{cases} \lceil h \rceil x & 0 \le x < \frac{\hat{h}}{2} \\ \frac{\hat{h}}{2}\left(\lceil h \rceil - \lfloor h \rfloor\right) + \lfloor h \rfloor x & \frac{\hat{h}}{2} \le x < \frac{1}{2} \\ \lfloor h \rfloor + \frac{\hat{h}}{2}\left(\lceil h \rceil - \lfloor h \rfloor\right) - \lfloor h \rfloor x & \frac{1}{2} \le x < 1 - \frac{\hat{h}}{2} \\ \lceil h \rceil - \lceil h \rceil x & 1 - \frac{\hat{h}}{2} \le x \le 1 \end{cases} . \tag{2.46}$$

It is again possible to remove $T_W(h)$ to obtain an infinite sum in terms of Eq.(2.46).

$$T_W(x) = \sum_{k=0}^{\infty} \left(\frac{-1}{2}\right)^k \left(t_W\left(\tilde{W}_h^k(x)\right) + \frac{1}{2} t_W\left(\tilde{W}_h^k(h)\right)\right). \tag{2.47}$$

Things are not so simple when we try to evaluate the Takagi functions for the lifted V map and the lifted Tent map. The fact that we have both a positive and a negative gradient in $V_h(x)$ and $\Lambda_h(x)$ makes it harder to simplify the recursion relation into one single sum. If we take the Takagi functions for the lifted V map as an example and let

$$f(x) = \begin{cases} -1 & 0 \le x < \frac{1}{2} \\ 1 & \frac{1}{2} \le x \le 1 \end{cases} , \tag{2.48}$$

$$g(x) = \begin{cases} T_V(h) & 0 \le x < \frac{1}{2} \\ -T_V(1-h) & \frac{1}{2} \le x \le 1 \end{cases} . \tag{2.49}$$

The sum for the Takagi function that we obtain is

$$T_V(x) = t_V(x) + \frac{1}{2} g(x) + \sum_{k=1}^{\infty} \frac{f(\tilde{V}_h^{k-1}(x))}{2^k} \left(t_V(\tilde{V}_h^k(x)) + \frac{1}{2} g(\tilde{V}_h^k(x))\right) \tag{2.50}$$

where

$$t_V(x) = \begin{cases} x & 0 \le x < \frac{h}{2} \\ \frac{h}{2} & \frac{h}{2} \le x < \frac{1}{2} \\ \frac{h+1}{2} - x & \frac{1}{2} \le x < \frac{1+h}{2} \\ 0 & \frac{1+h}{2} \le x \le 1 \end{cases} . \quad 0 \le h \le 1. \tag{2.51}$$

See figure 2.4 for an illustration of a selection of generalised Takagi functions. Note how figure 2.4.(a) reproduces the famous Takagi function (Takagi [1903]). An additional interesting observation is the similarity between the generalised Takagi function in figure 2.4.(b) with that of figure 4.(d) in Gaspard and Klages [1998]. This generalised Takagi function in Gaspard and Klages [1998] is for a different map where the gradient is varied as a parameter. The similarity between the generalised Takagi functions indicates a similarity between the underlying jumping process, despite the microscopic dynamics being different.

2.3 The structure of the diffusion coefficients

In this section the parameter dependent diffusion coefficients for the four maps will be illustrated, and their structure explained.

2.3.1 The lifted Bernoulli shift map

Figure 2.5.(a) gives the diffusion coefficient for the lifted Bernoulli shift map. The two striking features are the fractal region when h is between zero and a half, and the linear plateau when h is between a half and one. These regions will be explained in turn.

2.3.1.1 The fractal region

Firstly, the term 'fractal' has no strict mathematical definition so we use the term loosely. In particular we use it to refer to the fact that the diffusion coefficient exhibits non-trivial fine scale structure, and regions of scaling and self similarity, see figure 2.6. For a discussion of the 'fractality' of diffusion coefficients see for example Klages and Klauß [2003].

The topological instability of the map under parameter variation is reflected in the fractal structure of the diffusion coefficient. So in order to understand the fractality, we need to understand the topological instability. To this end, we take Eq.(2.1) modulo one, and analyse the behaviour of the Markov partitions of the interval map $\tilde{M}_h(x) : [0,1] \to [0,1]$

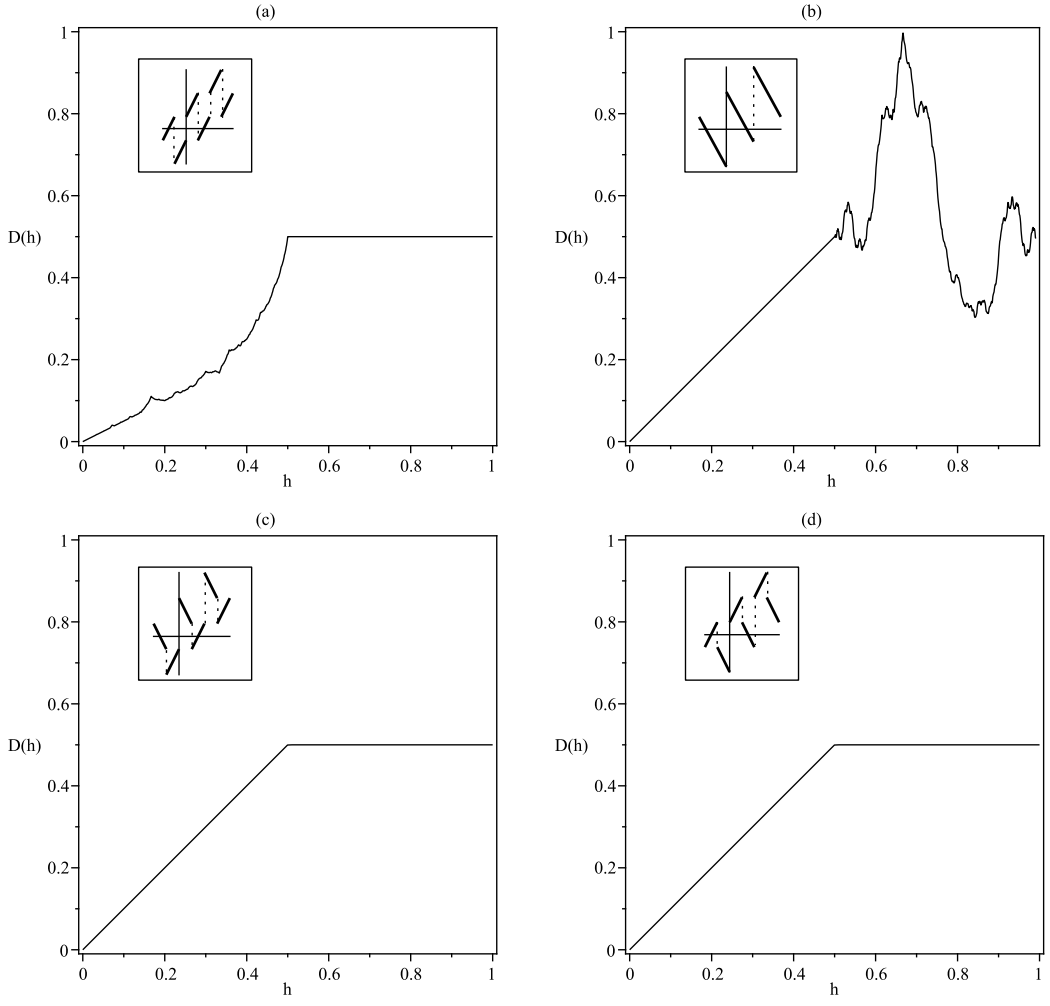

Figure 2.5: *The diffusion coefficients.* In this figure, the parameter dependent diffusion coefficients are illustrated. In **(a)** the lifted Bernoulli shift. In **(b)** the lifted negative Bernoulli shift. In **(c)** the lifted V map. In **(d)** the lifted tent map.

$$\tilde{M}_h(x) = \begin{cases} 2x + \hat{h} & 0 \leq x < \frac{1-\hat{h}}{2} \\ 2x + \hat{h} - 1 & \frac{1-\hat{h}}{2} \leq x < \frac{1}{2} \\ 2x - \hat{h} & \frac{1}{2} \leq x < \frac{1+\hat{h}}{2} \\ 2x - 1 - \hat{h} & \frac{1+\hat{h}}{2} \leq x < 1 \end{cases} . \tag{2.52}$$

The structure of the Markov partitions of (2.52) varies wildly under parameter

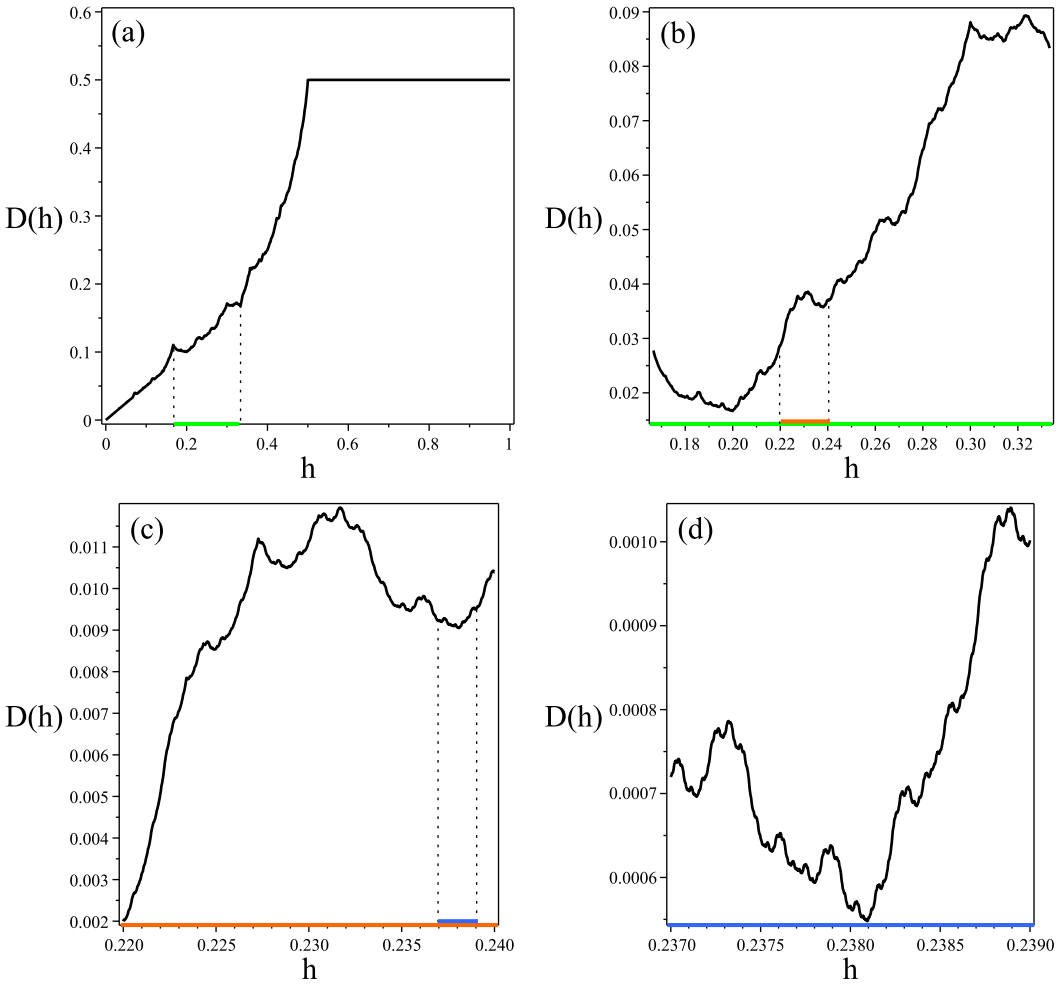

Figure 2.6: *Non-trivial fine-scale structure.* In this figure, certain sections of the parameter dependent diffusion coefficient in the lifted Bernoulli shift map have been enlarged to exhibit the non-trivial fine-scale structure. In **(b)** the highlighted region from **(a)** is illustrated, in **(c)** the highlighted region from **(b)** and in **(d)** the highlighted region from **(c)**.

variation. The method we employ to understand the Markov partitions involves iterating the critical point $x = 0.5$ (Klages [1996]; Klages and Dorfman [1995, 1999]). The set of iterates of this point, along with the set of points symmetric about $x = 0.5$, form a set of Markov partition points for the map. Hence we call the orbit of $x = \frac{1}{2}$ a 'generating orbit'. Furthermore, if the generating orbit is finite for a particular value of h, we obtain a finite Markov partition. We can then use the finite Markov partition to tell us about the diffusive properties of the map and hence the structure of the diffusion coefficient. For this purpose the following proposition is crucial.

Proposition 1 *The set of values of the parameter h which give a finite Markov partition are dense in the parameter space.*

Proof:

We show that when h is rational, the generating orbit is finite. This is achieved by showing that the denominator of h fixes the number of possible iterates of the generating orbit. Let $h = \frac{a}{b}$ where $a, b \in \mathbb{N}$ and $a \leq b$

$$\begin{aligned} \tilde{M}_{\frac{a}{b}}(0.5) &= 1 - h \\ &= \frac{b-a}{b}. \end{aligned} \tag{2.53}$$

Clearly, $b - a \in \{0, 1, 2, ..., b-1\}$. If $\tilde{M}_{\frac{a}{b}}(\frac{b-a}{b})$ is then evaluated, there are four possibilities due to the four branches of (2.52). For all four possibilities

$$\tilde{M}_{\frac{a}{b}}\left(\frac{b-a}{b}\right) = \frac{c}{b}, \quad c \in \{0, 1, 2, ..., b-1\}. \tag{2.54}$$

So for $n = 1$ and $n = 2$

$$\tilde{M}^n_{\frac{a}{b}}(0.5) = \frac{c}{b}, \tag{2.55}$$

with $c \in \{0, 1, 2, ..., b-1\}$. Now we assume that

$$\tilde{M}^m_{\frac{a}{b}}(0.5) = \frac{c}{b}, \tag{2.56}$$

for all $m \leq n$, and the result follows by induction that

$$\tilde{M}^n_{\frac{a}{b}}(0.5) = \frac{c}{b}, \quad c \in \{0, 1, 2, ..., b-1\} \quad \forall n \in \mathbb{N}. \tag{2.57}$$

The result in (2.57) puts a limit on the size of the subset of values that the orbit of $x = 0.5$ can hit at a given rational value of h. This size being equal to $|\{0, \frac{1}{b}, ..., \frac{b-1}{b}\}| = b$. Hence the orbit must be periodic or pre-periodic, and the Markov partition of the map must have a finite number of partition points when h is rational.

q.e.d.

The second important result is that the finite Markov partitions correspond to the local minima and maxima of the diffusion coefficient (Klages [1996]; Klages and Dorfman [1995, 1999]). If we extend our view back to the full maps, we see that if the generating orbit is periodic, i.e.

$$\tilde{M}^n_h(0.5) = 0.5, \quad n \in \mathbb{N}, \tag{2.58}$$

then this corresponds to a relatively high rate of diffusion for the parameter value, which is reflected in the diffusion coefficient as a local maximum. In contrast, if the generating orbit is pre-periodic, this corresponds to a relatively low rate of diffusion for the parameter value, which is reflected in the diffusion coefficient as a local minimum. So given that we have a dense set of local maxima and minima, we observe a fractal diffusion coefficient. Furthermore, Eq.(2.58) furnishes us with the means of pinpointing the local maxima of the diffusion coefficient. In Klages [1996] this technique gave an approximation of where the local extrema were, but this model allows to find them precisely. Each n gives us a set of simple linear equations for the variable h, the solutions of which are the local maxima in the diffusion coefficient. In addition, the smaller values of n give the most striking local maxima. One can apply a similar technique to locate the local minima of the graph, see figure 2.7. However, it's not a case of finding solutions to one simple equation like Eq.(2.58). Rather, there are many ways to define pre-periodic orbits as opposed to defining periodic orbits. In addition, the local

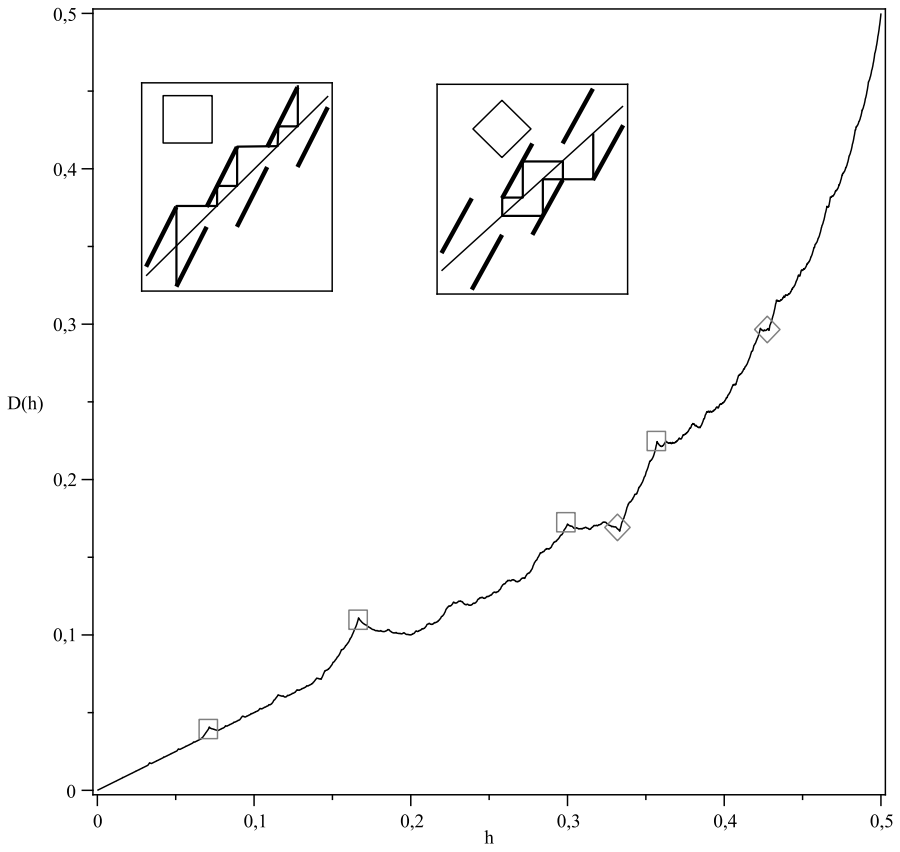

Figure 2.7: *Pinpointing the local extrema.* In this figure, some of the local extrema have been highlighted. At the points highlighted by squares we see the orbit of 0.5 is iterated to infinity resulting in a local maximum. At the points highlighted by diamonds we see the orbit of 0.5 is in a closed loop resulting in a local minimum.

minima do not adhere to such a strict ordering that the local maxima do. This is due to the fact that there are two components to a pre-periodic orbit, namely the transient length and the periodic orbit length. In summary, for h between zero and one half, there exists a dense set of points which correspond to either local maxima or local minima. Hence a fractal structure is observed.

2.3.1.2 The linear region

The second feature of the diffusion coefficient is the linear region where $h \in [0.5, 1]$. Not only is it striking because it very abruptly changes from fractal to

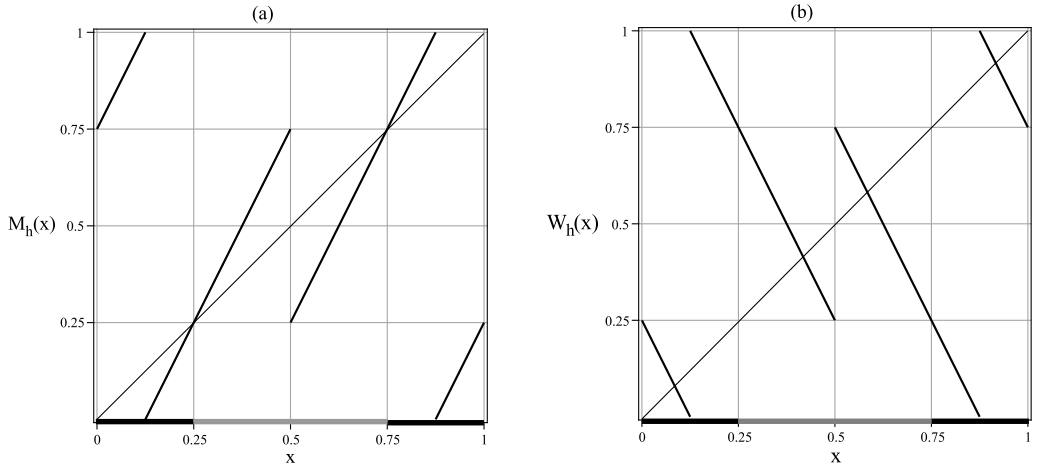

Figure 2.8: *Nonergodicity.* In this figure, the nonergodicity of the lifted Bernoulli shift map at $h = 0.75$ is shown in (a), and in the lifted negative Bernoulli shift at $h = 0.25$ in (b). For simplicity the dynamics have been reduced to the maps modulo 1. One can see that the black areas get mapped into themselves as do the grey areas. This splits up the phase space breaking ergodicity.

linear, it is also counter intuitive if we apply a simple random walk approximation to the map. That is, we can obtain a first order approximation of the diffusion coefficient by looking at the measure of the escape region of the map (the area where a point can move from one unit interval to the next) (Klages [1996]; Klages and Dorfman [1997]). This region clearly increases linearly with the parameter, so based on a first order approximation one would expect to see a general increase in the diffusion coefficient as the parameter increases. However, what is observed defies this. We explain this feature by noting the non-ergodicity of the map in this region.

When the parameter h reaches one half, a fixed point is born in the modulo one map. As the parameter increases further, the fixed point bifurcates and the two resulting fixed points split the phase space into two invariant sets, breaking the ergodicity of the map, see figure 2.8. Consequently, the invariant density $\rho^*(x)$, can be interpreted as the sum of two invariant densities $\rho_1^*(x)$ and $\rho_2^*(x)$ and the diffusion coefficient can be evaluated as

$$
\begin{aligned}
D_M(h) &= \lim_{n\to\infty} \frac{1}{2n} \int_0^1 \rho^*(x)(x_n - x_0)^2 dx \\
&= \lim_{n\to\infty} \frac{1}{2n} \left(\int_0^1 \rho_1^*(x)(x_n - x_0)^2 dx + \int_0^1 \rho_2^*(x)(x_n - x_0)^2 dx \right) \quad (2.59)
\end{aligned}
$$

We can then use the Taylor-Green-Kubo formula and derive two separate generalised Takagi functions, in order to evaluate the diffusion coefficient as

$$
\begin{aligned}
D_M(h) &= (1-h) + (h - \frac{1}{2}) \\
&= \frac{1}{2}. \quad (2.60)
\end{aligned}
$$

2.3.2 The negative Bernoulli shift map

Figure 2.5(b) shows the diffusion coefficient for the lifted negative Bernoulli shift map $W_h(x)$. Firstly we note how radically different the structure of the diffusion coefficient is from the lifted Bernoulli shift map. In addition, as $h \to 0$ the diffusion coefficient does not go to $\frac{h}{2}$ by reproducing the random walk solution as in the lifted Bernoulli shift map. However, as $h \to \infty$ the diffusion coefficient goes to $\frac{h^2}{2}$ as in the lifted Bernoulli shift. We also observe both a linear and a fractal region. For $0 \leq h \leq \frac{1}{2}$ the diffusion coefficient is a simple linear function equal to h. Again, the explanation for this is that the map is non-ergodic in this parameter range, see figure 2.8. The phase space is split up into two invariant regions, one of which does not contribute to diffusion as it is a trapping region, the other of which grows linearly with h so we observe a linear, increasing diffusion coefficient. When $\frac{1}{2} \leq h \leq 1$, the map becomes topologically unstable under parameter variation. Similar to the lifted Bernoulli shift map, this instability is reflected in the behaviour of the Markov partitions of Eq.(2.4) taken modulo one. We have that the finite Markov partitions are dense in the parameter space and that these finite Markov partitions correspond to the local maxima and minima of the diffusion coefficient. Hence we again observe a fractal diffusion coefficient.

2.3.3 The lifted V map

Mercifully, we need not turn to infinite sums like Eq.(2.50) when we evaluate the diffusion coefficient for the lifted V map. The diffusion coefficient for the V-map is given by

$$D_V(h) = \frac{h}{2} + \frac{1}{2}\left(T_V(h) + T_V(1-h)\right), 0 \leq h \leq 1. \tag{2.61}$$

Instead of evaluating the relevant Takagi function, Eq.(2.39), numerically we can use the helpful property that for h less than one half

$$\begin{aligned} T_V(h) &= -\frac{1}{2}T_V(1-h) + \frac{h}{2} + \frac{1}{2}T_V(h) \\ &= -T_V(1-h) + h. \end{aligned} \tag{2.62}$$

Using Eq.(2.62) in Eq.(2.61), the diffusion coefficient can be evaluated to

$$\begin{aligned} D_V(h) &= \frac{h}{2} + \frac{1}{2}\left(-T_V(1-h) + h + T_V(1-h)\right) \\ &= h. \end{aligned} \tag{2.63}$$

Furthermore, for h greater than one half

$$\begin{aligned} T_V(h) &= -h + \frac{1}{2}T_V(h) + \frac{h}{2} + \frac{1}{2} - \frac{1}{2}T_V(1-h) \\ &= -T_V(1-h) - h + 1. \end{aligned} \tag{2.64}$$

Using Eq.(2.64) in Eq.(2.61), the diffusion coefficient can again be evaluated

$$\begin{aligned} D_V(h) &= \frac{h}{2} + \frac{1}{2}\left(-T_V(1-h) - h + 1 + T_V(1-h)\right) \\ &= \frac{1}{2}. \end{aligned} \tag{2.65}$$

See figure 2.5.(c) for an illustration. We will explain this linearity after looking

at the diffusion coefficient for the lifted tent map.

2.3.4 The lifted tent map

For the lifted tent map $\Lambda_h(x)$, we can not perform the same trick with the Takagi functions, Eq.(2.38), that we did with the lifted V map in subsection 2.3.3. However we still do not need to resort to numerical computations to analyse the diffusion coefficient. We note that

$$\Lambda_h(x) = -V_h(-x). \tag{2.66}$$

Eq.(2.66) is important because it serves as a topological conjugacy of the form $f(x) = -x$. By using the Taylor-Green-Kubo formula Eq.(2.16) it was shown in Korabel and Klages [2004] that the diffusion coefficient is preserved under topological conjugacy, hence we observe an identical diffusion coefficient in the two maps which can be seen in figure 2.5. We can see why this is the case with this example by looking at Einstein's formula Eq.(2.6) to prove the following proposition:

Proposition 2 *The diffusion coefficients for the lifted tent map is identical to that of the lifted V map.*

Proof:

We note that the diffusion coefficient for the lifted V map is given by

$$D_V(h) = \lim_{n\to\infty} \frac{\left\langle (V_h^n(x_0) - x_0)^2 \right\rangle}{2n}, \tag{2.67}$$

and that the diffusion coefficient for the tent map ($D_\Lambda(h)$) can be given by

$$D_\Lambda(h) = \lim_{n\to\infty} \frac{\left\langle (\Lambda_h^n(-x_0) - (-x_0))^2 \right\rangle}{2n}, \tag{2.68}$$

where the p.d.f is in the interval, $[-1, 1]$ to make it symmetric about $x = 0$. By substituting (2.66) into (2.68)

$$D_\Lambda(h) = \lim_{n\to\infty} \frac{\left\langle (\Lambda_h^n(-x_0) - (-x_0))^2 \right\rangle}{2n}$$

$$
\begin{aligned}
&= \lim_{n\to\infty} \frac{\left\langle (-V_h^n(x_0) - (-x_0))^2 \right\rangle}{2n} \\
&= \lim_{n\to\infty} \frac{\left\langle (V_h^n(x_0) - x_0)^2 \right\rangle}{2n} \\
&= D_V(h). \qquad (2.69)
\end{aligned}
$$

we arrive at the desired relationship that $D_\Lambda(h) = D_V(h)$.

q.e.d.

From what we have seen in the lifted Bernoulli shift map and the lifted negative Bernoulli shift map, we would expect to find non-ergodicity in the lifted tent and lifted V maps. Furthermore we would expect to find it across the entire parameter range given the linear diffusion coefficients. However, there is no obvious non-ergodicity, and although a proof that the maps are ergodic across the entire parameter range remains elusive, we can check for ergodicity at individual values of the parameter by checking the reducibility of the transition matrices (Petersen [1983]). So we can confirm ergodicity for some values of h. Furthermore, the behaviour under parameter variation of the Markov partitions of the maps Eq.(2.4) and Eq.(2.5) taken modulo one indicate the presence of topological instability in the parameter space. So, although all the 'ingredients' for a fractal diffusion coefficient are present, we observe a linear one.

2.3.5 The dominating branch effect

In order to understand the linearity of the diffusion coefficient of the lifted V map (and hence the lifted tent map also), we first note the similarity of the linear regions in the diffusion coefficients of the two lifted Bernoulli shift maps, see figure 2.5. This presents the question, why do these maps have the same diffusion coefficients when they have such different microscopic dynamics?

We will explain the linearity of the diffusion coefficients of the lifted tent and lifted V map by showing why they have the same diffusion coefficients as the two Bernoulli shift maps in the relevant parameter ranges. We will take these ranges in turn starting with $0.5 \leq h \leq 1$. The diffusion coefficient for the lifted Bernoulli

shift map is given by Eq.(2.34) which for $h \in [0.5, 1]$ simplifies to

$$D_M(h) = \frac{h}{2} + T_M(h) \tag{2.70}$$

which using Eq.(2.44)can be rewritten as

$$D_M(h) = \frac{h}{2} + \sum_{k=0}^{\infty} \frac{1}{2^k} \left(t_M \left(\tilde{M}_h^k(h) \right) - \frac{1}{2} t_M \left(\tilde{M}_h^k(h) \right) \right). \tag{2.71}$$

Now using $\tilde{M}_h(h) = h$ for $h \in [0.5, 1]$ we can simplify Eq.(2.71) to

$$D_M(h) = \frac{h}{2} + \sum_{k=0}^{\infty} \frac{1}{2^k} \left(t_M (h) - \frac{1}{2} t_M (h) \right). \tag{2.72}$$

Which implies that our diffusion coefficient in this region is equal to

$$D_M(h) = \frac{h}{2} + \sum_{k=0}^{\infty} \frac{1}{2^{k+1}} \left(t_M(h) \right). \tag{2.73}$$

Now, keeping Eq.(2.73) in mind, we turn our attention to the lifted V map. The diffusion coefficient for the lifted V map with $h \in [0, 1]$ is given by Eq.(2.61). From Eq.(2.39) we can derive the useful recursion relation

$$T_V(h) = t_V(h) + \frac{1}{2} T_V(h) - \frac{1}{2} T_V(1 - h), \tag{2.74}$$

which if we repeatedly apply leads to

$$T_V(h) = \sum_{k=0}^{\infty} \frac{1}{2^k} t_V(h) - \sum_{k=0}^{\infty} \frac{1}{2^{k+1}} T_V(1 - h). \tag{2.75}$$

Substituting Eq.(2.75) into Eq.(2.61) the diffusion coefficient is given by

$$D_V(h) = \frac{h}{2} + \frac{1}{2} \left(\sum_{k=0}^{\infty} \frac{t_V(h)}{2^k} + T_V(1 - h) - \sum_{k=0}^{\infty} \frac{T_V(1 - h)}{2^{k+1}} \right). \tag{2.76}$$

We can see from Eq.(2.41) and Eq.(2.51) that $t_M(h) = t_V(h)$ when $h \in [0.5, 1]$ and hence the two diffusion coefficients are equal despite $M_h(x)$ being non-ergodic and $V_h(x)$ ergodic in this parameter range. However Eq.(2.76) and Eq.(2.73) tell

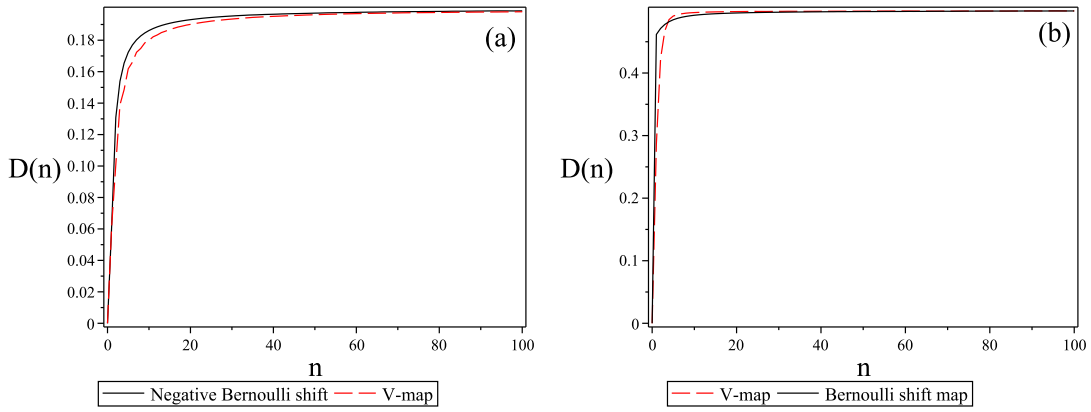

Figure 2.9: *The time dependent diffusion coefficients.* In this figure we see how the diffusion coefficient converges as n increases for certain parameter values. In (a) $h = 0.2$ for the lifted negative Bernoulli shift map and the lifted V map, in (b) $h = 0.7$ for the lifted Bernoulli shift map and the V map. We see that the diffusion coefficients tend to the same value but at different rates, indicating that the difference in the microscopic dynamics does not play a role in the limit. Rather we observe a dominating branch process where the common branch of the map determines the diffusion coefficient.

us that $D_M(h)$ and $D_V(h)$ converge at different rates, see figure (2.9) for an illustration of this phenomenon, and are hence only equal in the limit $n \to \infty$. We also note that in the limit the diffusion coefficient is only dependent on $t_M(h)$ or $t_V(h)$ and that these functions are only dependent on the branch of the map in $[0.5, 1]$, That is the microscopic effects of the other branch of the map in$[0, 0.5]$ cancel out in the limit and play no role in the final diffusion coefficient. We interpret this phenomenon physically as the diffusion undergoing a dominating branch process, i.e. the diffusion coefficient is only dependent on the contribution of one branch of the map in the limit as $n \to \infty$. Hence we see identical diffusion coefficients despite the different microscopic dynamics.

We find a similar situation for $h \in [0, 0.5]$, where the lifted negative Bernoulli shift map and the lifted V map have the same diffusion coefficient. They have the branch in $[0, 0.5]$ in common in this parameter range and it is this which creates the dominating branch process. Hence we also observe identical diffusion coefficients between these two maps in this parameter range.

2.3.6 Stability of the diffusion coefficient in the non-ergodic regions

In this subsection we look at the two lifted Bernoulli shift maps in the non-ergodic regions. We have already seen that changing the gradient of one branch of the map (resulting in the lifted V map or lifted tent map) has no effect on the diffusion coefficient in these regions, even though the microscopic dynamics are affected greatly. We will explore this phenomenon further.

For $h \in [0, 0.5]$ the lifted negative Bernoulli shift map has a linear diffusion coefficient. By changing the gradient and 'chopping up' the second branch of the map we obtain a map $\hat{W}_h(x) : [0, 1] \to \mathbb{R}$

$$\hat{W}_h(x) = \begin{cases} -2x + 1 + h & 0 \leq x < \frac{1}{2} \\ 2x - 1 & \frac{1}{2} \leq x \leq 1 - \frac{h}{2} \\ 2x - 2 & 1 - \frac{h}{2} \leq x < 1 \end{cases} . \tag{2.77}$$

The Takagi function for this map with $h \in [0, 1]$ is

$$T_{\hat{W}}(x) = \begin{cases} -\frac{1}{2}T_{\hat{W}}(-2x + h) + x + \frac{1}{2}T_{\hat{W}}(h) & 0 \leq x < \frac{h}{2} \\ -\frac{1}{2}T_{\hat{W}}(-2x + 1 + h) + \frac{h}{2} + \frac{1}{2}T_{\hat{W}}(h) & \frac{h}{2} \leq x < \frac{1}{2} \\ \frac{1}{2}T_{\hat{W}}(2x - 1) + \frac{h}{2} & \frac{1}{2} \leq x < 1 - \frac{h}{2} \\ \frac{1}{2}T_{\hat{W}}(2x - 1) + 1 - x & 1 - \frac{h}{2} \leq x < 1 \end{cases} \tag{2.78}$$

and the diffusion coefficient can be evaluated as

$$D_{\hat{W}}(h) = \frac{h}{2} + \frac{1}{2}\left(T_{\hat{W}}(h) + T_{\hat{W}}(1 - h)\right), 0 \leq h \leq 1. \tag{2.79}$$

Again for $h \in [0, 0.5]$ we have that

$$T_{\hat{W}}(h) = -T_{\hat{W}}(1 - h) + h. \tag{2.80}$$

which implies that for $h \in [0, 0.5]$ the diffusion coefficient is equal to h.

We can play a similar game with the lifted Bernoulli shift map which has a linear diffusion coefficient for $h \in [0.5, 1]$. We can change the gradient and chop up the first branch of the map to create $\hat{M}_h(x) : [0, 1] \to \mathbb{R}$

$$\hat{M}_h(x) = \begin{cases} -2x+1 & 0 \le x < \frac{1-h}{2} \\ -2x+2 & \frac{1-h}{2} \le x \le \frac{1}{2} \\ 2x-1-h & \frac{1}{2} \le x < 1 \end{cases} . \tag{2.81}$$

The Takagi function for this map with $h \in [0,1]$ is

$$T_{\hat{M}}(x) = \begin{cases} -\frac{1}{2}T_{\hat{M}}(-2x+1) & 0 \le x < \frac{1-h}{2} \\ -\frac{1}{2}T_{\hat{M}}(-2x+1) + x - \frac{1-h}{2} & \frac{1-h}{2} \le x < \frac{1}{2} \\ \frac{1}{2}T_{\hat{M}}(2x-h) - x + \frac{1+h}{2} - \frac{1}{2}T_{\hat{M}}(1-h) & \frac{1}{2} \le x < \frac{1+h}{2} \\ \frac{1}{2}T_{\hat{M}}(2x-1-h) - \frac{1}{2}T_{\hat{M}}(1-h) & \frac{1+h}{2} \le x < 1 \end{cases} \tag{2.82}$$

and the diffusion coefficient for this map is

$$D_{\hat{M}}(h) = \frac{h}{2} + \frac{1}{2}\left(T_{\hat{M}}(h) + T_{\hat{M}}(1-h)\right), 0 \le h \le 1. \tag{2.83}$$

We see that for $h \in [0.5, 1]$ we have

$$T_{\hat{M}}(h) = -T_{\hat{M}}(1-h) - h + 1 \tag{2.84}$$

which implies that for $h \in [0.5, 1]$ the diffusion coefficient is equal to 0.5.

So we have again seen that the diffusion coefficients for these maps are very stable in the relevant parameter ranges, i.e. the ranges where the maps are non-ergodic. This allows to conjecture that the diffusion coefficient in these parameter ranges is robust to changes that in the microscopic dynamics that leave the invariant density a constant function, despite the reintroduction of ergodicity.

2.4 Diffusion on the cylinder

In this section we will attempt to apply the functional recursion relation method used above to the pseudo-two-dimensional sawtooth map. We will see that the method fails to give the diffusion coefficient for all but a particular set of parameter values. We resort to numerical analysis to study the diffusion coefficient which gives evidence for a fractal structure.

2.4.1 The sawtooth map

We move away from simple maps on the real line and consider an area preserving, two-dimensional, Hamiltonian system called the 'sawtooth' map (Dana et al. [1989]), whose phase space X is the cylinder,

$$X = \{x, y \in \mathbb{R} : -0.5 \leq x < 0.5, -\infty < y < \infty\}, \tag{2.85}$$

where the lines $x = 0.5$ and $x = -0.5$ are identified. The sawtooth map moves points on the x axis according to

$$x_{n+1} = x_n + y_{n+1}, \tag{2.86}$$

modulo the interval $[-0.5, 0.5]$, where

$$y_{n+1} = y_n + Kx_n, \tag{2.87}$$

where $K \in \mathbb{R}$ is our control parameter and $n \in \mathbb{N}$ gives the discrete time steps where the lines $x = 0.5$ and $x = -0.5$ are identified. As the phase space is a cylinder, diffusion only occurs along the y axis. That is in this setting we only have diffusion in one-dimension. We can rewrite the dynamics for the sawtooth map as the matrix equation,

$$\Gamma_K \begin{pmatrix} x \\ y \end{pmatrix} = \begin{pmatrix} (K+1) & 1 \\ K & 1 \end{pmatrix} \begin{pmatrix} x \\ y \end{pmatrix}. \tag{2.88}$$

We see that when K is an integer we have a family of 'cat-maps' (Arnold and Avez [1968]).

2.4.2 The diffusion coefficient

As the density of points diffuses along the cylinder in one-dimension, the diffusion coefficient for the sawtooth map is given by Einstein's equation which in this setting is

$$D = \lim_{n\to\infty} \frac{\langle (y_n - y_0)^2 \rangle}{2n} \tag{2.89}$$

where

$$< ... >= \int_{-0.5}^{0.5} \int_{0}^{1} ...\rho^*(x,y)dydx \tag{2.90}$$

is an integral over the invariant density of initial conditions $\rho^*(x,y)$ located in the unit square $A = [-0.5, 0.5] \times [0, 1]$. The invariant density $\rho^*(x,y)$ is simply equal to 1.

We will attempt to evaluate the Taylor-Green-Kubo formula in order to derive the diffusion coefficient, which is given by

$$D = \lim_{n\to\infty} \left(\int \int_A v_0(x,y) J^n(x,y) dydx \right) - \frac{1}{2} \int \int_A v_0^2(x,y) dydx. \tag{2.91}$$

where the velocity function is given by

$$\begin{aligned} v_n(x,y) &= y_{n+1} - y_n \\ &= (Kx_n + y_n) - y_n \\ &= Kx_n, \end{aligned} \tag{2.92}$$

and the jump function by

$$\begin{aligned} J^n(x,y) &= \sum_{i=0}^{n} v_i(x,y) \\ &= v_0(x,y) + J^{n-1}(\tilde{\Gamma}_K(x,y)), \end{aligned} \tag{2.93}$$

with $\tilde{\Gamma}_K(x,y)$ equal to $\Gamma_K(x,y)$ taken modulo the initial unit square A. We can define generalised Takagi functions as

$$\begin{aligned} T^n(x,y) &= \int_0^y \int_{-0.5}^x J^n(s,t) dsdt \\ &= \int_0^y \int_{-0.5}^x Ksdsdt + \int_0^y \int_{-0.5}^x J^{n-1}(\tilde{\Gamma}_K(s,t)) dsdt. \end{aligned} \tag{2.94}$$

At this stage we would like to be able to rewrite the second integral in Eq.(2.94) in terms of $T^{n-1}(x,y)$, that is derive a recurrence relation for $T(x,y)$. However, we see that this is not possible if we rewrite the integral as

$$\int_0^y \int_0^x J^{n-1}(\tilde{\Gamma}_K(s,t)) = \int \int_{\tilde{\Gamma}_K(a)} J^{n-1}(s,t) ds dt, \tag{2.95}$$

where the integral is taken over the iteration under $\tilde{\Gamma}_K(x,y)$ of the square $a = [0,x] \times [0,y]$. As the sawtooth map is non-conformal, that is it does not preserve angles, this integral is not taken over a simple square, so there is no way to define a useable recurrence relation, as is possible in one dimension.

As we can not derive the diffusion coefficient analytically, we resort to a numerical investigation of the Taylor-Green-Kubo formula, Eq.(2.91). Rather than consider taking the limit $n \to \infty$, we can truncate this formula at a given value of n and define a 'time-dependent' diffusion coefficient.

$$D^n(K) = \int \int_A v_0(x,y) J^n(x,y) dy dx - \frac{1}{2} \int \int_A v_0^2(x,y) dy dx. \tag{2.96}$$

Then, starting from the zeroth order term $D^0(K)$, we can systematically add correlations into the system and observe how the structure of the diffusion coefficient builds up. The leading order term can be simply evaluated as,

$$D^0(K) = \frac{K^2}{24}, \tag{2.97}$$

which is exact at the integer values of K. See figure 2.10.(a) for an illustration of the parameter dependent diffusion coefficient. In this figure the diffusion coefficient appears to be a smooth function, which is the conclusion hinted at in Sano [2002]. However, if we remove the leading order term given by Eq.(2.97) we see that the picture is not so clear as there appears to be non-trivial fine-scale structure which gives evidence for a possible fractal structure. As we increase n, we see that $D^n(K)$ becomes an increasingly complex function as the higher-order correlations are added. See figures 2.10.(b), 2.10.(c) and 2.10.(d) for an illustration. However, the situation may be more subtle, it could also be the case that the diffusion coefficient lies between the 'fractals' that we saw in the one

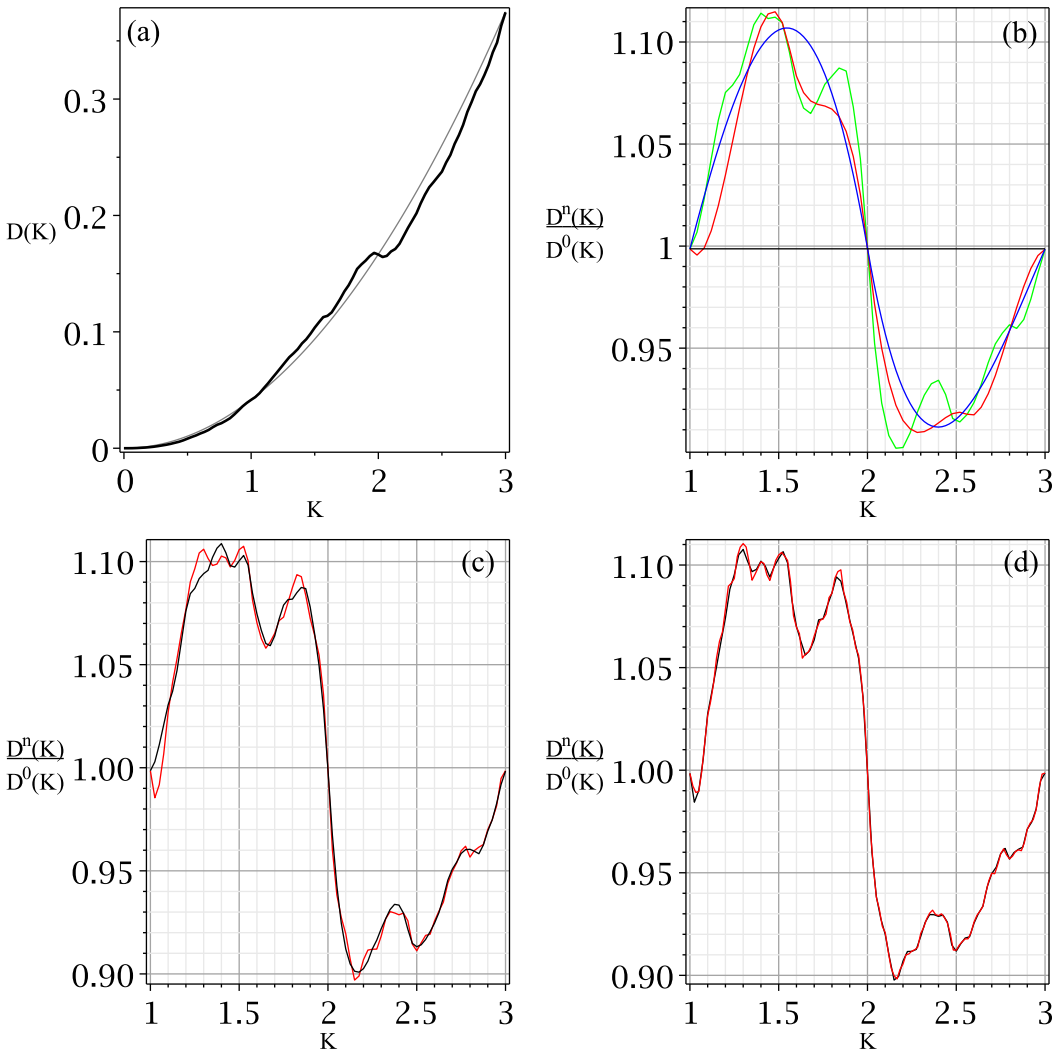

Figure 2.10: *Diffusion in the sawtooth map.* In figure **(a)** the numerically obtained diffusion coefficient for the sawtooth map as a function of the parameter K is illustrated for $0 \leq K \leq 3$ (thick black line) along with the leading order term $K^2/24$ (thin grey line). In figures **(b)**, **(c)** and **(d)** the 'time-dependent' diffusion coefficient $D^n(K)$, obtained from numerical evaluation of the Taylor-Green-Kubo formula, is illustrated after being normalised by dividing out the leading order term $D^0(K)$. In **(b)**, $D^n(K)$ is illustrated for $n = 0, 2, 3$ and 4 in black, blue, red and green respectively. $n = 1$ is not visible. In **(c)** $n = 5$ and 6 in black and red respectively. In **(d)** $n = 7$ and 8 in black and red respectively. Although the diffusion coefficient appears smooth in **(a)**, the increasingly complex functions that we observe in **(b)**, **(c)** and **(d)** suggest a potential fractal structure.

dimensional case and simple smooth functions. Investigations into diffusion in Hamiltonian particle billiards have led to conjectures of C^1 but not C^2 behaviour (Klages [2007]; Klages and Dellago [2000]) which fit in with what we observe in the sawtooth map.

2.5 Conclusion

In this chapter we studied four parameter-dependent, piecewise-linear, chaotic maps of the real line. We derived precise analytical expressions for the diffusion coefficients of these systems as a function of the parameter. These analytic expressions were derived via the Taylor-Green-Kubo formula which we solved using generalised fractal Takagi functions. The recursive solutions to these generalised Takagi functions allowed us to simply compute the diffusion coefficient to arbitrary precision. We also looked at the two-dimensional sawtooth map and numerically investigated the diffusion coefficient. This numerical investigation gave evidence for a fractal structure via a systematic inclusion of higher-order correlations, which produced an increasingly complex parameter dependent diffusion coefficient.

Under parameter variation we observed a curious mixture of fractal and linear behaviour in the diffusion coefficients across the family of one-dimensional maps. The fractality was explained in terms of the topological instability of the maps under parameter variation and this was understood by analysing the Markov partitions of the map. The linearity was explained in terms of the non-ergodicity of the maps in certain parameter ranges, which splits the phase space up into two separate ergodic components, each with their own diffusion coefficient. These individual diffusion coefficients complement each other to create a linear diffusion coefficient. We also observed linear diffusion coefficients despite all the hallmarks of the dynamics for generating fractality being present. In this case we found that in the relevant parameter ranges, the ergodic maps have a set of branches in common with the non-ergodic maps which dominate the diffusion process in the long time limit, hence we observe identical diffusion coefficients. Based on the study of a variety of models, in previous literature it was conjectured that sufficiently low-dimensional deterministically chaotic dynamical systems generating transport on

periodic lattices would typically exhibit irregular or fractal transport coefficients (Klages [1996, 2007]; Klages and Dorfman [1999]). Typicality does not exclude that there exist specific counterexamples. Here we have identified a non-trivial dynamical mechanism leading to piecewise linearity, despite the maps fulfilling these assumptions and even the fact that the dynamics are topologically unstable and ergodic under parameter variation. This also contradicts the intuition that a linear diffusion coefficient would imply that the corresponding dynamical system is topologically stable. The moral of this story is that if one observes a fractal diffusion coefficient, this phenomenon can be explained in terms of the topological instability of the dynamics under parameter variation. However, the converse is not necessarily true; if one observes topological instability of the dynamics under parameter variation, this does not necessarily imply the presence of a fractal diffusion coefficient.

So far this mechanism has only been confirmed for two piecewise linear maps whose microscopic symmetry is broken, which seems to be intimately associated with the existence of a dominating branch. An interesting open question is finding out under exactly which conditions we can manipulate the microscopic dynamics of such maps and still observe identical diffusion coefficients, that is to explore how strong the dominating branch process is. It would also be interesting to know whether there exist any more physically realistic, possibly higher-dimensional systems which display this dominating branch phenomenon. Also of interest is the consequences of introducing a bias into the system generating a current. It would be worthwhile to study whether analogous phenomena exist for this other transport property and whether they can be revealed by similar techniques. In addition, the true nature of the structure of the parameter dependent diffusion coefficient in the sawtooth map remains an open question. Answering this question will require the development of new, more powerful analytic techniques. We will discuss one possible line of enquiry in this direction in chapter 5.

Chapter 3

Capturing correlations

We investigate three different methods for systematically approximating the diffusion coefficient of a deterministic random walk on the line which contains dynamical correlations that change irregularly under parameter variation. Capturing these correlations by incorporating higher order terms, all schemes converge to the analytically exact result. Two of these methods are based on expanding the Taylor-Green-Kubo formula for diffusion, whilst the third method approximates Markov partitions and transition matrices by using the escape rate theory of chaotic diffusion. We check the practicability of the different methods by working them out analytically and numerically for a simple one-dimensional map, study their convergence and critically discuss their usefulness in identifying a possible fractal instability of parameter-dependent diffusion, in case of dynamics where exact results for the diffusion coefficient are not available.

3.1 Introduction

Diffusion is a fundamental macroscopic transport process in many-particle systems. It is quantifiable by the diffusion coefficient, which describes the linear growth in the mean-squared displacement of an ensemble of particles. The source of this growth is often considered to be a Brownian or random process of collisions between particles. However, on a microscopic scale the equations governing these collisions in physical systems are deterministic and typically chaotic. By studying

diffusion in chaotic dynamical systems we can attempt to take these deterministic rules into account and understand the phenomenon of diffusion from first principles (Cvitanović et al. [2010]; Dorfman [1999]; Gaspard [1998]; Klages [2007]). Of particular interest is the study of the diffusion coefficient under parameter variation in chaotic dynamical systems such as one-dimensional maps (Fujisaka and Grossmann [1982]; Geisel and Nierwetberg [1982]; Korabel and Klages [2004]; Schell et al. [1982]), area preserving two dimensional maps (Cary and Meiss [1981]; Rechester and White [1980]; Venegeroles [2007]) and particle billiards (Harayama and Gaspard [2001]; Harayama et al. [2002]; Machta and Zwanzig [1983]; Mátyás and Klages [2004]). Where exact analytical results for chaotic dynamical systems exist (Cristadoro [2006]; Groeneveld and Klages [2002]; Klages [1996]; Klages and Dorfman [1995, 1999]; Knight and Klages [2011b]) one finds that the diffusion coefficient is typically a complicated fractal function of control parameters. This phenomenon can be understood as a topological instability of the deterministic diffusive dynamics under parameter variation (Klages [1996, 2007]; Klages and Dorfman [1995, 1999]).

So far exact analytical solutions for the diffusion coefficient could only be derived for simple cases of low-dimensional dynamics. In higher dimensions even very fundamental properties of diffusion coefficients are often unknown, such as whether they are smooth or fractal functions of control parameters (Harayama and Gaspard [2001]; Jepps and Rondoni [2006]; Klages [2007]). For example, much effort was spent two decades ago studying more complicated systems like the two-dimensional sawtooth map (Cary and Meiss [1981]; Dana et al. [1989]; Eckhardt [1993]). However, despite a good understanding of the orbit structure (Percival and Vivaldi [1987a,b]) it was not possible to conclude whether the diffusion coefficient is fractal or not (Sano [2002]). If one wishes to achieve a microscopic understanding of diffusion in more realistic physical systems, one therefore has to rely either on numerical simulations or on approximation methods. We saw in chapter 2 how an analytical method which is very powerful in one dimension failed to yield the analytic diffusion coefficient of the sawtooth maps, in this case we resorted to a systematic approximation procedure to obtain evidence for a fractal structure.

In this chapter we compare three different methods for approximating pa-

rameter dependent diffusion coefficients with each other by working them out analytically and numerically for a simple one-dimensional map. This model has the big advantage that it is very amenable to rigorous analysis. Its diffusion coefficient has been calculated exactly in chapter 2 and in Knight and Klages [2011b] and was found to be a fractal function of a control parameter. Our goal is to assess the individual capabilities and limitations of these approximation methods in terms of practicability, physical interpretation, convergence towards the exact result, and identification of an underlying fractal structure in the diffusion coefficient.

In section 3.2 we define the deterministic dynamical system that provides our test case, which is a simple piecewise linear one-dimensional map. In section 3.3 the first approximation method is introduced, called correlated random walk in Klages and Korabel [2002], which consists of truncating the Taylor-Green-Kubo formula for diffusion. This method enables us to analytically build up a series of approximations which gives evidence for a fractal structure. In previous work this approximation scheme has successfully been applied to understand parameter dependent diffusion in models that are much more complicated than the one considered here (Harayama et al. [2002]; Klages [2007]; Korabel and Klages [2004]; Mátyás and Klages [2004]). Motivated by the criticism of this method in Gilbert and Sanders [2009] (see Klages and Knight [2011] for a discussion of this criticism), in this paper we provide further insight into the functioning of this method by working it out rigorously for our specific example. In section 3.4 the persistent random walk method for diffusion is studied (Haus and Kehr [1987]; Weiss [1994]). Persistence effects in diffusion were first developed within stochastic theory as a generalisation of simple Brownian motion in Fürth [1920] and in hydrodynamics Taylor [1922]. The physical motivation is that after performing one 'jump' a particle may have some momentum which means it is more likely to continue in the same direction. Alternatively, in particle diffusion in lattice structures like metals (Bardeen and Herring [1952]), a particle will leave a lattice space vacant behind it after jumping, meaning it is more likely to jump back. In both cases this leads to correlations between jumps. The method consists of approximating the Taylor-Green-Kubo formula by including memory in a self-consistent, persistent way. Recently this method has been worked out for chaotic diffusion

in Hamiltonian particle billiards (Gilbert and Sanders [2009, 2010]; Gilbert et al. [2011]). Here we apply this scheme to the different case of a one-dimensional map, and we obtain a series of approximations analytically and then numerically. In section 3.5 we look at a third method, defined within the framework of the escape rate theory of chaotic diffusion (Dorfman [1999]; Gaspard [1998]; Gaspard and Dorfman [1995]; Gaspard and Nicolis [1990]; Klages and Dorfman [1995, 1999]). It consists of evaluating the diffusion coefficient in terms of the decay rate of the dynamical system. The decay rate is in turn obtained by an approximation to the relevant Markov transition matrix. By this method we are able to build up a series of approximations which, through the functional form of the interpolation that we find, gives very strong evidence for fractality. Basic ideas defining this method have been sketched in Klages [2007], however, this is the first time that it has been fully worked out to understand fractal diffusion coefficients. Section 2.5 forms the conclusion. This work was performed in collaboration with Dr Rainer Klages of Queen Mary University of London and was published in Knight and Klages [2011a].

3.2 A one-dimensional map exhibiting chaotic diffusion

We use the simplest setting possible, where deterministic diffusion is generated by a parameter dependent one-dimensional dynamical system. The equations of motion are determined by a map $M_h(x) : \mathbb{R} \to \mathbb{R}$ so that

$$\begin{aligned} x_{n+1} &= M_h(x_n) \\ &= M_h^{n+1}(x) \quad x \in \mathbb{R}, h \geq 0, n \in \mathbb{N}, \end{aligned} \tag{3.1}$$

with $x = x_0$ (Fujisaka and Grossmann [1982]; Geisel and Nierwetberg [1982]; Klages and Dorfman [1995]; Schell et al. [1982]). In our case, the map $M_h(x)$ is based on the *Bernoulli shift* or *doubling map*, combined with a lift parameter h,

which gives the simple parameter dependent map of the interval

$$M_h(x) = \begin{cases} 2x + h & 0 \leq x < \frac{1}{2} \\ 2x - 1 - h & \frac{1}{2} \leq x < 1 \end{cases} . \tag{3.2}$$

This map exhibits 'escape', i.e., points leave the unit interval under iteration. It is copied and lifted over the real line by

$$M_h(x + z) = M_h(x) + z, \quad z \in \mathbb{Z} \tag{3.3}$$

in order to obtain a map from the real line to itself, see figure 3.1(a). The symmetry in this system ensures that there is no mean drift (Groeneveld and Klages [2002]). Note that the invariant density of the map Eq.(3.2) modulo one remains by construction simply uniform throughout the whole parameter range. This is in contrast to the related piecewise linear maps studied in Klages [1996, 2007]; Klages and Dorfman [1995, 1999], where the density becomes a highly complicated step function under parameter variation, which profoundly simplifies the situation. The model was first introduced in Gaspard and Klages [1998], where its parameter dependent diffusion coefficient $D(h)$ was obtained numerically, while in Dorfman [1999]; Gaspard [1992] the diffusion coefficient for a special single parameter value was calculated analytically. Exact analytical solutions for $D(h)$ for all $h \geq 0$ of this and related models were derived in chapter 2 and in Knight and Klages [2011b]. Since there is a periodicity with integer values of h, here we restrict ourselves to the parameter regime of $h \in [0, 1]$ without loss of generality. In Gaspard and Klages [1998]; Knight and Klages [2011b] and chapter 2 it was found that $D(h)$ displays both fractal and linear behaviour, see figure 3.1.(b). This is one of the simplest models that exhibits a fractal diffusion coefficient. Being nevertheless amenable to rigorous analysis, it thus forms a convenient starting point to learn about the power of different approximation methods for understanding complicated diffusion coefficients.

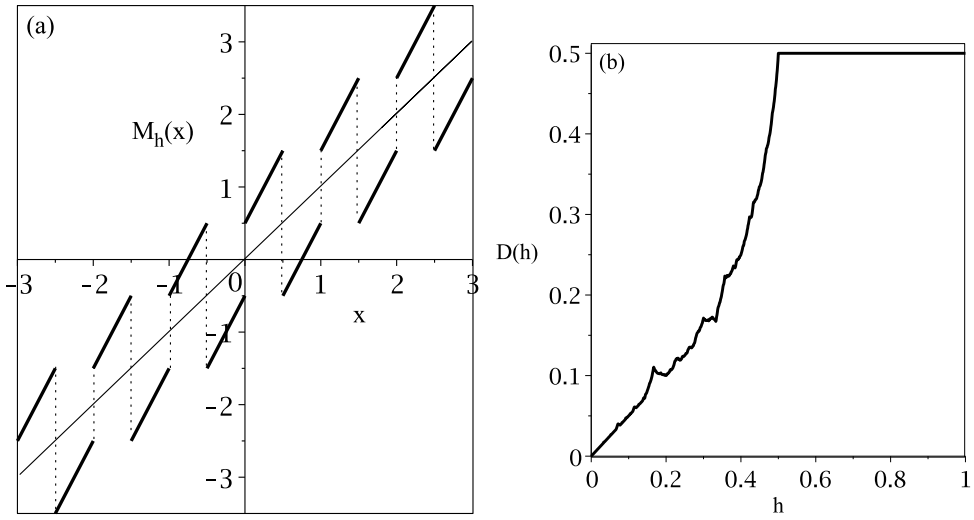

Figure 3.1: *The lifted Bernoulli shift map.* A section of the map $M_h(x)$, Eq.(3.2) and Eq.(3.3), is illustrated in **(a)** for the value of the control parameter $h = 0.5$. The corresponding parameter dependent diffusion coefficient $D(h)$, exactly calculated in chapter 2 and Knight and Klages [2011b], is shown in **(b)**.

3.3 Correlated random walk

The first approximation method starts with the diffusion coefficient expressed in terms of the velocity autocorrelation function of the map, called the Taylor-Green-Kubo formula, (Dorfman [1999]; Klages [2007]; Klages and Korabel [2002]) for derivations,

$$D(h) = \lim_{n\to\infty} \left(\sum_{k=0}^{n} \int_0^1 v_0(x) v_k(x) \rho^*(x) dx \right) - \frac{1}{2} \int_0^1 v_0^2(x) \rho^*(x) dx \,, \tag{3.4}$$

where $\rho^*(x)$ is the invariant density of the map Eq. (3.2) modulo one, this being equal to one throughout the parameter range as we have a family of doubling maps. The velocity function $v_k(x)$ calculates the integer displacement of a point at the k^{th} iteration,

$$v_k(x) = \lfloor x_{k+1} \rfloor - \lfloor x_k \rfloor \,. \tag{3.5}$$

In order to create an n^{th} order approximation we simply truncate Eq.(3.4) at a given n (Klages and Korabel [2002]). Hence we obtain the finite sum

$$D_n(h) = \sum_{k=0}^{n} \int_0^1 v_0(x)v_k(x)dx - \frac{1}{2}\int_0^1 v_0^2(x)dx \,, \tag{3.6}$$

which can physically be understood as a time dependent diffusion coefficient. Looking at how the sequence of $D_n(h)$ converges towards $D(h)$ thus corresponds to incorporating more and more memory in the decay of the velocity autocorrelation function and checking how this decay varies as a function of h for given n. Note that the functional form of $D_n(h)$ for finite n is to some extent already determined by the choice of integer displacements in Eq. (3.5), however, it has been checked that for the given model the deviations between using integer and non-integer displacements for finite time are minor. Secondly, we remark that by using this straightforward truncation scheme we have neglected further cross-correlation terms that do not grow linearly in n, cf. Dorfman [1999]. Still, by definition we have $D_n(h) \to D(h)$ $(n \to \infty)$. Going to lowest order, for $n = 0$ we immediately see that

$$D_0(h) = \frac{h}{2} \,, \tag{3.7}$$

which is the simple uncorrelated random walk solution for the diffusion coefficient (Knight and Klages [2011b]). In figure (3.2) one can see that $D_0(h)$ is asymptotically exact for $h \to 0$.

Of more interest however are the higher values of n capturing the higher order correlations that come into play. To evaluate these we define a jump function $J_h^n(x) : [0,1] \to \mathbb{R}$,

$$J_h^n(x) = \sum_{k=0}^{n} v_k\left(x\right) \,, \tag{3.8}$$

which gives the integer displacement of a point x after n iterations. Equation (3.8) can be written recursively as (Knight and Klages [2011b])

$$J_h^n(x) = v_0(x) + J_h^{n-1}\left(\tilde{M}_h(x)\right) , \tag{3.9}$$

where $\tilde{M}_h(x)$ is Eq. (3.2) taken modulo 1. This recursive formula will help when

we solve the integral in Eq. (3.6). Let $T_h^n(x) : [0,1] \to \mathbb{R}$ be defined as

$$T_h^n(x) = \int_0^x J^n(y)dy, \quad T_h^{-1}(x) := 0. \tag{3.10}$$

Using Eq. (3.9) we can solve Eq. (3.10) recursively as

$$T_h^n(x) = s_h(x) + \frac{1}{2}T^{n-1}\left(\tilde{M}_h(x)\right) \tag{3.11}$$

with

$$s_h(x) = \int_0^x v_0(y)dy = xv_0(x) + c, \tag{3.12}$$

where the constants of integration c can be evaluated using the continuity of $T_h^n(x)$ and the fact that $T_h^n(0) = T_h^n(1) = 0$ as there is no mean drift in this system. We obtain the following functional recursion relation for $T_h^n(x)$:

$$T_h^n(x) = \begin{cases} \frac{1}{2}T_h^{n-1}(2x+h) & -\frac{1}{2}T_h^{n-1}(h) & 0 \le x < \frac{1-h}{2} \\ \frac{1}{2}T_h^{n-1}(2x+h-1) & -\frac{1}{2}T_h^{n-1}(h) + x + \left(\frac{h-1}{2}\right) & \frac{1-h}{2} \le x < \frac{1}{2} \\ \frac{1}{2}T_h^{n-1}(2x-h) & -\frac{1}{2}T_h^{n-1}(h) - x + \left(\frac{h+1}{2}\right) & \frac{1}{2} \le x < \frac{1+h}{2} \\ \frac{1}{2}T_h^{n-1}(2x-1-h) & -\frac{1}{2}T_h^{n-1}(h) & \frac{1+h}{2} \le x < 1 \end{cases}. \tag{3.13}$$

Using Eq. (3.13) in Eq. (3.6) via Eq.(3.8) and Eq.(3.10) we can evaluate the n^{th} order approximation as

$$D_n(h) = \frac{h}{2} + T_h^{n-1}(h). \tag{3.14}$$

So we see that the higher order correlations are all captured by the cumulative integral functions $T_h^n(x)$. In order to evaluate Eq. (3.14) we construct a recursive relation from Eq. (3.13),

$$T_h^n(h) = \sum_{k=0}^{n} \frac{1}{2^k} t_h\left(\tilde{M}_h^k(h)\right) - \sum_{k=1}^{n} \frac{1}{2^k} T_h^{n-k}(h), \tag{3.15}$$

where

$$t_h(x) = \begin{cases} 0 & 0 \leq x < \frac{1-h}{2} \\ x + \frac{h-1}{2} & \frac{1-h}{2} \leq x < \frac{1}{2} \\ -x + \frac{h+1}{2} & \frac{1}{2} \leq x < \frac{1+h}{2} \\ 0 & \frac{1+h}{2} \leq x < 1 \end{cases} \tag{3.16}$$

is $s_h(x)$ with the $-\frac{1}{2}T_h^n(h)$ terms removed. In order to simplify Eq. (3.15) we write it entirely in terms of Eq. (3.16). Let

$$\tau_h(n) = \sum_{k=1}^{n} \frac{1}{2^k} T_h^{n-k}(h). \tag{3.17}$$

We can write Eq.(3.17) recursively as

$$\tau_h(n) = \frac{1}{2} T_h^{n-1}(h) + \frac{1}{2}\tau_h(n-1). \tag{3.18}$$

Substituting Eq.(3.17) and Eq.(3.18) into Eq.(3.15) we obtain

$$T_h^n(h) = \sum_{k=0}^{n} \frac{1}{2^k} t_h\left(\tilde{M}_h^k(h)\right) - \frac{1}{2} T_h^{n-1}(h) - \frac{1}{2}\tau_h(n-1). \tag{3.19}$$

Then substituting Eq.(3.15) back into Eq.(3.19)

$$\begin{aligned} T_h^n(h) &= \sum_{k=0}^{n} \frac{1}{2^k} t_h\left(\tilde{M}_h^k(h)\right) - \frac{1}{2}\left(\sum_{k=0}^{n-1} \frac{1}{2^k} t_h\left(\tilde{M}_h^k(h)\right)\right) \\ &+ \frac{1}{2}\tau_h(n-1) - \frac{1}{2}\tau_h(n-1) \end{aligned} \tag{3.20}$$

we arrive at the final expression

$$T_h^n(h) = \frac{1}{2^n} t_h\left(\tilde{M}_h^n(h)\right) + \sum_{k=0}^{n-1} \frac{1}{2^{k+1}} t_h\left(\tilde{M}_h^k(h)\right). \tag{3.21}$$

It is helpful to rewrite Eq.(3.15) in the form of Eq.(3.21) as it allows us to show that under this method, $D_n(h)$ converges exactly to $D(h)$ in finite time for particular values of h, see figure (3.2) for an illustration. This means that for

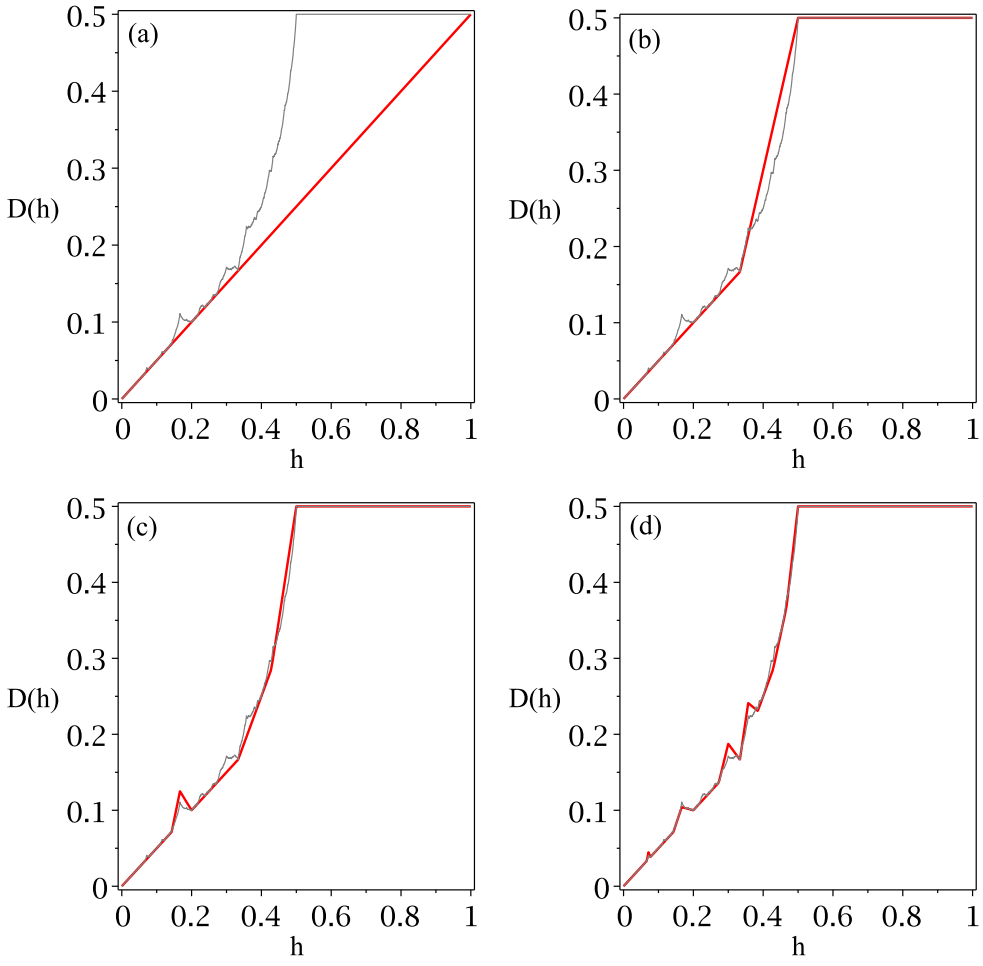

Figure 3.2: *Correlated random walk.* In this figure the first four approximations to the parameter dependent diffusion coefficient $D(h)$ are illustrated in bold (red) along with the actual diffusion coefficient. In **(a)** the zeroth order is shown, which is simply the random walk solution, in **(b)**,**(c)** and **(d)** the first, second, and third order approximations, respectively. At each stage one obtains a set of extrema with linear interpolation, which converge quickly to the exact diffusion coefficient $D(h)$. The amount of extrema increases exponentially with n, hence we see the fractal structure emerging.

a specific set of parameter values, we can fully capture the correlations of the map with a finite time approximation. This convergence is dependent upon the behaviour of the orbit of the point $x = h$ under the map $\tilde{M}_h(x)$. In particular, if this orbit is pre-periodic, and the values of the points in the periodic loop correspond to 0 in Eq. (3.16), then the time dependent diffusion coefficient $D_n(h)$ will converge to the exact value $D(h)$ on the n^{th} step, where n is given by the transient length of the orbit of h plus one. For example, let $h = 2/5$,

$$\begin{aligned} \tilde{M}_{2/5}(2/5) &= 1/5 \\ \tilde{M}_{2/5}(1/5) &= 4/5 \\ \tilde{M}_{2/5}(4/5) &= 1/5\,. \end{aligned} \tag{3.22}$$

So $h = 2/5$ is pre-periodic of transient length one. In addition

$$\begin{aligned} t_h(2/5) &= 1/10 \\ t_h(1/5) &= 0 \\ t_h(4/5) &= 0\,, \end{aligned} \tag{3.23}$$

thus $t_{2/5}\left(\tilde{M}^n_{2/5}(2/5)\right) = 0$ for $n > 1$. Hence we see finite time convergence to $D(h)$. This finite time convergence at a certain set of points is helpful in understanding the structure of $D(h)$ as the fractal diffusion coefficient can be seen emerging around these points in the same manner as an iterated function system like a Koch curve, see figure (3.2). This set of parameter values, whose number of elements becomes infinite for $n \to \infty$, holds the key to understanding the emergence of the fractal structure in the diffusion coefficient. There is a clear physical interpretation of this set of parameter values in terms of the orbits of the associated critical points of the map, as exemplified above. Under parameter variation these orbits generate complicated sequences of forward and backward scattering, which characterise the diffusive dynamics by physically explaining the origin of the fractal structure in terms of the topological instability of the associated microscopic scattering processes. This physical interpretation has been discussed in chapter 2 and is also explained in Klages [1996, 2007]; Klages and Dorfman [1995, 1999]; Knight and Klages [2011b].

Being able to analytically expose the fractal structure of parameter dependent diffusion coefficients is the main strength of this method. In addition, the convergence of the series of approximations is very quick due to the finite time convergence at certain values of h. Moreover, the fact that one only needs to directly put in the map dynamics makes it very user-friendly. However, due to the recurrence relation that this method is based on, applying it analytically is restricted to one-dimensional systems or higher dimensional systems whose dynamics can be projected down to one-dimensional systems, such as baker maps (Dorfman [1999]; Gaspard [1998]; Gaspard and Klages [1998]; Klages [2007]). In order to answer questions about more realistic, physical systems one would need to resort to numerical analysis. By using families of time and parameter dependent diffusion coefficients such as defined by Eq.(3.6) this is, on the other hand, straightforward, as has been demonstrated in Harayama et al. [2002]; Klages [2007]; Korabel and Klages [2004]; Mátyás and Klages [2004].

3.4 Persistent random walk

The next method we look at again starts with the Taylor-Green-Kubo formula for diffusion Eq. (3.4). However, rather than truncating it, we now approximate the correlations in a more self-consistent way by including memory effects persistently. The key difference to the previous method is that this approach models an exponential decay of the velocity autocorrelation function beyond the lowest order approximation. This method first emerged within stochastic theory as a persistent random walk (Haus and Kehr [1987]; Weiss [1994]) and was recently applied to understand chaotic diffusion in Hamiltonian particle billiards Gilbert and Sanders [2009, 2010]; Gilbert et al. [2011]. It is physically motivated by generalisations of simple random walk behaviour of diffusing particles. Diffusing particles may be more inclined to continue in a given direction due to momentum effects or to switch directions due to vacant lattice sites for example, giving rise to correlations between jumps. These effects were first studied in the context of Brownian motion in Fürth [1920] and in the setting of hydrodynamics in Taylor [1922].

The main task of evaluating the diffusion coefficient with this method is to find

an expression for the correlation function at the n^{th} time step by only including memory effects of a given length. We start by defining the velocity autocorrelation function as a sum over all possible velocities weighted by the corresponding parts of the invariant measure μ^* of the system,

$$\langle v_0(x)v_n(x)\rangle = \sum_{v_0(x),\ldots,v_n(x)} v_0(x)v_n(x)\mu^*(\{v_0(x),\ldots,v_n(x)\}). \tag{3.24}$$

The different parts of the invariant measure in Eq. (3.24) are approximated by the transition probabilities of the system, depending on the length of memory considered. These in turn are trivially obtained from the invariant probability density function $\rho^*(x)$. As a 0^{th} order approximation of this method, no memory is considered at all, that is, the movement of a particle is entirely independent of its preceding behaviour. In this case the correlations evaluate simply as

$$\langle v_0(x)v_n(x)\rangle = 0 \quad (n > 0), \tag{3.25}$$

thus we need only consider $\langle v_0^2(x)\rangle$. By Eq. (3.4) the approximate diffusion coefficient is obtained as

$$D_0(h) = \frac{1}{2}\int_0^1 \left\langle v_0^2(x)\right\rangle dx = \frac{h}{2}\,, \tag{3.26}$$

which reproduces again the random walk solution, as expected. For the higher order approximations, one must refine the level of memory that is used based upon the microscopic dynamics of the map.

3.4.1 One step memory approximation

We now include one step of memory in the system, i.e., we assume that the behaviour of a point at the n^{th} step is only dependent on the $(n-1)^{th}$ step. In Gilbert and Sanders [2009] Eq.(3.24) was evaluated for approximating the diffusion coefficient in a particle billiard. For this purpose it was assumed that a point moves to a neighbouring lattice point at each iteration. Hence the velocity function $v_n(x)$ could only take the values ℓ or $-\ell$, where ℓ defines the lattice spacing. In order to evaluate the one step memory approximation for the map

$M_h(x)$, we need to modify the method to include the probability that a point stays at a lattice point and does not move, hence the velocity function can take the values $1, -1$ or 0. This is physically motivated in persistent random walk theory by the presence of impurities in lattice structures. These impurities can trap diffusing particles with the trap time being far greater than the escape time. This has been observed experimentally in the case of hydrogen atoms diffusing in metallic crystals, see Okamura et al. [1980] for a study of persistent random walks in this setting.

Let $P(b|a)$ be the conditional probability that a point takes the velocity b given that at the previous step it had velocity a with $a, b \in \{0, 1, -1\}$. We use these probabilities to obtain a one step memory approximation. We can write the velocity autocorrelation function as

$$\langle v_0 v_n \rangle = \sum_{v_0,\ldots,v_n} v_0 v_n p(v_0) \prod_{i=1}^{n} P(v_i|v_{i-1}), \tag{3.27}$$

where we let $v_k(x) = v_k$ for brevities sake and $p(a)$ is the probability that a point takes the velocity a at the first step. We can capture the combinatorics of the sum over all possible paths by rewriting Eq.(3.27) as a matrix equation,

$$\langle v_0 v_n \rangle = \begin{pmatrix} 0 & 1 & -1 \end{pmatrix} \begin{pmatrix} P_{00} & P_{01} & P_{0-1} \\ P_{10} & P_{11} & P_{1-1} \\ P_{-10} & P_{-11} & P_{-1-1} \end{pmatrix}^n \begin{pmatrix} 0 \\ p(1) \\ -p(-1) \end{pmatrix} \tag{3.28}$$

where $P_{ba} = P(b|a)$. Eq.(3.28) can be simplified by using the fact that all the paths with a '0' state cancel each other out, therefore not contributing to diffusion, and by using the symmetries in the system, i.e.,

$$\begin{aligned} P_{-1-1} &= P_{11} \\ P_{-11} &= P_{1-1} \\ p(-1) &= p(1) \end{aligned} \tag{3.29}$$

Hence Eq. (3.27) can be simplified to

$$\langle v_0 v_n \rangle = \begin{pmatrix} 1 & -1 \end{pmatrix} \begin{pmatrix} P_{11} & P_{1-1} \\ P_{1-1} & P_{11} \end{pmatrix}^n \begin{pmatrix} 1 \\ -1 \end{pmatrix} p(1), \tag{3.30}$$

which is a simple quadratic form. By diagonalisation the expression for the n^{th} velocity autocorrelation function is obtained,

$$\langle v_0 v_n \rangle = 2p(1) \left(P_{11} - P_{1-1}\right)^n, \tag{3.31}$$

yielding the exponential decay of the velocity autocorrelation function,

$$< v_0 v_n > \sim \exp(n \log(P_{11} - P_{1-1})), \tag{3.32}$$

referred to above. Substituting Eq.(3.31) into the Taylor-Green-Kubo formula Eq.(3.4) by using the fact that $p(1) = h/2$ gives

$$\begin{aligned} D(h) &= \sum_{n=0}^{\infty} \langle v_0 v_n \rangle - \frac{1}{2} \langle v_0^2 \rangle \\ &= h \left(\sum_{n=0}^{\infty} \left(P_{11} - P_{1-1}\right)^n \right) - \frac{h}{2} \\ &= \frac{h}{1 - P_{11} + P_{1-1}} - \frac{h}{2}. \end{aligned} \tag{3.33}$$

The relevant parameter dependent probabilities can be worked out from the invariant density $\rho^*(x)$ of the system and are

$$P_{11} = \begin{cases} 0 & 0 \leq h < \frac{1}{3} \\ 1 - \frac{(1-h)}{2h} & \frac{1}{3} \leq h < \frac{1}{2} \\ \frac{1}{2} & \frac{1}{2} \leq h < 1 \end{cases} \tag{3.34}$$

and

$$P_{1-1} = \begin{cases} 0 & 0 \leq h < \frac{1}{3} \\ 0 & \frac{1}{3} \leq h < \frac{1}{2} \\ 1 - \frac{1}{2h} & \frac{1}{2} \leq h < 1 \end{cases} . \tag{3.35}$$

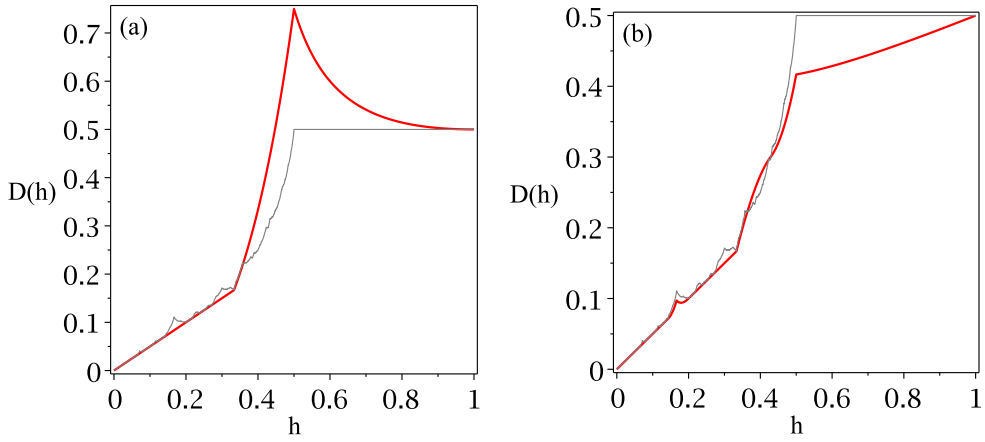

Figure 3.3: *Persistent random walk approximation.* In this figure the first order approximation Eq. (3.33) to the exact parameter dependent diffusion coefficient $D(h)$ is illustrated in **(a)**, the second order Eq. (3.37) is shown in **(b)**. Approximations are in bold (red) along with the diffusion coefficient. The major topological changes in the dynamics are picked out by piecewise-differentiable approximations.

Substituting Eq.(3.34) and Eq.(3.35) into Eq.(3.33) we obtain a persistent one-step memory approximation for the diffusion coefficient of the map $M_h(x)$. Figure (3.3) shows a plot of the final result as a function of the control parameter in comparison to the exact diffusion coefficient $D(h)$.

3.4.2 Two step memory approximation

We now extend the approximation to include two steps of memory, i.e., the behaviour of a point at the n^{th} step depends on what has happened at the $(n-1)^{th}$ and $(n-2)^{th}$ step. Let $P(c|b,a)$ be the conditional probability that a point has velocity c given that it had velocity b at the previous step and a at the step before that with $a, b, c \in \{0, 1, -1\}$. For this two step approximation, the velocity autocorrelations are given by

$$\langle v_0 v_n \rangle = \sum_{v_0,\ldots,v_n} v_0 v_n p(v_0, v_1) \prod_{i=2}^{n} P(v_i|v_{i-1}, v_{i-2}), \tag{3.36}$$

where $p(a,b)$ is the probability that a point takes velocity a at the first step followed by b. Again we proceed by the method of Gilbert and Sanders [2010] and rewrite Eq.(3.36) as a matrix equation in order to capture the combinatorics of the sum,

$$\langle v_0 v_n \rangle = \underline{r} \cdot \underline{\underline{A}}^n \cdot \underline{s} \tag{3.37}$$

where $\underline{r}$ evaluates v_n, $\underline{s}$ evaluates $v_0 p(v_0, v_1)$ and $\underline{\underline{A}}$ is the 9×9 probability transition matrix for the system. However, we are unable to evaluate Eq.(3.37) analytically (see Appendix A.1) so we resort to numerical evaluations. The result is depicted in figure 3.3. We see that this method picks out the same topological changes in the map dynamics that the previous method did and interpolates between them, however, the convergence at these points is not as accurate.

The strength of this method is in modelling the exponential decay of correlations that is often found in diffusive systems, particularly in Hamiltonian particle billiards (Bálint and Toth [2008]). When applied to these systems the method is not restricted by dimension making it very useful in this setting. However, generating by default an exponential decay of correlations is not an ideal approach for diffusive systems in which correlations do not decay exponentially. In contrast to the correlated random walk approach, this method is not designed to reveal possibly fractal structures of parameter dependent diffusion coefficients. It also requires a lot of input about the relevant transition probabilities (see Appendix A.1), making it unpractical when it comes to analysing higher order approximations.

3.5 Approximating Markov partitions

The final method we will look at does not involve the Taylor-Green-Kubo formula. Using the framework of the escape rate theory applied to dynamical systems as pioneered in Dorfman [1999]; Gaspard [1998]; Gaspard and Dorfman [1995]; Gaspard and Nicolis [1990], we consider a truncated map $M_h(x)$ defined on $[0, L]$, $L \in \mathbb{N}$ with periodic boundary conditions. The key quantity to understanding diffusion in this setting is the parameter-dependent decay rate $\gamma_{dec}(h)$, which measures the convergence of some initial density to the invariant one. As was

shown in Klages [1996]; Klages and Dorfman [1995, 1999], by this approach the diffusion coefficient as a function of the decay rate is given by,

$$D(h) = \lim_{L\to\infty} \frac{L^2}{4\pi^2}\gamma_{dec}(h). \tag{3.38}$$

That is one must calculate the decay rate for the truncated map on $[0, L]$ as a function of L and then take the limit $L \to \infty$. The decay rate can in turn be calculated exactly if the Frobenius-Perron equation can be mapped onto a Markov transition matrix. In case of $M_h(x)$ the second largest eigenvalue $\chi_1(h)$ of this transition matrix determines the decay rate, (Klages [1996]; Klages and Dorfman [1995, 1999]) and is given by

$$\gamma_{dec}(h) = ln\left(\frac{2}{\chi_1(h)}\right). \tag{3.39}$$

Unfortunately, constructing Markov transition matrices exactly for even the simplest parameter dependent maps can be a very complicated task. Hence the approximation method we employ here is based on approximating the transition matrix.

The approximation method starts as follows (see also Klages [1996]; Klages and Dorfman [1999] for details): For a given value of the parameter h, we restrict the dynamics to the unit interval by using Eq. (3.2) modulo 1. We then consider the set of iterates of the 'generating orbit' (see chapter 2), that is the orbit of the critical point $x = 0.5$. The set of values of the generating orbit form a set of Markov partition points for the map, yielding a finite partition if the generating orbit is periodic or pre-periodic. This set of points is then copied and lifted back onto the system of size L into each unit interval, defining a partition of $[0, L]$. By supplementing this partition with periodic boundary conditions, it defines a Markov partition for the whole system on $[0, L]$.

The key problem is that the behaviour of the orbit of the critical point under parameter variation is very irregular. Therefore we approximate Markov partitions by truncating this orbit for a given parameter value after a certain number of iterations. Typically, the resulting set of points will then not yield a Markov partition for this parameter value. In order to make up for this, we

introduce a weighted approximation into our transition matrix to account for any non-Markovian behaviour. For example, if partition part i gets mapped onto a fraction of partition part j then the entry $a_{i,j}$ in the approximate transition matrix will be equal to this fraction. See Appendix A.2 for the second and third order approximations to the transition matrix of the modulo one map.

The motivation behind this method is that at each stage of the approximation, whose level is defined by the number of iterates of the critical point, there will be certain values of the parameter whose Markov partitions are exact. So at least for these parameter values we will obtain the precise diffusion coefficient $D(h)$, with interpolations between these points as defined by the approximate transition matrix. That way, we will have full control and understanding over the convergence of our approximations.

We first work out the zeroth order approximation, for which we take the unit intervals as partition parts; see figure 3.4 for an illustration of $M_h(x)$ at system size $L = 3$. The corresponding approximate transition matrix $\underline{\underline{T}}(h)$ is cyclic and reads

$$\underline{\underline{T}}(h) = \begin{pmatrix} 2-2h & h & 0 & \dots & h \\ h & 2-2h & h & \dots & 0 \\ 0 & h & 2-2h & h & \dots \\ \vdots & \vdots & h & \ddots & h \\ h & 0 & \dots & h & 2-2h \end{pmatrix}, \tag{3.41}$$

therefore the eigenvalues can be evaluated analytically (Klages and Dorfman [1995, 1999]) as

$$\begin{aligned} \chi_1(h) &= 2-2h+2h\cos(2\pi/L) \\ &\simeq 2-2h+2h\left(1-\frac{2\pi^2}{L^2}\right) \ (L\to\infty)\,. \end{aligned} \tag{3.42}$$

By combining this result with Eq. (3.39), the decay rate is given as a function of the parameter and length L to

$$\gamma_{dec}(h) = \ln\left(\frac{1}{1-h+h\cos(2\pi/L)}\right) \simeq \frac{h2\pi^2}{L^2}\ (L\to\infty). \tag{3.43}$$

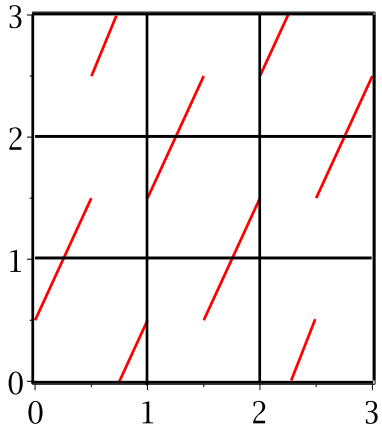

$$\underline{\underline{T}}(h) = \begin{pmatrix} 2-2h & h & h \\ h & 2-2h & h \\ h & h & 2-2h \end{pmatrix} \tag{3.40}$$

Figure 3.4: *Approximate Markov transition matrix.*Illustrated here is the map $M_h(x)$ truncated on $[0, L]$ with $L = 3$ and periodic boundary conditions. The map is given by the diagonal lines (red) and the zeroth order approximation to the Markov partition is shown by the thick black lines. The partition parts are simply the unit intervals. Note the periodic boundary conditions. The corresponding transition matrix is shown below. Note that this partition is only Markov when $h = 0$ or 1.

Using Eq. (3.43) in Eq. (3.38), the diffusion coefficient is finally given by

$$D(h) = \frac{h}{2}\,, \tag{3.44}$$

which again yields the familiar random walk approximation.

The next stage of approximation involves two partition parts per unit interval, and for this we simply include the critical point $x = 0.5$ as a partition point. So our partition parts are the half-unit intervals on the real line. These approximations do not yield cyclic matrices so their eigenvalues are worked out numerically. See figure 3.5 for an illustration of the eigenvalues for a selection of parameters that yield Markov transition matrices at the first and second order approximation (see Appendix A.2).

For the next iteration level we include the first iteration of $x = 0.5$, $\tilde{M}_h(0.5) =$

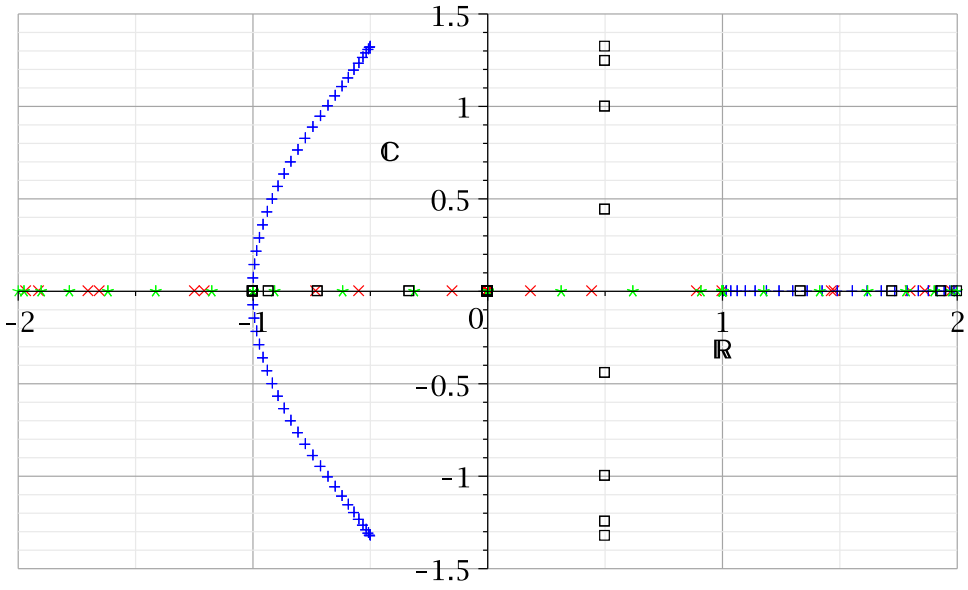

Figure 3.5: *First and second order eigenvalues.* In this figure the eigenvalues of Markov transition matrices of size $L = 120$ are illustrated. The parameters have been chosen such that the first and second order approximations are identical to the actual transition matrix. That is, $h = 1/2$ (red diagonal cross), converges at the first order approximation, and $h = 1/6$ (blue cross), $h = 1/4$ (green asterix) and $h = 1/3$ (black squares) converge at the second order. We observe a relatively simple structure in the eigenvalues, particulary at $h = 1/2$ and $h = 1/4$ who have no complex values.

$1 - h$ as a partition point and its mirror image about $x = 0.5$ which is h, and for each higher approximations we include one more iterate. However, again with these higher approximations we no longer obtain a cyclic matrix, so we have to resort to numerics to evaluate the eigenvalues. See figure 3.6 for an illustration of the eigenvalues of a selection of Markov transition matrices. The parameter values are chosen such that the approximation procedure yields a fully Markov transition matrix at the third order approximation. We observe a more complicated structure in the eigenvalues than that of the first and second order Markov transition matrices (see figure 3.5), this being related to the stronger higher order correlations in the system.

The first three approximations obtained by this method are displayed in figure

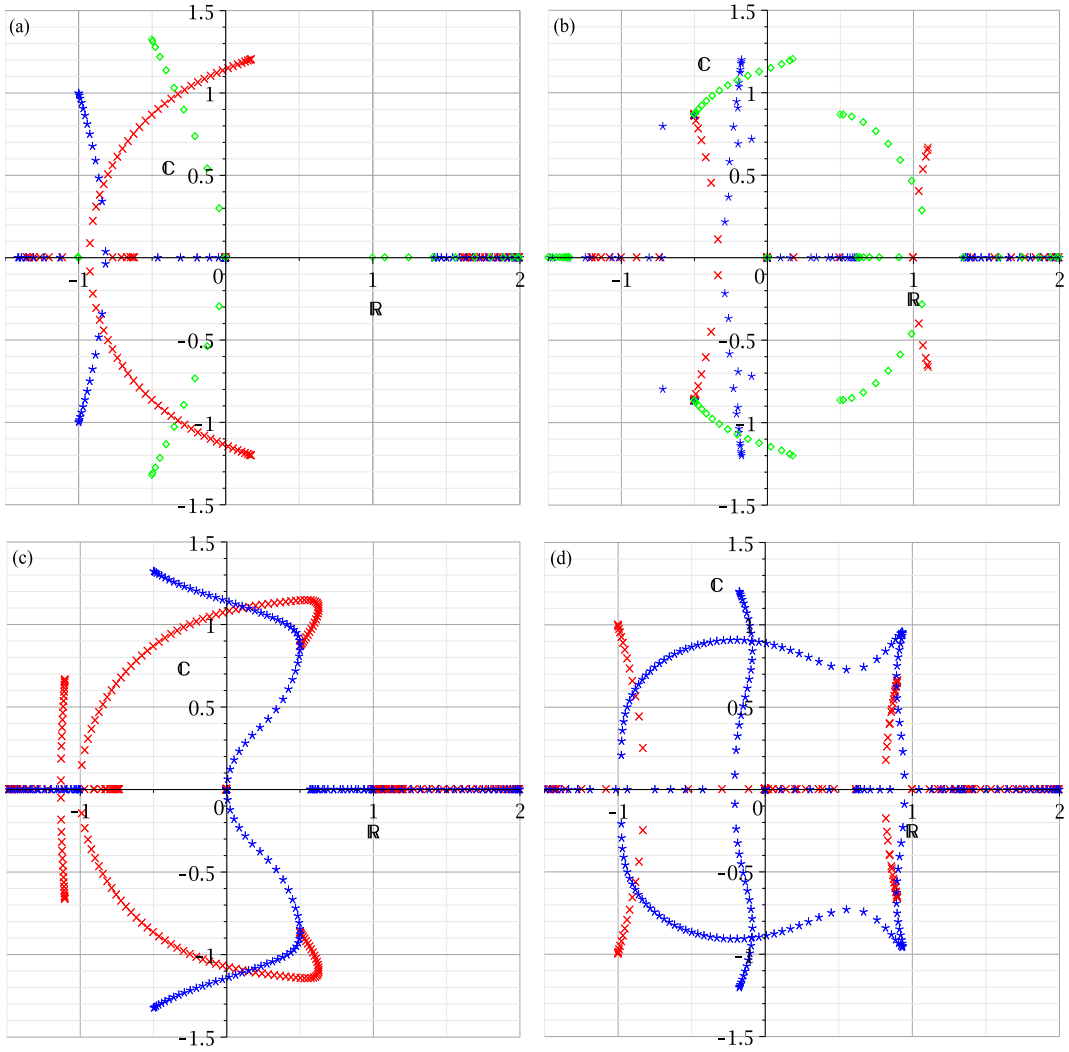

Figure 3.6: *Third order eigenvalues.* In this figure, the eigenvalues of Markov transition matrices are illustrated at the set of parameter values which converge at the third-order approximation. In **(a)**, $h = 1/14$ (red diagonal cross), $h = 1/10$ (blue asterix) and $h = 1/8$ (green box), the system size is $L = 120$. In **(b)**, $h = 1/7$ (red diagonal cross), $h = 1/5$ (blue asterix) and $h = 3/10$ (green box), the system size is $L = 120$. In **(c)**, $h = 5/14$ (red diagonal cross) and $h = 3/8$ (blue asterix) the system size is $L = 300$. In **(d)**, $h = 2/5$ (red diagonal cross) and $h = 3/7$ (blue asterix) the system size is $L = 300$. We observe much more complicated structure in the eigenvalues compared with the first and second order case (figure 3.5).

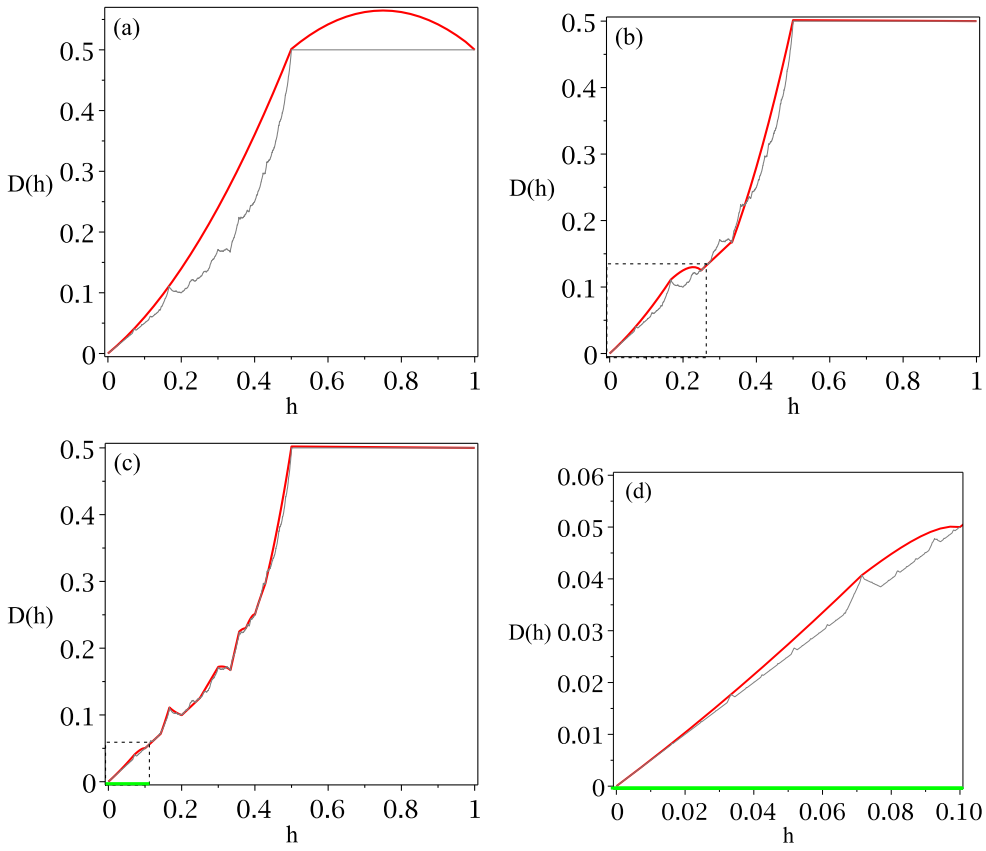

Figure 3.7: *Approximating the transition matrices.* In this figure, the first order approximation to the parameter dependent diffusion coefficient $D(h)$ obtained by this method is illustrated in **(a)**, and the second and third orders are illustrated in **(b)** and **(c)**, respectively, whilst a blow up of **(c)** is shown in **(d)**. The approximations are shown in bold (red) along with the diffusion coefficient diffusion coefficient. We see that the functional form of the interpolation in **(a)** is repeated in **(b)** at a smaller scale (see the contents of the dashed line box). This functional form is again repeated on a still smaller scale in **(c)** as illustrated in **(d)**. This self-similarity provides evidence that the final function $D(h)$ is fractal.

3.7. The main strength of this method is that we know, by definition, where our approximations are going to converge exactly in finite time, namely at Markov partition parameter values h picked out by each subsequent approximation. In addition, the functional form of the interpolation between these points highlights areas of self-similarity and therefore gives one evidence for fractal behaviour even at low-level approximations, see figure 3.7. However this method quickly relies on numerical computation and again requires considerable input from the user making it unpractical at higher level approximations.

3.6 Conclusion

In this chapter, we studied three methods for approximating the parameter dependent diffusion coefficient by applying them analytically and numerically to a simple dynamical system that exhibits diffusion. For this model the exact parameter-dependent diffusion coefficient was derived in chapter 2 (Knight and Klages [2011b]). Using these results as a reference, the motivation was to learn about the capabilities and the weaknesses of the individual methods. These are of course not a comprehensive list of the many possible ways to approximate the diffusion coefficient of a system, see Rechester and White [1980]; Venegeroles [2007] for diffusion in sawtooth and standard maps. However, what they do illustrate is the fact that even in our simple model studied here, the results that one obtains are very much dependent upon the individual method used, and these results vary greatly between the methods.

By the first method, based on a systematic truncation of the Taylor-Green-Kubo formula, we saw the fractal structure building up analytically over a series of correlated random walk approximations, as we were able to exactly capture the correlations of the system in finite time at certain parameter values. This yielded in turn quick convergence to the exact results. Using a persistent random walk approach, the second method retained an exponential decay of correlations even in finite time approximations. However, for the model under consideration this approximation yielded convergence that was significantly weaker than in case of the other two methods. Based on the escape rate approach to chaotic diffusion and approximate transition matrices, the third method had our attention focused on

areas of self-similarity giving us particularly strong evidence for fractal structures in the diffusion coefficient. This method generated again very quick convergence. Comparing the three different methods with each other demonstrates that one is able to tailor the approximate results one gets by applying a specific method to the specific questions one wishes to answer, or to the specific setting.

Accordingly, the quest for a 'unique' way to approximate the diffusion coefficient of a dynamical system, as suggested in Gilbert and Sanders [2009], is unnecessarily restrictive. Here we looked at a different class of systems than the Hamiltonian particle billiards considered in Gilbert and Sanders [2009]. This had the advantage that the different approximation methods could be studied more rigorously. We can conclude that the persistent random walk method favoured in Gilbert and Sanders [2009] may be more appropriate for dispersing billiards, because an integral part of this method is modelling an exponential decay of correlations, as it is quite common in these systems. However, one may question the usefulness of this method for diffusive dynamical systems where exponential decay is not guaranteed. Here other methods, such as the first and the third one discussed above, may yield superior results in terms of speed of convergence and identification of possible fractal structures in diffusion coefficients. Particularly the first method has the advantage that it is conceptually very simple and quite universally applicable, without making any assumptions on the decay of correlations.

Each of the three approximation methods discussed here has, for a given model, its own virtue. When one looks to understand, or display, a particular property of a system and cannot achieve this analytically, resorting to one of these approximation methods is thus a sensible course of action.

A final point worth emphasising is that the structure of the diffusion coefficients in more physical systems such as Lorentz gases and sawtooth maps are still not fully understood Klages [2007]; Venegeroles [2007]. Particularly, to which extent these systems diffusion coefficients are fractal remains an open question. Further refining approximation methods, such as the ones presented in this paper, to highlight areas of self-similarity in parameter dependent diffusion coefficients in these systems, or to show the emergence of fractal structures, would be of great help in answering these questions.

Chapter 4

Diffusion through different holes

The dependence of the diffusion coefficient on the size and the position of dynamical channels ('holes') linking spatial regions in periodically lifted, one-dimensional dynamical systems is considered. The system properties can be obtained analytically via a Taylor-Green-Kubo formula in terms of a functional recursion relation, leading to a diffusion coefficient varying with the hole positions and non-monotonically on their size. Analytic formulas for small holes in terms of periodic orbits covered by the holes are derived. The asymptotic regimes observed show deviations from a simple random walk approximation, a phenomenon that should be ubiquitous in dynamical systems and could potentially be observed experimentally. The escape rate of the corresponding open system is also calculated. The resulting parameter dependencies are compared with those of the diffusion coefficient and explained in terms of periodic orbits.

4.1 Introduction

Recently there has been a surge of interest from mathematicians and physicists on dynamical systems with holes, that is, subsets of phase space that allow trajectories to escape. Work on the escape rate of such systems has revealed fundamental results regarding its dependence on position, the small hole size limit (Bunimovich and Yurchenko [2011]; Keller and Liverani [2009]) and the effect of noise in such systems (Altmann and Endler [2010]) to name a few; for reviews of this work

see for example Altmann and Tél [2009]; Demers and Young [2006]; Dettmann [2011]. Here we pose the question: How do other system properties depend upon the position and size of escape holes? In this chapter we answer this question for the diffusion coefficient, interpreting the holes now as the links between spatially separate regions. Diffusion is an essential process of many-particle systems, the study of which cross-links transport theory in statistical mechanics with dynamical systems theory (Dorfman [1999]; Gaspard [1998]; Klages [2007]). In addition, diffusive systems provide a setting where the complex interaction between different holes can be studied, an area that has yielded interesting results regarding escape rates from circular (Bunimovich and Dettmann [2005]) and diamond (Bunimovich and Dettmann [2007]) billiards with two holes, and very recently regarding transmission and reflection rates in stadium billiards (Dettmann and Georgiou [2011]) and the bouncer model (Dettmann and Leonel [2012]). A general relation between escape and diffusion has been established by the escape rate theory of chaotic diffusion, which provides exact formulas expressing transport coefficients in terms of escape rates in spatially extended systems with absorbing boundary conditions (Dorfman [1999]; Gaspard [1998]; Gaspard and Nicolis [1990]; Klages [1996, 2007]).

Much research has gone into studying the parameter dependence of the diffusion coefficient in simple one-dimensional maps (Fujisaka and Grossmann [1982]; Geisel and Nierwetberg [1982]; Schell et al. [1982], see also chapter 2 of this thesis). For low-dimensional, spatially periodic chaotic dynamical systems the diffusion coefficient is often found to be a fractal function of control parameters, exhibiting non-trivial fine scale structure even in apparently simple examples (Gaspard and Klages [1998]; Klages [2007]; Klages and Dorfman [1995]). The source of this fractality is typically explained in terms of topological instability under parameter variation of the underlying dynamics (Cristadoro [2006]; Cvitanović et al. [2010]). However there exist systems that display these hallmarks of fractality but nevertheless have a linear diffusion coefficient as we saw in chapter 2. Therefore there is still work to be done explaining the phenomenon of fractal diffusion coefficients in one dimension, let alone attempting to answer questions about higher dimensional, more physical systems like sawtooth maps (Dana et al. [1989]), standard maps (Rechester and White [1980]) or particle billiards (Harayama and Gaspard

[2001]; Harayama et al. [2002]) where analytical results are lacking, as are answers to basic questions about the structure of the diffusion coefficient. Previous work has focused on deriving and understanding the diffusion coefficient under smooth variation of control parameters of the dynamics (Klages [2007]). In this setting the reduced, modulo one dynamics of a system will change with parameter variation (Cvitanović et al. [2010]). In this chapter we will switch focus and study a system where the reduced dynamics does not change (Gaspard and Klages [1998]; Knight and Klages [2011a,b]).

In section 4.2 we define the dynamical system that we will study. It is a simple piecewise-linear chaotic map of the real line which is a deterministic realization of a random walk. It is constructed by copying and periodically lifting the Bernoulli shift or doubling map over the whole real line (Gaspard and Klages [1998]; Knight and Klages [2011a,b]). We choose the doubling map so that we can compare with the results on escape rates from Bunimovich and Yurchenko [2011]; Keller and Liverani [2009] where the doubling map was also studied. In addition, the invariant measure of the doubling map is simply Lebesgue, which helps make it amenable to analysis with the method we will employ. The process of copying and periodically lifting a map is the classical way to study chaotic diffusion in one-dimension (Fujisaka and Grossmann [1982]; Geisel and Nierwetberg [1982]; Schell et al. [1982]). However we do not introduce transport into the system through variation of a control parameter such as a shift or by varying the slope, rather we dig escape holes into the map that serve as intervals where points can be iterated to a neighbouring interval in analogy with the work in Bunimovich and Yurchenko [2011]; Keller and Liverani [2009].

We then derive the diffusion coefficient as a function of the size and position of the escape holes in this system via the Taylor-Green-Kubo formula (Dorfman [1999]; Klages [2007]), in terms of a functional recursion relation. There are various methods for analytically deriving diffusion coefficients Cristadoro [2006]; Cvitanović et al. [2010]; Groeneveld and Klages [2002]; Klages [2007] but the method we use, developed in Gaspard and Klages [1998]; Klages [1996]; Knight and Klages [2011a,b] and employed in chapter 2 of this thesis, is the best suited to this setting. In section 4.3 we look at the analytical formulas derived in section 4.2 and find that the diffusion coefficient varies as the position of the escape

holes is varied, in analogy with results on the escape rate. We also find that the diffusion coefficient decreases non-monotonically as the size of the escape holes decreases, a result that is different to the escape rate.

Following this, we analyze the diffusion coefficient for small hole size by deriving analytical expressions which capture the asymptotic regime. We find that the asymptotic regime is dependent upon the orbit structure of the limiting point in an escape region, a result which goes beyond a simple random walk approximation (Fujisaka and Grossmann [1982]; Klages [1996]; Klages and Dorfman [1997]; Schell et al. [1982]). We explain the results on position dependence, non-monotonicity and asymptotic regimes by looking at the periodic orbit structure of the map. Moreover, we build a periodic orbit expansion for small but finite holes giving a more intuitive insight of the above. In section 4.4 we numerically calculate the escape rate for the corresponding open system in order to compare with the diffusion coefficient. Conclusions are made in section 4.5. The results presented in this chapter are from collaborative work with Dr. Rainer Klages of Queen Mary University of London, Dr. Carl Dettmann of the University of Bristol and Dr. Orestis Georgiou of the Max-Planck-Institut für Physik Komplexer Systeme and were submitted for publication in December 2011 (Knight et al. [2011]).

4.2 Diffusion coefficient as a function of the escape holes

In this section we will introduce the particular dynamical system that we will consider. It is a periodically lifted, piecewise linear map of the real line that exhibits chaotic diffusion. We will explain the concept of 'escape hole' in this context and then analytically derive the diffusion coefficient as a function of the escape holes.

4.2.1 Deterministic dynamical system

The dynamical system that we will study is based on the doubling map modulo one $\tilde{M}(x) : [0,1] \to [0,1]$,

$$\tilde{M}(x) = \begin{cases} 2x & 0 \leq x < \frac{1}{2} \\ 2x-1 & \frac{1}{2} \leq x < 1 \end{cases} . \tag{4.1}$$

The tilde in Eq.(4.1) will be used throughout to signify a self-map. We turn Eq.(4.1) into a dynamical system that exhibits diffusion in two steps. Firstly, we dig two symmetric holes into $\tilde{M}(x)$. Let $0 \leq a_1 < a_2 \leq 0.5 \leq a_3 < a_4 \leq 1$, with $a_4 = 1 - a_1$ and $a_3 = 1 - a_2$. For simplicity we let $h = a_2 - a_1$ which is the size of an escape hole. We lift the map dynamics by one for $x \in [a_1, a_2]$ and we lower the dynamics by one for $x \in [a_3, a_4]$ to create a map $M(x) : [0,1] \to [-1,2]$,

$$M(x) = \begin{cases} 2x & 0 \leq x < a_1 \\ 2x+1 & a_1 \leq x < a_2 \\ 2x & a_2 \leq x < \frac{1}{2} \\ 2x-1 & \frac{1}{2} \leq x < a_3 \\ 2x-2 & a_3 \leq x < a_4 \\ 2x-1 & a_4 \leq x \leq 1 \end{cases} . \tag{4.2}$$

We label the intervals $I_L = [a_1, a_2]$ and $I_R = [a_3, a_4]$ for convenience. We call I_L and I_R escape holes as they allow points to escape from the unit interval to a neighbouring interval. One can of course consider non-symmetric escape holes and non-symmetric maps such as the tent map. The necessary calculations in these cases are essentially no more complicated than shown here. The results for the diffusion coefficient differ only quantitatively, so presented here is only the case with symmetric escape holes in the doubling map. Secondly, we periodically copy $M(x)$ over the entire real line with a lift of degree one such that,

$$M(x+n) = M(x) + n, \quad n \in \mathbb{Z}, \tag{4.3}$$

so that $M(x) : \mathbb{R} \to \mathbb{R}$. A uniform distribution of points on the unit interval will spread out when iterated under Eq.(4.2) and Eq.(4.3). The diffusion coefficient D,

is defined as the linear increase in the mean square displacement of a distribution of points and is given by Einstein's formula in one-dimension as

$$D = \lim_{n\to\infty} \frac{\left\langle (x_n - x_0)^2 \right\rangle}{2n}, \tag{4.4}$$

where x_n is the position of a point x_0 at time n which is given by $M^n(x_0)$ in the system we consider. The angular brackets represent an average over a distribution of points. In the setting we consider, this distribution is the invariant density of the system $\rho^*(x) = 1$, and the average we interpret as an integral,

$$\langle ... \rangle = \int_0^1 ... \rho^*(x) dx. \tag{4.5}$$

4.2.2 Deriving the diffusion coefficient

Eq.(4.4) can be rewritten in terms of the velocity autocorrelation function of the system as the Taylor-Green-Kubo formula (Dorfman [1999]; Klages [2007]),

$$D = \lim_{n\to\infty} \left(\sum_{k=0}^{n} \langle v_0(x) v_k(x) \rangle \right) - \frac{1}{2} \left\langle v_0(x)^2 \right\rangle , \tag{4.6}$$

where $v_k(x) = \lfloor x_{k+1} \rfloor - \lfloor x_k \rfloor$ gives the integer value of the displacement of a point x_0 at time k. Considering Eq.(4.2) $v_k(x)$ takes the form,

$$v_k(x) = \begin{cases} 0 & 0 \le x_k < a_1 \\ 1 & a_1 \le x_k < a_2 \\ 0 & a_2 \le x_k < a_3 \\ -1 & a_3 \le x_k < a_4 \\ 0 & a_4 \le x_k \le 1 \end{cases} . \tag{4.7}$$

The leading order term of Eq.(4.6), D_{rw}, is simply equal to

$$\begin{aligned} D_{rw} &= \frac{1}{2} \int_0^1 v_0(x)^2 dx, \\ &= \frac{(a_4 - a_3) + (a_2 - a_1)}{2} = h. \end{aligned} \tag{4.8}$$

Eq.(4.8) is the simple random walk result for diffusion that one obtains if higher order correlations are neglected (Fujisaka and Grossmann [1982]; Klages [1996]; Klages and Dorfman [1997]; Schell et al. [1982]). In order to fully evaluate Eq.(4.6) we define a recursive function $J^n(x) : [0,1] \to \mathbb{Z}$ (Gaspard and Klages [1998]; Klages [1996]; Knight and Klages [2011a,b]),

$$\begin{aligned} J^n(x) &= \sum_{k=0}^{n} v_k(x) \\ &= v_0(x) + \sum_{k=0}^{n-1} v_k(\tilde{M}(x)) \\ &= v_0(x) + J^{n-1}(\tilde{M}(x)). \end{aligned} \tag{4.9}$$

We then define a cumulative function which integrates over Eq.(4.9) as in Eq.(4.6),

$$T(x) = \lim_{n\to\infty} T^n(x) = \int_0^x J^n(y)dy. \tag{4.10}$$

Due to the chaotic nature of the map $M(x)$, $J^n(x)$ will be a very complicated step function for high values of n, hence in the limit $n \to \infty$ $T(x)$ will be a fractal function exhibiting non-trivial fine scale structure (Dorfman [1999]; Klages [1996, 2007]; Knight and Klages [2011b]). By combining Eq.(4.9) and Eq.(4.10) we can solve $T(x)$ as a functional recursion relation. We use the conditions that $T(0) = T(1) = 0$ and that the function $T(x)$ is continuous to obtain

$$T(x) = \begin{cases} \frac{1}{2}T(2x) & 0 \le x < a_1 \\ \frac{1}{2}T(2x) + x - a_1 & a_1 \le x < a_2 \\ \frac{1}{2}T(2x) + a_2 - a_1 & a_2 \le x < \frac{1}{2} \\ \frac{1}{2}T(2x-1) + a_2 - a_1 & \frac{1}{2} \le x < a_3 \\ \frac{1}{2}T(2x-1) + 1 - x - a_1 & a_3 \le x < a_4 \\ \frac{1}{2}T(2x-1) & a_4 \le x \le 1 \end{cases} . \tag{4.11}$$

Repeated application of the recurrence relation means we can solve Eq.(4.11) as an infinite sum,

$$T(x) = \lim_{n\to\infty} \sum_{k=0}^{n} \frac{1}{2^k} t(\tilde{M}^k(x)), \tag{4.12}$$

where

$$t(x) = \begin{cases} 0 & 0 \leq x < a_1 \\ x - a_1 & a_1 \leq x < a_2 \\ a_2 - a_1 & a_2 \leq x < a_3 \\ 1 - x - a_1 & a_3 \leq x < a_4 \\ 0 & a_4 \leq x \leq 1 \end{cases} . \tag{4.13}$$

Eq.(4.6) can now be evaluated in terms of the functional recursion relation of Eq.(4.11) as

$$\begin{aligned} D &= \lim_{n\to\infty} \left(\int_0^1 v_0(x) \sum_{k=0}^{n} v_k(x) dx \right) - \frac{1}{2} \int_0^1 v_0^2(x) dx \\ &= \lim_{n\to\infty} \left(\int_{a_1}^{a_2} J^n(x) dx - \int_{a_3}^{a_4} J^n(x) dx \right) - h \\ &= T(a_2) - T(a_1) - T(a_4) + T(a_3) - h. \end{aligned} \tag{4.14}$$

Finally, due to the condition that I_L and I_R are symmetrically positioned, $T(x)$ is a symmetric function. We can use this to simplify Eq.(4.14) to

$$D = 2T(a_2) - 2T(a_1) - h. \tag{4.15}$$

Eq.(4.15) and Eq.(4.12) provide us with a very efficient way to evaluate the diffusion coefficient for any choice of position or size of I_L and I_R. For a more detailed discussion of this method see for example Gaspard and Klages [1998]; Klages [1996, 2007]; Knight and Klages [2011a,b] or chapter 2 of this thesis. We will evaluate Eq.(4.15) for a series of choices in the following section.

4.3 Analyzing the diffusion coefficient

In this section we look at how the diffusion coefficient varies with the position of the escape holes and the asymptotic behaviour as the hole size goes to zero.

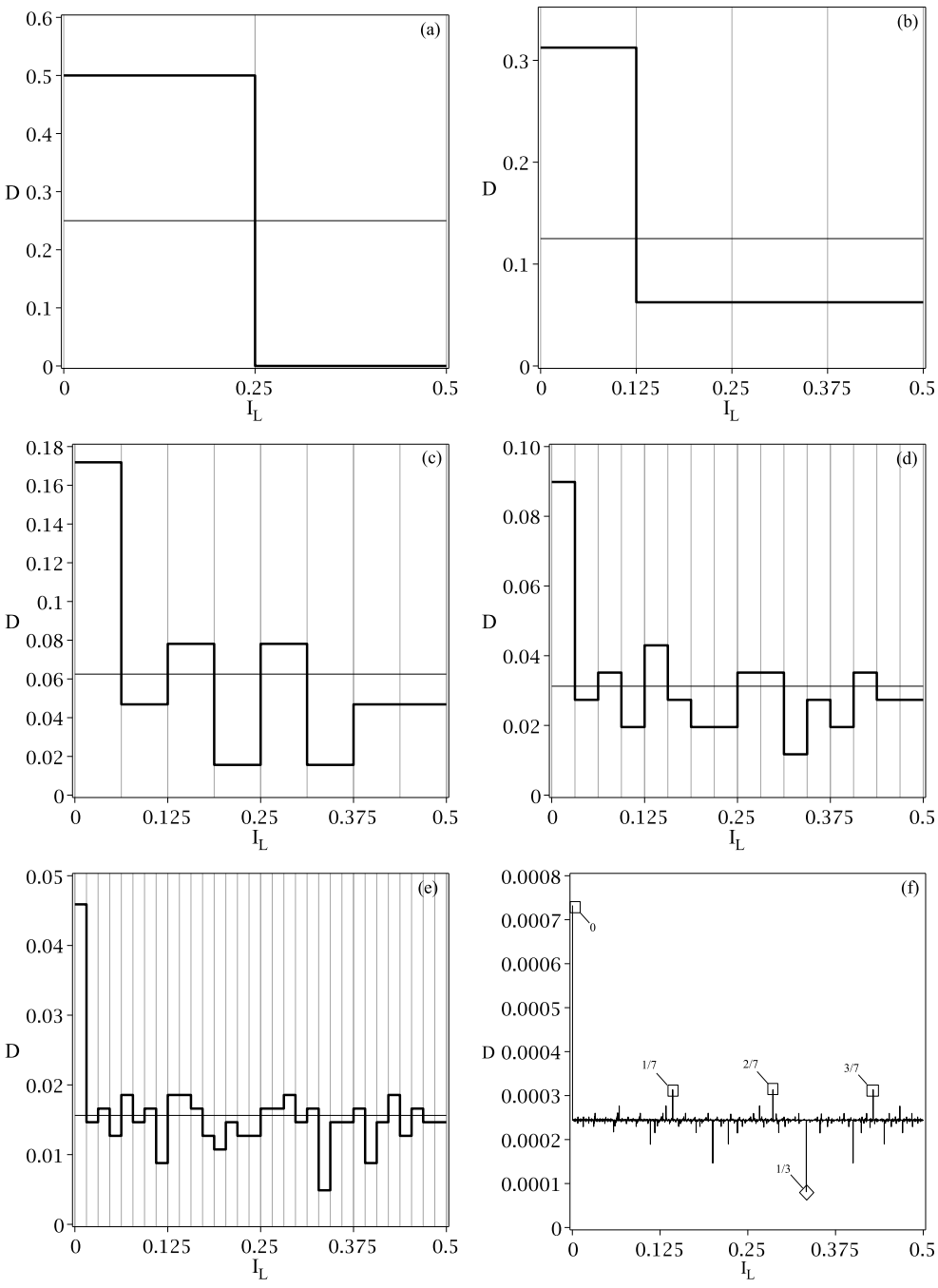

Figure 4.1: *The diffusion coefficients* In these figures the diffusion coefficient D is illustrated for the doubling map $M(x)$ as a function of the position of the escape hole I_L of size $1/2^s$. In (a), (b), (c), (d), (e) and (f) it is $s = 2, 3, 4, 5, 6$ and 12 respectively. D is given by the thick black lines whilst the escape intervals are highlighted by the thin vertical lines. The thin horizontal lines are a guide to show the average value $1/2^s$. The symbols in (f) refer to specific periodic orbits as discussed in the text.

4.3.1 Position dependence

We evaluate Eq.(4.15) in a specialised setting where we restrict I_L and I_R to Markov intervals. That is, we choose the points $a_i, (i \in \{1,2,3,4\})$ to be dyadic rationals, i.e., for some fixed integer $s > 0$ the points a_i are of the form $r/2^s$ with $r \in \mathbb{Z}$ and $0 \leq r \leq 2^s$. The points a_i will then be pre-images of $1/2$ under the map $\tilde{M}(x)$. As $T(0.5) = a_2 - a_1$, $T(a_i)$ can be evaluated with a finite sum rather than the infinite sum of Eq.(4.12). For each value of s there are 2^{s-1} places to position an interval I_L of size 2^{-s}, with I_R being determined by the symmetry condition. We can evaluate the diffusion coefficient at each of these choices via Eq.(4.15) and compare the results as the choices vary. For example, when $s = 1$ there is only one choice for I_L, namely $a_1 = 0, a_2 = 1/2$, exactly corresponding to a simple random walk, with $1/2$ probability of moving left or right at each step. The diffusion coefficient for this system is well known to be $1/2$, in agreement with the more general expressions given here, Eq.(4.8) for $h = 1/2$ and Eq.(4.15), as

$$\begin{aligned} D &= 2T(1/2) - 2T(0) - (1/2) \\ &= 1/2. \end{aligned} \tag{4.16}$$

For higher values of s the diffusion coefficient varies with the position of the escape holes, see figure 4.1. We see a step function that behaves increasingly erratically as the partition is refined and s is increased. We further note that the average of this step function can be calculated to be $\langle D_s \rangle = 2^{-s} = h$ for a given s, which is the simple random walk solution of Eq.(4.8).

The structure of the step functions in figure (4.1) can be explained in terms of the periodic orbits of the map $\tilde{M}(x)$ which correspond to *standing* or *running* orbits of $M(x)$ (Cvitanović et al. [2010]; Klages [2007]; Korabel and Klages [2004]). For example, if an image of I_L overlaps I_R, one will find a lot of backscattering in the system, i.e., points that escape the unit interval via I_L find themselves getting sent back via I_R (and vice versa). This has the result of decreasing the diffusion coefficient relative to the random walk solution derived in Eq.(4.8). In order to find intervals where this overlap occurs, we look for standing orbits by solving the simple equation $\tilde{M}^p(x) = x$ where $\tilde{M}^q(x) = 1 - x$ for $q < p$. Due

to the symmetry of the escape intervals, the image of I_L containing the solution of this equation will, after q iterations, overlap with I_R and backscattering will occur. The smaller values of p will correspond to values of x which give the most overlap and hence the most backscattering. For example,

$$\tilde{M}(x) = 1 - x, \quad x \in [0, 0.5], \quad \Rightarrow x = \frac{1}{3}. \tag{4.17}$$

Therefore if one places I_L so that $x = 1/3$ is in its interior, one will find the system has a relatively small diffusion coefficient due to the backscattering. This phenomenon is highlighted in figure 4.1 and is therefore due to *standing* orbits (Klages [2007]; Korabel and Klages [2004]).

Alternatively, if the image of I_L overlaps with itself consistently then one will find a higher diffusion coefficient. This is due to the presence of *running* orbits (Cvitanović et al. [2010]; Klages [2007]; Korabel and Klages [2004]) in such a system. In order to find such orbits, we solve the simple equation $\tilde{M}^p(x) = x$ where $\tilde{M}^q(x) \neq 1 - x$ for $q < p$. For example $p = 1$ gives

$$\tilde{M}(x) = x, \quad x \in [0, 0.5], \quad \Rightarrow x = 0, \tag{4.18}$$

and we can see in figure 4.1 that when the escape interval contains the point $x = 0$ one has a high diffusion coefficient relative to the simple random walk result. When $p = 2$,

$$\tilde{M}^2(x) = x, \quad \Rightarrow x = 0, \frac{1}{3}. \tag{4.19}$$

we can immediately throw the solution $x = 1/3$ away as this result corresponds to $\tilde{M}(x) = 1 - x$. However, for $p = 3$

$$\tilde{M}^3(x) = x, \quad \Rightarrow x = 0, \frac{1}{7}, \frac{2}{7}, \frac{3}{7}, \tag{4.20}$$

and again we see in figure 4.1 that these values correspond to relatively high diffusion coefficients when they are in the interior of I_L. This process of pinpointing standing and running periodic orbits can be continued for higher iterations with relative ease as we are dealing with a full shift map and there is no need to prune any solutions. This technique helps explain the increasingly complicated step

function that one obtains as s is increased.

At first sight, the step functions illustrated in figure 4.1 do not appear to contain much interesting structure. However, upon closer inspection we notice that every 'parent' hole of size 2^{-s} and associated diffusion coefficient D_s splits into two 'child' holes of size $2^{-(s+1)}$ and associated diffusion coefficients D^0_{s+1} and D^1_{s+1} respectively, such that

$$D_s \;\; = \;\; 2D^0_{s+1} + 2D^1_{s+1} - 2^{-s}. \tag{4.21}$$

where superscripts $0, 1$ correspond to left and right child hole respectively. To see this, one first needs to define cumulative functions $T^0(x)$ and $T^1(x)$ for the respective left and right child holes. Now since the cumulative functions are additive with respect to the holes we have that $T(a_i) = T^0(a_i) + T^1(a_i)$ for $i = 1 \ldots 4$. Moreover, since the iterate of the parent hole endpoint a_i always avoids both parent and child holes then $T^0(a_i) = T^1(a_i)$. Finally, considering the midpoint $a_m = (a_2 + a_1)/2$ of the parent hole which is also the right and left endpoint of the left and right child holes respectively, it follows from Eq.(4.11) that $T^0(a_m) - T^1(a_m) = (a_2 - a_1)/2$. Eq.(4.21) follows after expanding in terms of T^0 and T^1 and substituting the above relations. Notice that recursive iteration of Eq.(4.21) n times gives an expression for D_s in terms of the 2^n child diffusion coefficients

$$D_s = (1 - 2^n)2^{-s} + 2^n \sum_{j \in \{0,1\}^n} D^j_{s+n}, \tag{4.22}$$

where the sum runs over all 2^n binary permutations of length n. Rearranging this we find

$$\frac{D_s - 2^{-s}}{2^{-s}} = \sum_{j \in \{0,1\}^n} \frac{D^j_{s+n} - 2^{-s-n}}{2^{-s-n}} \tag{4.23}$$

that is, the relative deviation of each diffusion coefficient from its mean is exactly additive.

The above scaling and self-similarity structure (often considered to be properties of fractal structures) of the step functions illustrated in figure 4.1 can be further investigated by defining a set of continuous, cumulative functions which integrate over the step function, in the same way that $T(x)$ integrates over the

step function $J^n(x)$. In order to define such a function, $\Phi_s(x)$, for a given s, we firstly subtract the average diffusion coefficient $\langle D_s \rangle = 1/2^s$, and integrate over the resulting step function. We then normalise this integral by multiplying it with 2^{s+1} so that it can be easily compared with other values of s. Let

$$\Phi_s(x) = 2^{s+1} \int_0^x \left(D(y) - 2^{-s} \right) \quad dy, \tag{4.24}$$

where $D(y)$ refers to the diffusion coefficient of the dyadic interval I_L containing y. The solution to Eq.(4.24) is illustrated for several examples of s in figure 4.2. We see that as s increases, Eq.(4.24) becomes a fractal function exhibiting non-trivial fine scale structure and regions of scaling and self-similarity. This structure is symptomatic of the dense set of periodic orbits which exists in $\tilde{M}(x)$. In the limit of s going to infinity, each periodic orbit makes the diffusion coefficient deviate from the average hence one obtains a dense step function. When this function is integrated over one sees a function that contains a dense set of maxima and minima, hence a fractal.

4.3.2 Asymptotic behaviour

In this subsection, we will analyze the behaviour of the diffusion coefficient as the hole size $h = a_2 - a_1$ goes to zero. By doing this, the hole will converge to a point which could be a running orbit, a standing orbit, or a non-periodic orbit. We derive equations which give the asymptotic behaviour in all three cases and use them to obtain the diffusion coefficient in terms of all periodic orbits in a hole of small but finite size. In order to do this, we first rewrite the $(T(a_2) - T(a_1))$ term from Eq.(4.15) with Eq.(4.12) to

$$\begin{aligned} &T(a_2) - T(a_1) = \\ &\lim_{n\to\infty} \sum_{k=0}^{n} \frac{1}{2^k} \left(t\left(\tilde{M}^k\left(a_2\right)\right) - t\left(\tilde{M}^k\left(a_1\right)\right)\right). \end{aligned} \tag{4.25}$$

First consider the case that I_L converges to a running orbit, that is, a periodic point x_p of period p, which does not enter I_R under forward iteration. In this

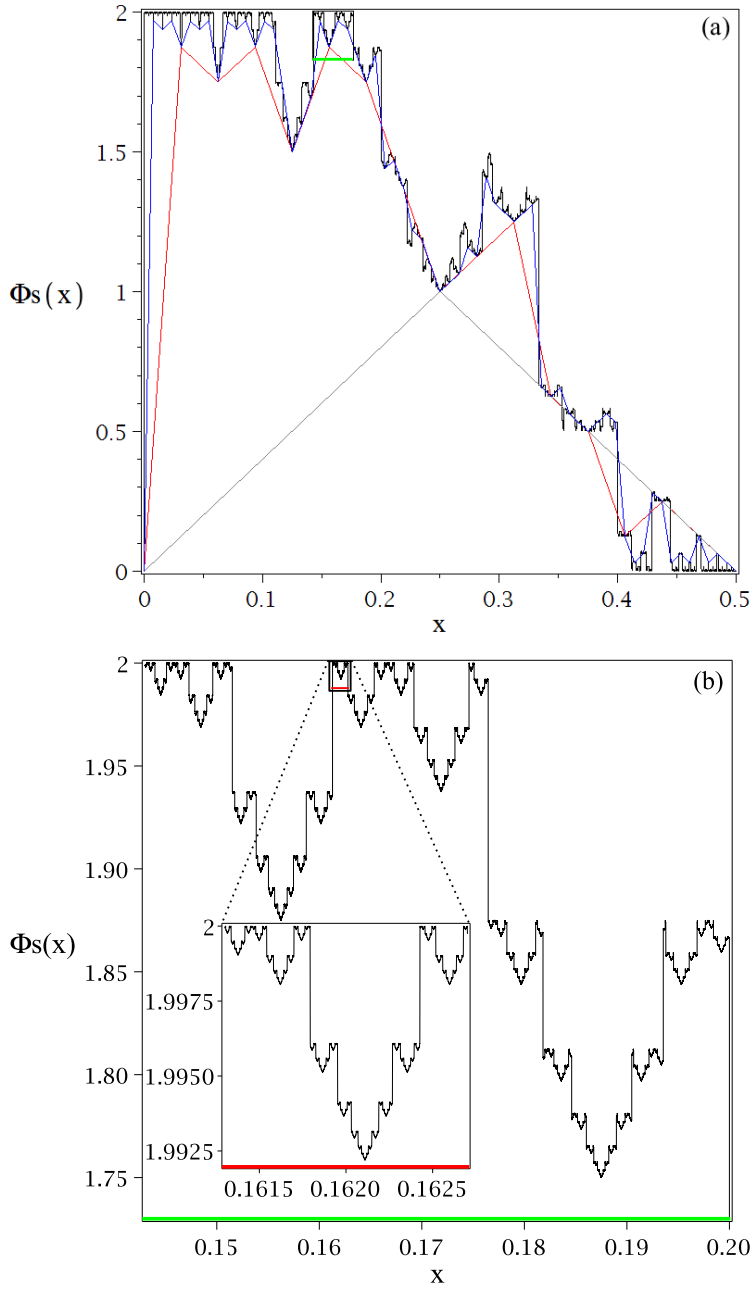

Figure 4.2: *Cumulative integral function* $\Phi_s(x)$. In this figure the self similarity and scaling that one sees by integrating over the position dependent diffusion coefficient for the doubling map is illustrated. In (a) the structure is seen emerging as the hole size $1/2^s$ is decreased. From $(0.1, 0)$ upwards, $s = 2$ (grey), $s = 5$ (red), $s = 8$ (blue) and $s = 20$ (black). In (b) the region highlighted in (a) is blown up whilst the inset shows the highlighted region in (b) blown up in order to illustrate the self similarity and non-trivial fine-scale structure of the diffusion coefficient.

case, from Eq.(4.13) we see that the only contributions to Eq.(4.25) come when $k = lp, l \in \mathbb{N}$

$$\begin{aligned} T(a_2) - T(a_1) &\sim \lim_{n\to\infty} h\left(\sum_{l=0}^{n} \frac{1}{2^{lp}}\right) \quad (h \to 0) \\ &= h\left(\frac{1}{1-2^{-p}}\right) \quad (h \to 0)\,. \end{aligned} \tag{4.26}$$

Evaluating Eq.(4.15) with Eq.(4.26) we get

$$D(x_p) \sim hJ_p^r = h\left(\frac{1+2^{-p}}{1-2^{-p}}\right) \quad (h \to 0)\,, \tag{4.27}$$

where the superscript r denotes a running orbit. Now consider the case where I_L converges to a standing orbit, that is, a periodic point x_p of period p, which enters I_R under forward iteration. Note that due to the symmetry of the holes this will always occur at time $p/2$ and hence standing orbits always have even periods. In this case we get a positive contribution to Eq.(4.25) when $k = lp$, and a negative contribution when $k = lp/2$,

$$\begin{aligned} T(a_2) - T(a_1) &= \lim_{n\to\infty} h\left(\sum_{l=0}^{n} \frac{(-1)^l}{2^{\frac{lp}{2}}}\right) \quad (h \to 0) \\ &\sim h\left(\frac{1}{1+2^{-\frac{p}{2}}}\right) \quad (h \to 0)\,. \end{aligned} \tag{4.28}$$

In this case Eq.(4.15) evaluates as

$$D(x_p) \sim hJ_p^s = h\left(\frac{1-2^{-\frac{p}{2}}}{1+2^{-\frac{p}{2}}}\right) \quad (h \to 0)\,. \tag{4.29}$$

The final case to consider is where I_L converges to a point which is non-periodic. In this setting the only contribution to Eq.(4.25) comes from the $k = 0$ term and therefore

$$D \sim J_p^n h = h \quad (h \to 0)\,, \tag{4.30}$$

which reproduces the simple random walk result. In summary, we have

$$D \sim J_p^{\wp} h = \begin{cases} h\frac{1+2^{-p}}{1-2^{-p}} & \wp = r \\ h\frac{1-2^{-p/2}}{1+2^{-p/2}} & \wp = s \\ h & \wp = n \end{cases} . \tag{4.31}$$

Eq.(4.31) gives us a good explanation for the structure that we see in figure 4.1 with improved agreement for small holes (large s). As s is increased, the different asymptotic regimes can be seen in the step function. For example, when I_L is placed on a running orbit such as $x = 0$ where $p = 1$, Eq.(4.27) tells us that $D = 3h$ for small h. When I_L is placed on a standing orbit like $x = 1/3$ with $p = 2$, Eq.(4.29) tells us that $D = h/3$ for small h. These deviations from the average value of h are observed in figure 4.1.

A further consequence of Eq.(4.31) is the intriguing result that for small hole size, one can not rely on the simple random walk approximation for an accurate description of the diffusion coefficient (Fujisaka and Grossmann [1982]; Klages [1996]; Klages and Dorfman [1997]; Schell et al. [1982]). Rather, one must go beyond this theory and take into account the periodic orbit structure of the system, and in particular, the periodic orbits contained in the escape holes. The asymptotic regime that one obtains for small h will be dependent upon the type of point that the escape holes converge to. The authors are aware of only one other published result on a one-dimensional system in which the random walk approximation theory is violated (Knight and Klages [2011b]). In this case the phenomenon was explained in terms of ergodicity breaking, which is not the case here.

We can now go beyond the small hole limit by combining the above results with the parent-child hole relation of Eq.(4.22). For large n we have that

$$D_{s+n} = 2^{-s-n} J_p^{\wp} \quad (n \to \infty) , \tag{4.32}$$

with $\wp \in \{r, s, n\}$ depending on the limiting point of the hole as in Eq.(4.31). Hence, we may now express D_s in terms of all periodic orbits of period p which

intersect the holes,

$$D_s = 2^{-s}\left(1 + \sum_p (J_p^{\wp} - 1)\right) \quad (n \to \infty)\,. \tag{4.33}$$

Note that a periodic orbit that intersects the parent hole more than once just gets added each time. Also, as discussed below, all periodic orbits are counted as running if they occur at the end of the interval. Eq.(4.33) suggests that the observed fluctuations of D_s from its average $\langle D_s \rangle = 2^{-s}$ are due to the individual fluctuations of the infinitely many periodic orbits which intersect the holes.

As expected from periodic orbit theory (Cvitanović et al. [2010]), a very large number of periodic orbits is needed to trace the hole accurately. However, if the periodic orbits are ordered appropriately the sum may be truncated to produce good approximations to D_s (Dettmann and Morriss [1997]). Note that the optimal ordering (for fast convergence) of periodic orbits is by a modified version of the length of the orbit; $J^r_{p_1} \approx J^s_{p_2}$ for $2p_1 \approx p_2$. In other words backscattering is much more dominant for orbits of equal period (see figure 4.3).

We can further study the asymptotic behaviour for the three different cases derived above and the finite hole size result by reducing I_L continuously. Figure 4.3.(a) illustrates these different regimes.

When using Eq.(4.31), care needs to be taken when I_L converges to a point from the left or the right, i.e., it is not centred on a point and reduced in size. In this case a boundary point of the escape region, a_1 or a_2, is kept fixed. If the boundary point is periodic, points near it in the interior of I_L miss I_R, and so it is always a running orbit. For example, as illustrated in figure 4.1 and figure 4.3.(a), $x = 1/3$ is a period two standing orbit when $1/3$ is in the interior of I_L and the asymptotic regime for small h when I_L converges to $1/3$ is given by Eq.(4.29) as $h/3$. However, if $a_1 = 1/3$ is fixed and h goes to zero, we must use Eq.(4.27) to evaluate the asymptotic regime as in this case $1/3$ is a running orbit. Eq.(4.27) tells us that the asymptotic regime is in fact $5h/3$. This additional topological subtlety that must be considered is illustrated in figure 4.3.(b).

Another interesting feature that we find in this system is that reducing the size of the escape holes can sometimes have no effect on the diffusion coefficient. As

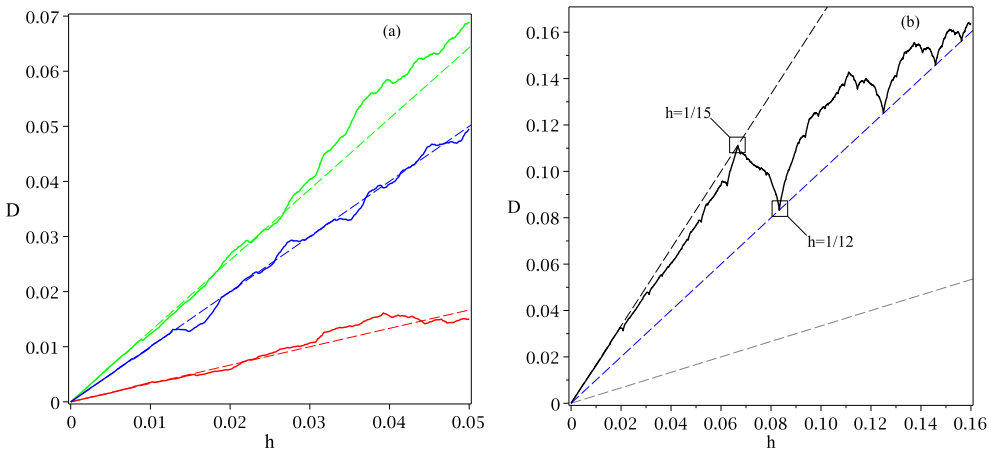

Figure 4.3: *The asymptotic regimes* In (a) the diffusion coefficient $D(h)$ for escape holes centred on three different classes of points in $M(x)$ is illustrated as a function of the hole size h (from top to bottom); $x = 1/3$ a standing orbit (red), $x = \sqrt{5}/2 - 17/25$ a non-periodic orbit (blue) and $x = 1/7$ a running orbit (green) along with the different asymptotic regimes $h/3$, h and $9h/7$ respectively shown by dashed lines. These asymptotic regimes correspond to the result of Eq.(4.31). In (b), the position of the left boundary of the hole $a_1 = 1/3$ is fixed and h is again decreased continuously. We observe that $x = 1/3$ becomes a running orbit when a critical point, and the asymptotic regime of $5h/3$ (black dashed, top) illustrates this. The line $h/3$ (grey dashed, bottom) is what one would expect if $x = 1/3$ was contained in I_L yielding a standing orbit, and the random walk solution is given by the blue dashed line (middle). The two symbols (squares) identify parameter values where the right boundary point a_2 of the hole generates a standing orbit, respectively a running orbit.

we calculated in Eq.(4.16), if the escape holes are $I_L = [0, 0.5]$ and $I_R = [0.5, 1]$, the diffusion coefficient is equal to 0.5. However, we can reduce the escape hole so that $I_L = [0, 0.25]$ and $I_R = [0.75, 1]$ and the diffusion coefficient remains equal to 0.5 as illustrated in figure 4.1.(a). We also see that if the escape holes are $I_L = [0.25, 0.5]$ and $I_R = [0.5, 0.75]$, the diffusion coefficient is equal to 0. This is due to a simple trapping mechanism in which no diffusion occurs. In addition, reducing the size of the escape holes can result in an increase of the diffusion coefficient, i.e., the diffusion coefficient decreases non-monotonically in some regions as the size of the escape holes is decreased. One can check this by comparing the figures in figure 4.1. One can also observe this phenomenon by

looking at the fractal structure illustrated in figure 4.3.(b). While $a_1 = 1/3$ is fixed, the various maxima and minima that we see can be explained by looking at the orbit of the point a_2. We see that when $a_2 = 5/12$ (corresponding to $h = 1/12$), the orbit of a_2 is a standing orbit and hence we see a striking minimum in the diffusion coefficient. If we reduce h so that $h = 1/15$ with $a_2 = 2/5$, the orbit of a_2 is now a running orbit and we observe a maximum in the diffusion coefficient. These points are highlighted in figure 4.3.(b). This explanation in terms of topological instability under parameter variation is discussed further in Klages [1996, 2007]; Klages and Dorfman [1995]; Knight and Klages [2011b].

4.4 The escape rate

The escape rate theory of diffusion has established an exact analytical relationship between the escape rate of a spatially extended diffusive dynamical system with absorbing boundaries and its diffusion coefficient (Dorfman [1999]; Gaspard [1998]; Gaspard and Nicolis [1990]; Klages [1996, 2007]). However, motivated by Bunimovich and Yurchenko [2011]; Keller and Liverani [2009] where the complicated dependence of the escape rate on position and size of a hole has been studied, here we focus on the relationship between the open map $\tilde{M}(x)$ on the unit interval with the escape holes I_L and I_R serving as absorbing regions and the diffusion coefficient of the corresponding coupled, spatially extended system. That is, for calculating the escape rate any orbit that enters either of these intervals is removed from the system, and in this way points from an initial density escape, while for calculating the diffusion coefficient all points remain within the system by performing 'jumps' when hitting these intervals, as defined by the lift Eq.(4.3). An interesting question is to which extent the coupled diffusive 'jump dynamics' of the spatially extended system is already captured by the escape rate of the interval map that defines the unit cell of this lattice.

The main result from Bunimovich and Yurchenko [2011] concerning the escape rate is that escape will occur fastest through a hole whose minimal period is highest, or equivalently, the escape rate will be slowest through the hole which has the smallest minimal period. By minimal period we mean the smallest period of all the periodic points in a hole.

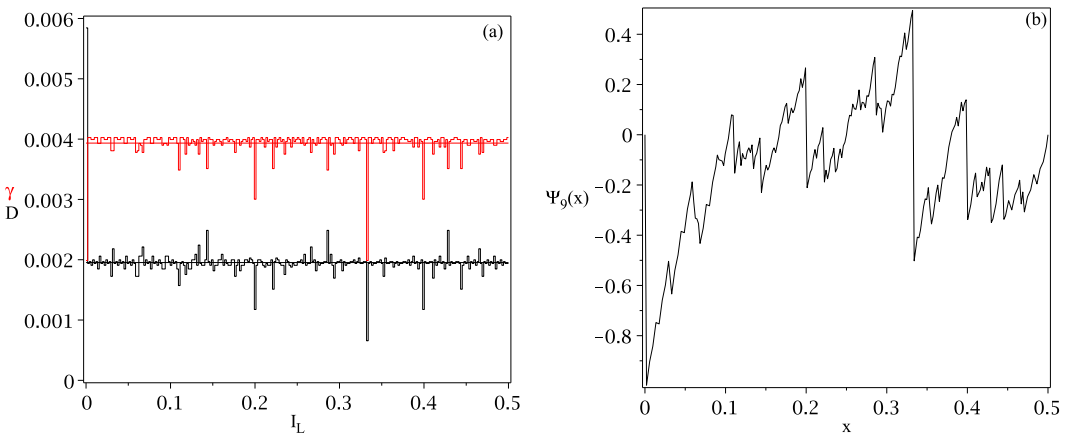

Figure 4.4: *Comparing the diffusion coefficient with the escape rate.* In figure **(a)**the diffusion coefficient for the doubling map is illustrated in black (bottom) alongside the escape rate of the corresponding open system in red (top) as a function of the escape interval I_L. The thin horizontal lines illustrate the average value to aid visual comparison of the fluctuations: $< D >= 1/2^9$ and $< \gamma > \simeq 0.00393$ (3s.f.) $\simeq 1/2^8$. There is a clear relationship between the structure of these functions although intervals which give relatively high diffusion coefficients will give relatively low escape rates. The calculation has been performed for intervals I_L of size $1/2^9$. In **(b)** the corresponding cumulative integral function $\Psi_s(x)$ for the escape rate with $s = 9$ is illustrated, displaying the fractal structure of the escape rate.

In order to calculate the escape rate of our system we look at the transition matrix induced by the dynamics. The escape rate γ can be evaluated via the largest eigenvalue ν of this transfer matrix (Gaspard [1998]; Gaspard and Klages [1998]; Klages [1996, 2007]; Klages and Dorfman [1995])

$$\gamma = -\ln \nu. \tag{4.34}$$

In figure 4.4.(a) solutions to Eq.(4.34) are illustrated for $s = 9$ and compared with the diffusion coefficient in the corresponding extended system. In analogy with Eq.(4.24), we can define a function $\Psi_s(x)$ which integrates over the step-function escape rate to give a cumulative function which exposes the self-similarity and fractal structure, this is illustrated in figure 4.4.(b). In figure 4.4.(a) we observe structural similarities between the escape rate and the diffusion coefficient, with

deviations from the average occurring for both phenomena on the same intervals. In order to quantify these deviations we can compare Eq.(4.31) with Theorem 4.6.1 from Bunimovich and Yurchenko [2011], which is a special case of Theorem 2.1 from Keller and Liverani [2009]. It gives the escape rate for small hole size in the doubling map with one escape hole and can easily be generalised to escape through two holes as is the case here. This theorem states that the escape rate for small h with a running orbit (no iterate of the orbit reaches the second hole) is given by

$$\frac{\gamma(x_p)}{h} \to 2\left(1 - \frac{1}{2^p}\right) \quad (h \to 0)\,, \tag{4.35}$$

where x_p is the lowest period point in the escape interval with period p. For a standing orbit (the periodic orbit is in both holes) the period is effectively halved and we get

$$\frac{\gamma(x_p)}{h} \to 2\left(1 - \frac{1}{2^{p/2}}\right) \quad (h \to 0)\,. \tag{4.36}$$

When the escape interval converges to a non-periodic point, the theorem states that the escape rate is given by

$$\frac{\gamma(x)}{h} \to 2 \quad (h \to 0)\,. \tag{4.37}$$

From Eq.(4.35) the relative deviation from the average escape rate $\langle\gamma\rangle = 2h$ is given by

$$\gamma(x_p) - \langle\gamma\rangle = -\frac{2h}{2^p}. \tag{4.38}$$

for a running orbit and

$$\gamma(x_p) - \langle\gamma\rangle = -\frac{2h}{2^{p/2}}. \tag{4.39}$$

for a standing orbit. Similarly, the relative deviation from the average diffusion coefficient $\langle D\rangle = h$, for a running orbit, can be obtained from Eq.(4.27) as

$$D(x_p) - \langle D\rangle = \frac{2h}{2^p - 1}, \tag{4.40}$$

whilst for standing orbits, via Eq.(4.29), the relative deviation is given by

$$D(x_p) - \langle D \rangle = -\frac{2h}{2^{p/2}+1}, \tag{4.41}$$

Eqs.(4.38),(4.39),(4.40) and (4.41) help us explore the relationship between the diffusion coefficient of the extended system with the escape rate of the open system. An obvious difference is the absence of backscattering in the escape rate. However a more striking one is that the average escape rate does not equal the algebraic mean of all escape rates as for diffusion coefficients. That is $\langle \gamma \rangle \neq \frac{1}{2^{s-1}} \sum_{j=1}^{2^{s-1}} \gamma_s^j$ which is obvious from figure 4.4 but is also suggested by Eq.(4.35). The two symmetric holes are coupled differently for the escape problem and in a much more complicated way than as in Eq.(4.21) by involving the eigenvalues of $2^{s-1} \times 2^{s-1}$ transfer matrices. However, for small holes this coupling decays rapidly revealing the similarities which are seen in figure 4.4.

4.5 Conclusion

In this chapter we have analytically derived the diffusion coefficient for a one-dimensional, piecewise-linear dynamical system as a function of the size and position of the coupling regions of the dynamics which we called 'escape holes'. We showed that the diffusion coefficient is a complicated function of the position and a non-monotonic function of the size of the escape holes, despite the fact that the underlying reduced dynamics is not changed, as is the case in previously studied models (Gaspard and Klages [1998]; Klages [2007]; Klages and Dorfman [1995]; Knight and Klages [2011b]).

We found that the asymptotic regime that one obtains for small hole size is a function of the type of periodic orbit that the escape holes converge to. This result implies that the simple uncorrelated random walk approximation may not always give accurate estimates for the diffusion coefficient of a system. We have obtained an expansion for the diffusion coefficient of finite size holes in terms of periodic orbits and discussed their relative importance. In our setting, a periodic orbit can either be a running or a standing orbit. The presence of a standing orbit has the effect of reducing the diffusion coefficient relative to the average

value whilst the presence of a running orbit has the effect of increasing it relative to the average value.

We numerically calculated the escape rate of the corresponding open system and compared it with the diffusion coefficient. We found that the diffusion coefficient and escape rate are both dependent upon the underlying periodic orbit structure of the map, although subtle differences arise which we explain as a difference in the coupling between holes.

An interesting open question is to which extent the above effects can be observed in computer simulations of diffusion in higher dimensional, more physically realistic systems such as suitably adapted periodic Lorentz gases (Gaspard [1998]; Klages [2007]) and related particle billiards (Harayama and Gaspard [2001]; Harayama et al. [2002]). We conjecture that these phenomena may even be observable in cold atom experiments on atom-optics billiards (Friedman et al. [2001]; Milner et al. [2001]).

Chapter 5

We knead the diffusion coefficient

In this chapter we look at an alternative method to the functional recursion relation discussed in Chapter 2 for fully analytically evaluating the parameter dependent diffusion coefficient of a periodically lifted one-dimensional map. The method we employ is based upon finding the zeros of dynamical zeta functions via the orbits of the critical points called the kneading orbits. We will look at how the dynamical zeta function is related to the generating function for diffusion before defining a 'kneading determinant' which in turn is related to the dynamical zeta function via its zeros. We will then analytically evaluate the kneading determinant for the full parameter range and from this obtain the diffusion coefficient.

5.1 Introduction

In chapter 2 we saw how a physically intuitive method for determining the diffusion coefficient via a functional recursion relation was essentially based upon the orbits of the critical points of the dynamical system. These orbits called 'kneading orbits' (see for example Devaney [1989]; Katok and Hasselblatt [1995]) were encoded into the solutions of fractal 'generalised Takagi functions'. In this chapter we approach things the other way around and we will derive the diffusion coefficient using the kneading orbits as a starting point.

In Milnor and Thurston [1988],the determinant of a certain kneading matrix of

an interval map was related to the corresponding topological zeta function. The elements of this kneading matrix are infinite order formal polynomials whose coefficients are defined by the kneading orbits of the critical points. The 'topological' or 'Artin-Mazur' zeta function counts periodic points of a dynamical system and encodes information about the topological entropy into its leading zero (see for example Cvitanović et al. [2010]). Therefore, the result of Milnor and Thurston permitted the evaluation of the topological entropy by considering only the trajectories of a finite number of points rather than having to take into account the evolution of the entire density. Before this result, one needed to resort to a periodic orbit expansion of the zeta function, a technique hampered by the rate at which the number of periodic orbits of a dynamical system increases with orbit length, this rate actually being given by the topological entropy itself. This topic of expansion techniques is extensively discussed in the online 'chaos book', see Cvitanović et al. [2010] and references therein.

The result of Milnor and Thurston was extended in Baladi and Ruelle [1994] to zeta functions that take into account a constant weight function on the orbits. Baladi and Ruelle were able to show that the determinant of a weighted kneading matrix was equal to the dynamical zeta function multiplied by a certain rational function. The dynamical zeta function is also known as the generalised dynamical zeta function (Cristadoro [2006]), Ruelle zeta function (Baladi and Keller [1990]), Ruelle dynamical zeta function (Baladi [1998]), weighted dynamical zeta function (Baladi [1995]), zero-order Ruelle zeta function (Cvitanovic and Pikovsky [1993]) and probably other variants. We will stick with the terminology of Cvitanović et al. [2010] and refer to it as the dynamical zeta function. The dynamical zeta function is of interest in this current setting as it was shown in Baladi and Keller [1990] that the zeros of the dynamical zeta function are related to the eigenvalues of the corresponding weighted transfer operator, a generalisation of the Perron-Frobenius operator that includes a constant weight function. In turn, the weighted Perron-Frobenius operator can be used to study the diffusion coefficient of a dynamical system via the generating function for diffusion (Dorfman [1999]).

In Cristadoro [2006] the Baladi-Ruelle generalisation of Milnor and Thurstons result was used to construct a weighted kneading matrix whose determinant could be explicitly related to the parameter dependent diffusion coefficient of a one-

dimensional map where the gradient is varied as a parameter (Klages and Dorfman [1995]). In this chapter we will apply the method used in Cristadoro [2006] to the piecewise linear map studied in chapter 2 where the parameter lifts the branches of the map. This map has the advantage that we can derive a relatively simple expression for the parameter dependent diffusion coefficient. This allows us to analyse the convergence of the diffusion coefficient under this method in depth.

In section 5.2 we will look at how the diffusion coefficient of a dynamical system is related to the zeros of a particular dynamical zeta function. We will then look at how to analytically derive the weighted kneading determinant for a simple piecewise linear map of the real line in section 5.3. Conclusions are drawn in section 5.4.

5.2 Generating zeta functions

In this section we will look at how the dynamical zeta function is related to the generating function for diffusion. The objective is to give the main ideas underpinning the theory. A more detailed study of this material is covered in Cvitanović et al. [2010] and relevant material can also be found in Artuso [2000]; Cvitanovic and Pikovsky [1993].

5.2.1 The generating function

Consider a one-dimensional hyperbolic map $f(x) : \mathbb{R} \to \mathbb{R}$ defined periodically such that

$$f(x+n) = f(x) + n \quad n \in \mathbb{R} \tag{5.1}$$

As discussed in previous chapters, a density of points on a given interval will spread out under iteration of Eq.(5.1) and can display diffusion, this phenomena being first observed in Geisel and Nierwetberg [1982]; Grossmann and Fujisaka [1982]; Schell et al. [1982]. The function

$$Q(\beta) = \lim_{t\to\infty} \frac{1}{t} \ln \left\langle e^{\beta\left(f^t(x)-x\right)} \right\rangle \tag{5.2}$$

where the angular brackets represent an average taken over the initial density of points is a diffusion 'generating function' because the derivatives with respect to the variable β give the moments of the deterministic process generated by the dynamical system of Eq.(5.1). In particular, the first derivative evaluated at $\beta = 0$,

$$\begin{aligned} \left.\frac{\partial Q(\beta)}{\partial \beta}\right|_{\beta=0} &= \lim_{t\to\infty} \frac{1}{t} \left.\frac{\left\langle (f^t(x) - x)\, e^{\beta\left(f^t(x)-x\right)} \right\rangle}{\left\langle e^{\beta(f^t(x)-x)} \right\rangle}\right|_{\beta=0} \\ &= \lim_{t\to\infty} \frac{1}{t} \left\langle f^t(x) - x \right\rangle, \end{aligned} \tag{5.3}$$

gives the drift of the process. Whilst we can see that the second derivative evaluated at $\beta = 0$,

$$\left.\frac{\partial^2 Q(\beta)}{\partial \beta^2}\right|_{\beta=0} = \lim_{t\to\infty} \frac{1}{t} \left(\left\langle \left(f^t(x) - x\right)^2 \right\rangle - \left\langle \left(f^t(x) - x\right) \right\rangle^2 \right), \tag{5.4}$$

can be related to the diffusion coefficient via

$$D = \frac{1}{2} \left.\frac{\partial^2 Q(\beta)}{\partial \beta^2}\right|_{\beta=0}. \tag{5.5}$$

5.2.2 The weighted transfer operator

In order to extract the required information from the generating function of Eq.(5.2) we observe that

$$\left\langle e^{\beta\left(f^t(x)-x\right)} \right\rangle = \int_0^1 dx \int_0^1 dy \delta(y - \tilde{f}^t(x)) e^{\beta\left(f^t(x)-x\right)}, \tag{5.6}$$

where $\delta(...)$ is the Dirac-delta function which is equal to one when its argument is zero and is equal to zero otherwise, whilst $\tilde{f}^t(x) : [0,1] \to [0,1]$ is the map dynamics of Eq.(5.1) taken modulo one. Formally all we have done is insert the identity

$$\int_0^1 dy \delta(y - \tilde{f}^t(x)) = 1, \tag{5.7}$$

into the left hand side of Eq.(5.6). Note that we only consider the dynamics of the reduced map modulo one (represented by the tilde). This reduction from considering the full phase-space trajectories to only considering the modulo one trajectories will help greatly simplify the analytical evaluation of the diffusion coefficient.

Eq.(5.6) allows us to define the operator

$$\mathcal{L}^t = e^{\beta(\sigma_x)}\delta(y - \tilde{f}^t(x)), \tag{5.8}$$

where $\sigma_x = \lfloor f^t(x) - x \rfloor$ gives the integer displacement of a point x when its orbit is taken over the whole real line. We observe that the operator in Eq.(5.8) reduces to the Perron-Frobenius operator when we set $\beta = 0$. Therefore we can think of the operator in Eq.(5.8) as a weighted Perron-Frobenius operator (Dorfman [1999]). The underlying Perron-Frobenius operator evolves the density of points on the unit interval according to the modulo one dynamics of the dynamical system whilst the weight keeps track of how far points have been displaced when their orbits are folded out onto the real line.

As Eq.(5.6) is an integral over exponentials, it too will grow exponentially with time, with the rate of growth being controlled by the leading eigenvalue of the relevant weighted Perron-Frobenius operator of Eq.(5.8) (Ruelle [2004]), that is

$$\left\langle e^{\beta\left(f^t(x)-x\right)} \right\rangle \backsimeq a(e^{\lambda})^t, \tag{5.9}$$

where a is a constant and e^{λ} is the leading eigenvalue of the transfer operator in Eq.(5.8).

If we substitute the right-hand-side of Eq.(5.9) into Eq.(5.2)

$$\begin{aligned} Q(\beta) &= \lim_{t\to\infty} \frac{1}{t} \ln \left\langle e^{\beta\left(f^t(x)-x\right)} \right\rangle \\ &= \lim_{t\to\infty} \frac{1}{t} \ln a(e^{\lambda})^t, \end{aligned} \tag{5.10}$$

and evaluate the right-hand-side of Eq.(5.10) we see that

$$Q(\beta) = \lambda. \tag{5.11}$$

Hence we can conclude that the leading eigenvalue of the weighted Perron-Frobenius operator in Eq.(5.8) is equal to $e^{Q(\beta)}$. We immediately observe that at $\beta = 0$ the leading eigenvalue is thankfully equal to one which is as expected of the un-weighted Perron-Frobenius operator and corresponds to the invariant density of the system, as stated by the Perron-Frobenius theorem.

5.2.3 The dynamical zeta function

In order to gain access to the information contained in the leading eigenvalue and hence the generating function of Eq.(5.2) we look for the smallest root of the equation

$$\det(\mathbf{1} - z\mathcal{L}) = 0, \tag{5.12}$$

which will be given by

$$z_0(\beta) = e^{-Q(\beta)}, \tag{5.13}$$

where the subscript zero represents the fact that this z is a zero of the determinant.

So we see that we can evaluate the diffusion coefficient by solving the eigenvalue problem of the relevant transfer operator. This can be done by rewriting the determinant in terms of the trace of the operator via the matrix identity

$$\det(\mathbf{1} - z\mathcal{L}) = e^{tr(\ln(\mathbf{1} - z\mathcal{L}))}. \tag{5.14}$$

We now expand the logarithm function in the right-hand-side of Eq.(5.14) as a power series and obtain the relation

$$\det(\mathbf{1} - z\mathcal{L}) = \exp\left(-\sum_{n=1}^{\infty} \frac{z^n}{n} \mathrm{tr}\mathcal{L}^n\right). \tag{5.15}$$

The important result of Eq.(5.15) is that we have now obtained a relation between the determinant of the operator on the left-hand-side and the periodic orbits of

the dynamical system in terms of the trace of the operator on the right-hand-side.

$$\mathrm{tr}\mathcal{L}^n = \sum_{x=\tilde{M}^n(x)} \frac{e^{\beta\left(f^t(x)-x\right)}}{|1-\Lambda_{x,n}|}, \tag{5.16}$$

where

$$\Lambda_{x,n} = \prod_{i=0}^{n-1} \tilde{f}'(\tilde{f}^i(x)), \tag{5.17}$$

is the instability of the orbit of x after n iterations. Substituting Eq.(5.16) into Eq.(5.15) we obtain

$$\det(\mathbf{1} - z\mathcal{L}) = \exp\left(-\sum_{n=1}^{\infty} \frac{z^n}{n} \sum_{x=\tilde{M}^n(x)} \frac{e^{\beta\left(f^t(x)-x\right)}}{|1-\Lambda_{x,n}|}\right). \tag{5.18}$$

We can expand the denominator in Eq.(5.16) as a geometric series and use the subsequent relation

$$\frac{1}{|\,1-\Lambda_{x,n}\,|} = \frac{1}{|\,\Lambda_{x,n}\,|}\Sigma_{k=0}^{\infty}\Lambda_{x,n}^{-k}, \tag{5.19}$$

in Eq.(5.18) to express the determinant as a product over dynamical zeta functions

$$\det(\mathbf{1} - z\mathcal{L}) = \prod_{k=0}^{\infty} \zeta_k^{-1}(z,\beta). \tag{5.20}$$

Where the k^{th} order dynamical zeta function, introduced in Ruelle [1976] is given by

$$\zeta_k^{-1}(z,\beta) = \exp\left(-\sum_{n=1}^{\infty} \frac{z^n}{n} \sum_{x=\tilde{M}^n(x)} \frac{e^{\beta\left(f^t(x)-x\right)}}{|\Lambda_{x,n}|}\Lambda_{x,n}^{-k}\right). \tag{5.21}$$

In Baladi and Keller [1990] it was shown that the zeros of the zeroth order dynamical zeta function coincide with the eigenvalues of the corresponding weighted transfer operator so in our setting we need only consider $\zeta_0^{-1}(z,\beta)$. That is, the smallest zero of $\zeta_0^{-1}(z,\beta)$ (we will drop the 0 subscript in the following), is equal

to the leading eigenvalue of weighted Perron-Frobenius operator 5.8, $z_0(\beta)$, this eigenvalue being related to the generating function of Eq.(5.2) that we are interested in by Eq.(5.13). There exists a vast literature on the study of these interesting zeta functions, for surveys relating to this area see for example Baladi [1998]; Parry and Pollicott [1990]; Ruelle [1994] and references therein.

Given Eq.(5.13), we can derive a formula for the drift J in terms of the smallest zero of $\zeta^{-1}(z,\beta)$

$$J = \left.\frac{dz_0(\beta)}{d\beta}\right|_{\beta=0}. \tag{5.22}$$

If we assume that $J = 0$, i.e. there is no mean drift in our system then the diffusion coefficient is given by

$$D = -\frac{1}{2}\left.\frac{d^2 z_0(\beta)}{d\beta^2}\right|_{\beta=0}. \tag{5.23}$$

Rewriting Eq.(5.23) using the fact that $z_0(0) = 1$ we can obtain an expression for the diffusion coefficient in terms of $\zeta^{-1}(z,\beta)$

$$D = \frac{1}{2}\left.\left(\frac{\partial^2\zeta^{-1}(z,\beta)}{\partial\beta^2}\left(\frac{\partial\zeta^{-1}(z,\beta)}{\partial z}\right)^{-1}\right)\right|_{z=1,\beta=0} \tag{5.24}$$

One possible way to proceed from here is to rewrite $\zeta^{-1}(z,\beta)$ using the Euler expansion technique, that is in terms of only prime periodic orbits instead of periodic orbits. A prime periodic orbit is one that can not be broken down into a product of shorter period orbits. This is reminiscent of the way prime numbers can not be factorised into a product of smaller numbers and leads to the name prime periodic orbit,

$$\zeta^{-1}(z,\beta) = \prod_{\{p\}}\left(1 - \frac{z^{n_p}e^{\beta\sigma_p}}{|\Lambda_p|}\right), \tag{5.25}$$

where the product is taken over all the prime periodic orbits and n_p is the corresponding period. Eq.(5.25) can now be expanded as a series and in the case where one is dealing with a map that has a finite Markov partition, $\zeta^{-1}(z,\beta)$ can be written in terms of a finite polynomial. This is the cycle expansion technique

that was pioneered in the early 1990's in application to simple one dimensional maps (Artuso [1991]), the Lorentz gas (Cvitanović et al. [1992]) and later on in the sawtooth maps (Artuso and Strepparava [1997]). However, in even very simple cases it is very hard to obtain a good understanding of the periodic orbit structure due to the exponential increase in number as the period is increased, this increase being given by the topological entropy, and the complicated pruning rules that comes along with these longer orbits. That is, if one encodes the orbits with symbolic sequences, it is hard to get a good understanding of which sequences are allowed by the dynamics and which are not. In the next section we will discuss a method which manages to bypass these problems and allows us to obtain the crucial information about $z_0(\beta)$.

5.3 Generalised Milnor-Thurston kneading determinant

In this section we will derive the parameter dependent diffusion coefficient for a one dimensional map of the interval via a generalised Milnor-Thurston kneading determinant, this construction being based upon the kneading orbits of the map.

5.3.1 Kneading orbits

The map we will study is $M_h(x) : \mathbb{R} \to \mathbb{R}$ defined by

$$M_h(x) = \begin{cases} 2x + h & 0 \leq x < \frac{1}{2} \\ 2x - 1 - h & \frac{1}{2} \leq x < 1 \end{cases}, \tag{5.26}$$

along with the lift condition

$$M_h(x + n) = M_h(x) + n, \quad n \in \mathbb{Z}, \tag{5.27}$$

where $h \in [0, 1]$ is a control parameter. We derived the diffusion coefficient for this map in chapter 2 and found it to be a fractal function of h and that this fractal structure is periodic over the integers. Therefore we will restrict the parameter h to the interval $[0, 1]$ for simplicity. The periodicity of the lift condition means

that we need only consider the reduced dynamics of $M_h(x)$, that is Eq.(5.26) taken modulo one,

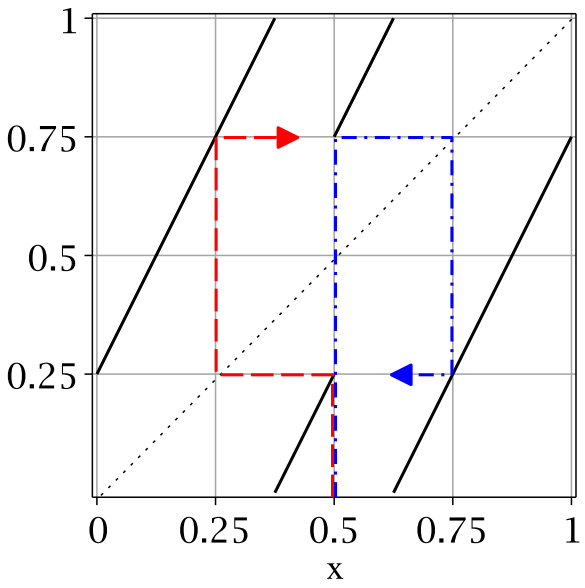

Figure 5.1: *Kneading orbits.* In this figure, the two kneading orbits of the point $x = 0.5$ are illustrated for the lifted doubling map modulo one. The point $x = 0.5$ is split into two points 0.5^+ and 0.5^- corresponding to the two choices of iteration induced by the discontinuity. See the text for definitions of these points. The orbit of 0.5^+ is given in blue (dash-dot-dashed line) whilst the orbit of 0.5^- is given in red (dashed line). Note the similarity between the kneading orbit and the Markov partition 'generating orbit' discussed in chapter 2.

$$\tilde{M}_h(x) = \begin{cases} 2x + h & 0 \leq x < \frac{1-h}{2} \\ 2x + h - 1 & \frac{1-h}{2} \leq x < \frac{1}{2} \\ 2x - h & \frac{1}{2} \leq x < \frac{1+h}{2} \\ 2x - 1 - h & \frac{1+h}{2} \leq x < 1 \end{cases} . \tag{5.28}$$

For the points of discontinuity in Eq.(5.28) there is a choice for the possible iterates. In order to remove this choice the points are split into two points and we define the action of functions on these points of the form a^+ or a^- as

$$\phi(a^\pm) = \lim_{x \to a^\pm} \phi(x), \tag{5.29}$$

where $\phi(x)$ is an arbitrary function. See figure 5.1 for an illustration of kneading orbits. For an introduction to kneading theory see for example Devaney [1989]; Katok and Hasselblatt [1995]. As a side remark, in Groeneveld and Klages [2002] the points a^+ and a^- are interpreted as positive and negative electrostatic charges respectively. This interpretation is then used to derive the diffusion coefficient via an alternative method to the one we will present.

5.3.2 Weighted kneading matrix

We will now look at how to construct the weighted kneading determinant for $\tilde{M}_h(x)$. We will use similar terminology and notation from Baladi and Ruelle [1994]; Cristadoro [2006] for ease of comparison. Let $0 = a_0 < a_1 < ... < a_N = 1$ be the points of discontinuity of a given one-dimensional map of the interval where $N \in \mathbb{N}$ is finite. In our case with $\tilde{M}_h(x)$ this means

$$a_0 = 0, \quad a_1 = \frac{1-h}{2}, \quad a_2 = 0.5, \quad a_3 = \frac{1+h}{2}, \quad a_4 = 1. \tag{5.30}$$

Furthermore, let $\epsilon(x) = \pm$ give the sign of the gradient of the map at x, which for $\tilde{M}_h(x)$, is equal to one for all x. We now introduce the specific constant weight function $t(x) : [0,1] \to \{t_i\}, i = 1..N$, which will be defined individually on each interval $[a_{i-1}, a_i]$ as $t_i = ze^{\beta\sigma_i}/\Lambda$ where as before Λ is the Lyapunov exponent of the map and hence equal to two in this setting whilst $\sigma_i = \lfloor M_h(x) - x \rfloor$ for $x \in [a_{i-1}, a_i]$ gives the integer displacement of a point under iteration, σ_i is essentially just the 'velocity function' from chapter 2, c.f. Eq.(2.11). For $\tilde{M}_h(x)$ these weights are given by

$$t_1 = \frac{z}{2}, \quad t_2 = \frac{ze^{\beta}}{2}, \quad t_3 = \frac{ze^{-\beta}}{2}, \quad t_4 = \frac{z}{2}. \tag{5.31}$$

In order to define the important 'invariant coordinate' of a point x, we give each point x an 'address vector' $\vec{\alpha}(x) : [0,1] \to \mathbb{Z}^{N-1}$. In our case $N = 4$ and $\vec{\alpha}(x)$ is defined as

$$\vec{\alpha}(x) = [\mathrm{sgn}(x - a_1), \mathrm{sgn}(x - a_2), \mathrm{sgn}(x - a_3)]. \tag{5.32}$$

This leads to the invariant coordinate of x

$$\vec{\theta}(x) = \sum_{n=0}^{\infty} \left[\prod_{k=0}^{n-1} \epsilon \left(\tilde{M}_h^k(x) \right) t \left(\tilde{M}_h^k(x) \right) \right] \vec{\alpha}(\tilde{M}_h{}^n(x)). \tag{5.33}$$

For n equals zero the product is conventionally set to one. Eq.(5.33) defines an $N-1$ dimensional vector whose entries are infinite degree polynomials in z. The coefficients of the polynomials are determined by the iterates of the point x and the corresponding weight functions. We now define the 'discontinuity vector' of the critical points a_i. For each critical point $a_1, ..., a_{N-1}$ define the discontinuity vector

$$\vec{K}_i(z,\beta) = \frac{1}{2} \left[\vec{\theta}(a_i^+) - \vec{\theta}(a_i^-) \right]. \tag{5.34}$$

The $(N-1) \times (N-1)$ kneading matrix $\underline{\underline{K}}(z,\beta)$ mentioned above is defined using the $N-1$ discontinuity vectors of size $N-1$ from Eq.(5.34). The determinant of this kneading matrix $\Delta(z,\beta)$ is the kneading determinant that we are after and that will allow us to derive the diffusion coefficient. More specifically, it was shown in Baladi and Ruelle [1994] that

$$\Delta(z,\beta) = R(z,\beta)\zeta_0^{-1}(z,\beta), \tag{5.35}$$

where $R(z,\beta)$ is a rational function that depends upon the set of periodic points $\tilde{p}$ that hit a critical point under iteration. For a system with N critical points $R(z,\beta)$ is defined as

$$R(z,\beta) = \left[1 - \frac{1}{2}(\epsilon_1 t_1 + \epsilon_N t_N)) \right] \prod_{\{\tilde{p}\}} [1 - t_{\tilde{p}}]^{-1}, \tag{5.36}$$

where $t_{\tilde{p}}$ is defined by the weight on the interval containing the point $\tilde{p}$. For our purposes however we need not concern ourselves with $R(z,\beta)$ as from Eq.(5.35) we see that the smallest zero of the kneading determinant is equal to the smallest zero of the dynamical zeta function. This means we can evaluate the diffusion coefficient by only considering the kneading determinant.

5.3.3 Evaluating the diffusion coefficient

Each entry of the kneading matrix $\underline{\underline{K}}(z,\beta)$ is an infinite degree polynomial in z, so working out the determinant may appear to be a daunting task. However, due to the form of the parameter dependence, $\underline{\underline{K}}(z,\beta)$ is a 3×3 matrix for all parameter values $h\in(0,1)$. Hence the simplest way to evaluate the kneading determinant is by brute force calculation.

Let $k_{i,j}(z,\beta)$ be the $(i,j)^{th}$ entry of $\underline{\underline{K}}(z,\beta)$. The kneading determinant is then equal to

$$\Delta(z,\beta)=k_{1,1}k_{2,2}k_{3,3}+k_{1,2}k_{2,3}k_{3,1}+k_{1,3}k_{2,1}k_{3,2}-k_{1,1}k_{2,3}k_{3,2}-k_{1,2}k_{2,1}k_{3,3}-k_{1,3}k_{2,2}k_{3,1}, \tag{5.37}$$

where the dependence on z and β has been dropped for convenience. In analogy with Eq.(5.24), the diffusion coefficient as a function of the parameter h is then given by

$$D(h)=\frac{1}{2}\left(\frac{\partial^2\Delta_h(z,\beta)}{\partial\beta^2}\left(\frac{\partial\Delta_h(z,\beta)}{\partial z}\right)^{-1}\right)\Bigg|_{z=1,\beta=0}, \tag{5.38}$$

where the subscript h indicates that the kneading determinant is dependent upon the parameter.

5.3.4 A simple example

To illustrate the method, we look at the simplest case possible (other than $h=0$ of course which is trivial). We set the parameter $h=1$ and this means that $N=2$ as opposed to 3 for the other parameter values. At this value $\underline{\underline{K}}(z,\beta)$ is a 1×1 'matrix' that is equal to its determinant. Therefore from Eq.(5.34) we have

$$\begin{aligned}\Delta_1(z,\beta) &= \underline{\underline{K}}_1(z,\beta)\\ &= \frac{1}{2}\left[\vec{\theta}(0.5^+)-\vec{\theta}(0.5^-)\right].\end{aligned} \tag{5.39}$$

Furthermore the weights are given by

$$t_1 = \frac{ze^{\beta}}{2}, \quad t_2 = \frac{ze^{-\beta}}{2}, \tag{5.40}$$

and $\tilde{M}_1(x)$ is just the doubling map modulo one. The point 0.5^+ gets mapped onto the fixed point at $x = 0$ after one iteration. Hence from Eq.(5.33)

$$\begin{aligned} \vec{\theta}(0.5^+) &= 1 - t_2 \sum_{n=0}^{\infty} t_1^n \\ &= 1 - \frac{t_2}{1 - t_1}. \end{aligned} \tag{5.41}$$

Similarly, the point 0.5^- gets mapped onto the fixed point at $x = 1$ after one iteration so

$$\vec{\theta}(0.5^-) = -1 + \frac{t_1}{1 - t_2} \tag{5.42}$$

Substituting Eq.(5.40), Eq.(5.42) and Eq.(5.41) into Eq.(5.39) yields,

$$\Delta_1(z, \beta) = 0.5 \left[2 - \frac{0.5ze^{-\beta}}{1 - 0.5ze^{\beta}} - \frac{0.5ze^{\beta}}{1 - 0.5ze^{-\beta}} \right]. \tag{5.43}$$

Differentiating we obtain

$$\left. \frac{\partial^2 \Delta_1(z, \beta)}{\partial \beta^2} \right|_{z=1, \beta=0} = -2, \quad \left. \frac{\partial \Delta_1(z, \beta)}{\partial z} \right|_{z=1, \beta=0} = -2. \tag{5.44}$$

From Eq.(5.38) we therefore obtain the required result that $D(1) = 0.5$.

5.3.5 Step-function convergence

Even though Eq.(5.37) may look daunting, we can solve Eq.(5.38) for the full parameter range with a little help from a computer. It involves defining nine polynomials whose coefficients are determined by the kneading orbits of the three critical points $\frac{1-h}{2}, 0.5$ and $\frac{1+h}{2}$. From Eq.(5.28) we have that

$$\tilde{M}_h(0.5^+) = (1 - h)^+, \quad \tilde{M}_h(0.5^-) = h^-$$

$$\begin{aligned}
\tilde{M}_h^2\left(\left(\frac{1-h}{2}\right)^+\right) &= h^+, \quad \tilde{M}_h^2\left(\left(\frac{1-h}{2}\right)^-\right) = (1-h)^- \\
\tilde{M}_h^2\left(\left(\frac{1+h}{2}\right)^+\right) &= h^+, \quad \tilde{M}_h^2\left(\left(\frac{1+h}{2}\right)^-\right) = (1-h)^-. \qquad (5.45)
\end{aligned}$$

Hence the orbits of the three critical points reduce to the orbits of the two points $x = h$ and $x = 1 - h$. In addition, as this map is symmetric about the point $x = 0.5$ the orbit of $x = 1 - h$ is just the mirror image of the orbit of $x = h$. Therefore we see that the diffusion coefficient is a function of the orbit of the point $x = h$. This result is in good analogy with the result for the functional recursion method discussed in chapter 2 (cf. Eq.(2.34)) in which the diffusion coefficient is also evaluated as a function of the orbit of $x = h$.

We can analyse the convergence of the diffusion coefficient by truncating the sum in Eq.(5.33) and systematically adding terms to the polynomials in Eq.(5.37). Firstly, we observe that the zeroth order truncation $D_0(h) = 0$ does not reproduce the random walk solution for diffusion D_{rw}, i.e. the solution one would obtain if one took no higher order correlations into account (Fujisaka and Grossmann [1982]; Klages [1996]; Klages and Dorfman [1997]; Schell et al. [1982]), which in this case is $D_{rw} = h/2$. Secondly, we observe a series of increasingly complex step-functions which converge to the diffusion coefficient as different parameter regions pick up different weights through the orbit of $x = h$. See figure 5.2 for an illustration of the convergence of the diffusion coefficient in the full parameter range $h = [0, 1]$. The precise location of the discontinuities in the n^{th} step function are given by the discontinuities of the equation $\tilde{M}_h(h)$ which can be solved with Eq.(5.28). For example for $n = 1$ we obtain

$$\tilde{M}_h(h) = \begin{cases} 3h & 0 \le h < \frac{1}{3} \\ 3h - 1 & \frac{1}{3} \le h < \frac{1}{2} \\ h & \frac{1}{2} \le h < 1 \end{cases}, \qquad (5.46)$$

which is discontinuous at $h = 1/3$ and $h = 1/2$ as reflected in figure 5.2.(a). As n is increased, $\tilde{M}_h^n(h)$ becomes increasingly discontinuous as reflected in figures 5.2.(b),..,(f). These step functions have the interesting additional property that they pick out regions of self similarity through their functional form. For instance,

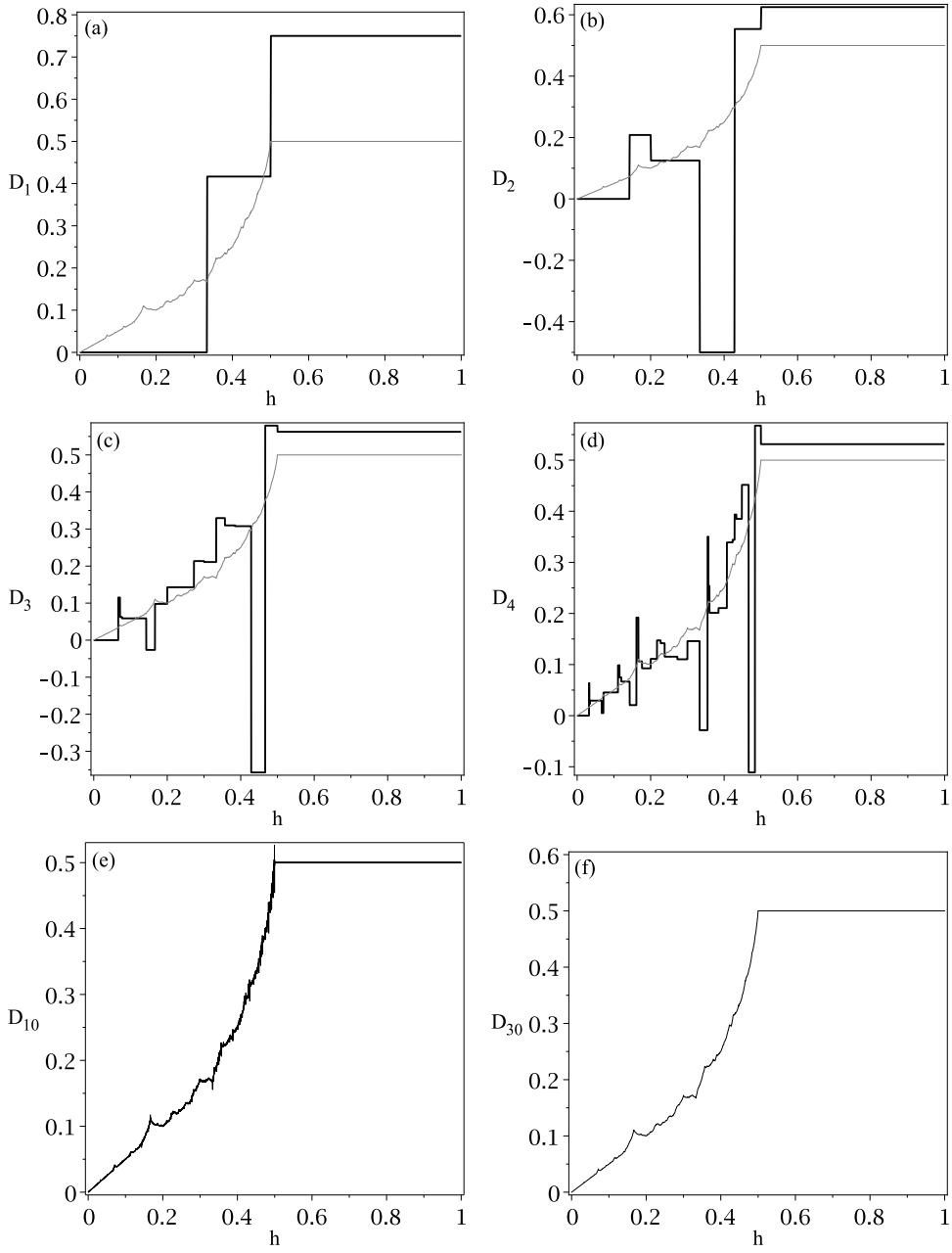

Figure 5.2: *Step function convergence of the diffusion coefficient.* In this figure, the convergence of the parameter dependent diffusion coefficient of the lifted Bernoulli shift map is illustrated. It has been evaluated using a method based upon the kneading orbits of the map. In **(a)**, **(b)**, **(c)**, **(d)**, **(e)** and **(f)** the diffusion coefficient is illustrated at the first, second, third, fourth, tenth and thirtieth order truncation of the kneading orbit respectively (see text for definition). We observe an increasingly complex series of step functions which converge to the diffusion coefficient.

compare the region $h \in [0, 0.5]$ in figure 5.2.(b) with that of the region $h \in [0, 0.2]$ in figure 5.2.(c). This phenomenon of self similarity on fine scales is indicative of the fine scale structure found in $D(h)$. Although in comparison with alternative methods for 'approximating' a diffusion coefficient (Knight and Klages [2011a]) or chapter 3) the lower order approximations give us little information about the structure of the diffusion coefficient due to their step-function form and we have to go to relatively high order before we observe the diffusion coefficient.

5.4 Conclusion

In this chapter we showed how the zeros of dynamical zeta functions are directly related to the diffusion coefficient of a corresponding dynamical system. Using this background theory, we employed a method based on the generalisation of the Milnor-Thurston kneading theory, by Baladi and Ruelle, to analytically derive the parameter dependent diffusion coefficient for a piecewise linear map of the real line. The classic way to derive information from the dynamical zeta function is the cycle expansion method which has the advantage that it takes into account the evolution of a density of points by using only the periodic orbits. The kneading theory technique presented in this chapter has the added strength that it requires only the information from a finite number of orbits of critical points, in order to derive information about the entire density. We showed further that for the map under consideration, this information is captured by the orbit of a single point, in analogy with the recursive functional relation method discussed in chapter 2. However, the convergence to the diffusion coefficient was shown to be drastically different in that the random walk solution was not reproduced at any stage and we observed a series of increasingly complicated step functions, this result being different to the approximation methods discussed in chapter 3.

Although the kneading method we presented is powerful as we can fully analytically derive the diffusion coefficient at any parameter value to very high degrees of accuracy, it relies heavily on the assumption of hyperbolicity. Without this assumption the analytic structure of the dynamical zeta functions is drastically changed and the dynamical systems exhibit power law decay of correlations rather than exponential leading to anomalous diffusion where the mean square

displacement no longer increases linearly, see for example Artuso and Cristadoro [2004]; Artuso and Cristadoro [2005] or for a comprehensive introduction see Klages et al. [2008]. We also saw in figure 5.2 that the structure of the convergence to the diffusion coefficient is quite poor relative to other methods (see Knight and Klages [2011a] or chapter 3 of this thesis). Little information can be gleaned from the lower order approximations about the structure of the diffusion coefficient.

An important open question is to what extent the method employed in this chapter can be generalised to higher dimensions. Considerable research has gone into extending the results of Baladi and Ruelle Baladi [2004]. Potentially applying this work to higher dimensional systems like the sawtooth maps (Dana et al. [1989]), standard maps (Rechester and White [1980]) or particle billiards (Harayama and Gaspard [2001]; Harayama et al. [2002]; Klages [2007]) and being able to analytically answer questions about the structure of the parameter dependent diffusion coefficients presents an intriguing line of future research.

Chapter 6

Concluding remarks and outlook

In this thesis we have explored the complicated, parameter-dependent diffusion coefficients that are found in simple, one-dimensional dynamical systems. The parameter-dependent diffusion coefficients we studied exhibit non-trivial, fine-scale structure and regions of scaling and self-similarity leading to the term 'fractal' diffusion coefficients. The fractality in these simple systems is a result of the topological sensitivity under parameter variation in the microscopic, deterministic dynamics.

In chapter 2, we employed a method which evaluates the Taylor-Green-Kubo formula for diffusion in terms of the recursive solutions of certain fractal 'generalised Takagi functions' to analytically evaluate the parameter-dependent diffusion coefficients of a family of piecewise-linear maps. The specific form of the maps we looked at allowed us to fully explore the analytic capability of this particular method for deriving the diffusion coefficient and allowed us to fully explain the fractal structure we observed. This led to the observation of linear, as opposed to fractal, diffusion coefficients which in some cases were caused by ergodicity breaking. However in other cases the linearity is due to the newly discovered 'dominating-branch' process. The dominating-branch process causes ergodic maps, which at first-look one may expect to exhibit a fractal diffusion coefficient, to mimic their non-ergodic cousins resulting in linear diffusion coefficients. This leads to the important conclusion that topological instability does not necessarily imply fractality. In addition we numerically explored the two-dimensional sawtooth map to show how the recursion relation method fails in this

higher-dimensional setting, and to illustrate the subtle behaviour of parameter-dependent diffusion coefficients in higher dimensions.

Inspired by the work on higher-dimensional systems and the lack of analytical results in this area (Klages [2007]), in chapter 3 we investigated various methods for systematically approximating the diffusion coefficient in a dynamical system. Approximation methods are, more often than not, the only tool available for studying the diffusion coefficient, along with numerical experiments. Here we showed that the approximations that one obtains, drastically vary between the approximation methods that one employs, this being indicative of the fact that there is no unique way to systematically approximate the diffusion coefficient.

Inspired by recent work on open systems, we took the powerful method used in chapter 2 and applied it to a novel type of parameter-dependence in chapter 4. Here we looked at what effect the size and position of the coupling regions in the dynamics called 'escape holes' has on the diffusion coefficient. This led to the discovery of a fractal structure based upon the periodic orbits of the reduced dynamics. We also discovered a variety of asymptotic regimes for small hole size which are also dependent upon the periodic structure of the reduced dynamics. This result generalises the random walk approximation for small hole size (Fujisaka and Grossmann [1982]; Klages [1996]; Klages and Dorfman [1997]; Schell et al. [1982]).

In chapter 5, we looked at an alternative method for fully analytically deriving the parameter-dependent diffusion coefficient of a dynamical system. This method evaluates the zeros of the systems dynamical zeta function via the kneading orbits which are the orbits of the critical points. The zeros can in turn be related to the diffusion coefficient via the generating function. The power of this method is that it bypasses the need to take full account of the periodic orbit structure which is an alternative way to evaluate the dynamical zeta function and diffusion coefficient (Cvitanović et al. [2010]). An interesting observation was the behaviour of the convergence with this kneading theory method. We observed an increasingly complex set of step functions which only reproduce the leading order term in the limit, this being different to the alternative methods we studied in the previous chapters.

We have seen what can be achieved analytically in terms of deriving and

explaining the fractal structures found in simple dynamical systems, but there are still many open questions. We saw in chapter 2 how the powerful recursion-relation method fails analytically in the higher-dimensional setting, but one possible generalisation would be to use it to analytically derive the other moments of the spreading process. Firstly, this could involve adapting the method to obtain the first moment known as the 'current' or 'drift' in a system that exhibits a bias. Secondly, the Taylor-Green-Kubo formula could be suitably adapted to evaluate the higher-order 'Burnett-coefficients' (Burnett [1935]), which correspond to the higher-order moments and attract much interest (Beijeren [1982]; Chernov and Dettmann [2000]; Cvitanović et al. [2010]; Gaspard [1998]). It would be interesting to see whether the above mentioned dominating-branch process can be seen in the other moments or whether these moments can distinguish between the microscopic dynamics. In addition it would be useful to know how common the dominating-branch process is and if it exists in higher dimensional systems. It would also be worthwhile to study the asymptotic regimes for small hole size, mentioned above in reference to chapter 4, in the higher dimensional setting and see whether corresponding results can be found here. Potential crosslinks with experiment could also be made.

Of crucial importance in the research of parameter-dependence is the link to experiment (Klages [2007]). In particular, to what extent these complicated fractal structures can be observed in a physical setting remains an open question. Along these lines the effect of introducing noise into the dynamics is an important topic (Klages [2002a,b]) as with any experiment comes some level of noise. In Klages [2002a,b] numerical investigations of the effect of noise on fractal diffusion coefficients were performed, developing the methods used in this thesis could put this work on a more rigorous footing. In addition, developing algorithms to subtract the noise and expose an underlying fractal structure would be of great help.

Understanding diffusion in higher dimensional, more physically realistic systems presents a challenging goal. Fundamental questions regarding the parameter-dependent diffusion coefficient in area preserving maps (Dana et al. [1989]; Rechester and White [1980]) and particle billiards (Harayama and Gaspard [2001]; Harayama et al. [2002]; Klages [2007]) in particular remain unanswered. Devel-

oping suitable analytic techniques to derive these coefficients would be a big step forward in answering these questions.

Finally, the process of 'anomalous diffusion', where the mean square displacement grows nonlinearly, which can be observed in experiment (Barthelemy et al. [2008]) and is used to explain a large number of physical phenomena is an important generalisation of normal diffusion (Klages et al. [2008]). Increasing the understanding of anomalous diffusion in experiments through the development of suitable mathematical techniques is currently a very active area of research (Seri et al. [2011]).

Appendix

A.1 Two-step transition matrix

The velocity correlation functions for the two-step persistent random walk are,

$$\langle v_0 v_n \rangle = \underline{r} \cdot \underline{\underline{A}}^n \cdot \underline{s} \tag{1}$$

where $\underline{r}$ evaluates v_n, $\underline{s}$ evaluates $v_0 p(v_0, v_1)$,

$$\underline{\mathbf{r}} = \begin{pmatrix} 0 & 0 & 0 & 1 & 1 & 1 & -1 & -1 & -1 \end{pmatrix}, \tag{2}$$

$$\underline{\mathbf{s}} = \begin{pmatrix} 0 & p(1,0) & -p(-1,0) & 0 & p(1,1) & -p(-1,1) & 0 & p(1,-1) & -p(-1,-1) \end{pmatrix}^T$$

and $\underline{\underline{A}}$ is the 9×9 probability transition matrix for the system.

$$\begin{pmatrix} P_{000} & P_{001} & P_{00-1} & 0 & 0 & 0 & 0 & 0 & 0 \\ 0 & 0 & 0 & P_{010} & P_{011} & P_{01-1} & 0 & 0 & 0 \\ 0 & 0 & 0 & 0 & 0 & 0 & P_{0-10} & P_{0-11} & P_{0-1-1} \\ P_{100} & P_{101} & P_{10-1} & 0 & 0 & 0 & 0 & 0 & 0 \\ 0 & 0 & 0 & P_{110} & P_{111} & P_{11-1} & 0 & 0 & 0 \\ 0 & 0 & 0 & 0 & 0 & 0 & P_{1-10} & P_{1-11} & P_{1-1-1} \\ P_{-100} & P_{-101} & P_{-10-1} & 0 & 0 & 0 & 0 & 0 & 0 \\ 0 & 0 & 0 & P_{-110} & P_{-111} & P_{-11-1} & 0 & 0 & 0 \\ 0 & 0 & 0 & 0 & 0 & 0 & P_{-1-10} & P_{-1-11} & P_{-1-1-1} \end{pmatrix}, \tag{3}$$

The two-step parameter dependent transition probabilities associated with Eq.(3) are,

$$P_{000} = \begin{cases} (1-3h)/(1-2h) & 0 \le h < \frac{1}{7} \\ (3-5h)/(4-8h) & \frac{1}{7} \le h < \frac{1}{5} \\ (2-5h)/(2-4h) & \frac{1}{5} \le h < \frac{1}{3} \\ 1/2 & \frac{1}{3} \le h < 1 \end{cases}, \tag{4}$$

$$P_{001} = \begin{cases} 1 & 0 \le h < \frac{1}{7} \\ (1-3h)/(4h) & \frac{1}{7} \le h < \frac{1}{5} \\ 1/2 & \frac{1}{5} \le h < 1 \end{cases}, \tag{5}$$

$$P_{101} = \begin{cases} 0 & 0 \le h < \frac{1}{7} \\ (7h-1)/(4h) & \frac{1}{7} \le h < \frac{1}{6} \\ 1/4 & \frac{1}{6} \le h < \frac{1}{3} \\ (1-2h)/(2-2h) & \frac{1}{3} \le h < \frac{1}{2} \\ 0 & \frac{1}{2} \le h < 1 \end{cases}, \tag{6}$$

$$P_{101} = \begin{cases} 0 & 0 \le h < \frac{1}{7} \\ (7h-1)/(4h) & \frac{1}{7} \le h < \frac{1}{6} \\ 1/4 & \frac{1}{6} \le h < \frac{1}{3} \\ (1-2h)/(2-2h) & \frac{1}{3} \le h < \frac{1}{2} \\ 0 & \frac{1}{2} \le h < 1 \end{cases}, \tag{7}$$

$$P_{010} = \begin{cases} 1 & 0 \le h < \frac{1}{3} \\ (2-4h)/(1-h) & \frac{1}{3} \le h < \frac{3}{7} \\ 1/2 & \frac{3}{7} \le h < 1 \end{cases}, \tag{8}$$

$$P_{110} = \begin{cases} 0 & 0 \le h < \frac{1}{3} \\ (3h-1)/(1-h) & \frac{1}{3} \le h < \frac{3}{7} \\ 1/2 & \frac{3}{7} \le h < 1 \end{cases}, \tag{9}$$

$$P_{011} = \begin{cases} 1 & 0 \le h < \frac{3}{7} \\ (1-h)/(6h-2) & \frac{3}{7} \le h < \frac{1}{2} \\ (1-h)/2h & \frac{1}{2} \le h < 1 \end{cases}, \tag{10}$$

$$P_{111} = \begin{cases} 0 & 0 \leq h < \frac{3}{7} \\ (7h-3)/(6h-2) & \frac{3}{7} \leq h < \frac{1}{2} \\ 1/2 & \frac{1}{2} \leq h < 1 \end{cases}, \tag{11}$$

$$P_{1-11} = \begin{cases} 0 & 0 \leq h < \frac{1}{2} \\ (2h-1)/(2h) & \frac{1}{2} \leq h < 1 \end{cases}, \tag{12}$$

We also have the following properties of the transition probabilities which we can use to simplify Eq.(3).

$$\begin{aligned} P_{100} &= (1-P_{000})/2, \quad P_{10-1} = 1-(P_{101}+P_{001}), \\ P_{1-10} &= 1-(P_{110}+P_{010}), \quad P_{1-1-1} = 1-(P_{111}+P_{011}) \\ P_{-1-11} &= P_{1-11}, \quad P_{01-1} = 0, \\ p(-1,0) &= p(1,0), \quad p(-1,-1) = p(1,1). \end{aligned} \tag{13}$$

Let m_{ij}^n be the ij^{th} entry of $\underline{\underline{A}}^n$. By splitting Eq.(3) into three vectors $(000), (111)$ and $(-1-1-1)$, Eq.(1) can be split into a sum involving three 3×9 matrices. The first of these terms cancels as it is multiplied by the vector (000) and we can gather the remaining terms to obtain,

$$\langle v_0 v_n \rangle = \begin{pmatrix} 1 & 1 & 1 \end{pmatrix} \begin{pmatrix} (m_{41}^n - m_{71}^n) & ... & (m_{49}^n - m_{79}^n) \\ (m_{51}^n - m_{81}^n) & ... & (m_{59}^n - m_{89}^n) \\ (m_{61}^n - m_{91}^n) & ... & (m_{69}^n - m_{99}^n) \end{pmatrix} \underline{\mathbf{s}}. \tag{14}$$

We can then remove the first, fourth and seventh columns in the matrix in Eq.(14) corresponding to the zeros in $\underline{\mathbf{s}}$. We can then use the symmetries in $p(a,b)$ to reduce $\underline{\mathbf{s}}$ to a 3×1 vector and rearrange the entries in the matrix of Eq.(14) accordingly. Using the property that the symmetries of $\underline{\underline{A}}^n$ are the same as those of $\underline{\underline{A}}$ we can reduce Eq.(14) to one involving a 3×3 matrix,

$$\langle v_0 v_n \rangle = \begin{pmatrix} 2 & 2 & 2 \end{pmatrix} \begin{pmatrix} (m_{42}^n - m_{43}^n) & (m_{45}^n - m_{49}^n) & (m_{48}^n - m_{46}^n) \\ (m_{52}^n - m_{53}^n) & (m_{55}^n - m_{59}^n) & (m_{58}^n - m_{56}^n) \\ (m_{62}^n - m_{63}^n) & (m_{65}^n - m_{69}^n) & (m_{68}^n - m_{66}^n) \end{pmatrix} \begin{pmatrix} p(1,0) \\ p(1,1) \\ p(1,-1) \end{pmatrix}. \tag{15}$$

In order to obtain an analytical expression for the matrix in Eq.(15), we would like to obtain a solvable recurrence relation, however, on inspection we see that this matrix is equal to

$$\begin{pmatrix} P_{100} & P_{101} & P_{10-1} \\ 0 & 0 & 0 \\ 0 & 0 & 0 \end{pmatrix} \begin{pmatrix} 0 & 0 & 0 \\ (m_{33}^{n-1} - m_{32}^{n-1}) & (m_{39}^{n-1} - m_{35}^{n-1}) & (m_{36}^{n-1} - m_{38}^{n-1}) \\ (m_{32}^{n-1} - m_{33}^{n-1}) & (m_{35}^{n-1} - m_{39}^{n-1}) & (m_{38}^{n-1} - m_{36}^{n-1}) \end{pmatrix}$$
$$+ \begin{pmatrix} 0 & 0 & 0 \\ P_{110} & P_{111} & P_{-1-11} \\ 0 & 0 & 0 \end{pmatrix} \begin{pmatrix} (m_{42}^{n-1} - m_{43}^{n-1}) & (m_{45}^{n-1} - m_{49}^{n-1}) & (m_{48}^{n-1} - m_{46}^{n-1}) \\ (m_{52}^{n-1} - m_{53}^{n-1}) & (m_{55}^{n-1} - m_{59}^{n-1}) & (m_{58}^{n-1} - m_{56}^{n-1}) \\ (m_{62}^{n-1} - m_{63}^{n-1}) & (m_{65}^{n-1} - m_{69}^{n-1}) & (m_{68}^{n-1} - m_{66}^{n-1}) \end{pmatrix}$$
$$+ \begin{pmatrix} 0 & 0 & 0 \\ 0 & 0 & 0 \\ P_{1-10} & P_{1-11} & P_{1-1-1} \end{pmatrix} \begin{pmatrix} (m_{43}^{n-1} - m_{42}^{n-1}) & (m_{49}^{n-1} - m_{45}^{n-1}) & (m_{46}^{n-1} - m_{48}^{n-1}) \\ (m_{53}^{n-1} - m_{62}^{n-1}) & (m_{69}^{n-1} - m_{65}^{n-1}) & (m_{66}^{n-1} - m_{68}^{n-1}) \\ (m_{63}^{n-1} - m_{52}^{n-1}) & (m_{59}^{n-1} - m_{55}^{n-1}) & (m_{56}^{n-1} - m_{58}^{n-1}) \end{pmatrix}$$

and unlike for the one-step approximation, a recurrence relation is unobtainable.

A.2 Transition matrices

In this section we explicitly give the parameter dependent Markov transition matrix approximations of the interval map $\tilde{M}_h(x)$. In order to transfer this to the system on $[0, L]$ one must use the following $n \times n$ matrices as the diagonal elements of an $Ln \times Ln$ matrix and insert the periodic boundary conditions appropriately. The elements that correspond to periodic boundary conditions are given in brackets.

A.2.1 Second order

$h \in [0, 1/6]$ and $h \in [1/6, 1/4]$:

$$\begin{pmatrix} 0 & (1) & 1 & 0 \\ \frac{4h}{1-2h} & \frac{1-6h}{1-2h} & 1 & 0 \\ 0 & 1 & \frac{1-6h}{1-2h} & \frac{4h}{1-2h} \\ 0 & 1 & (1) & 0 \end{pmatrix}, \begin{pmatrix} 0 & (1) & 1 & 0 \\ 1 & 0 & \frac{2-8h}{1-2h} & \frac{6h-1}{1-2h} \\ \frac{6h-1}{1-2h} & \frac{2-8h}{1-2h} & 0 & 1 \\ 0 & 1 & (1) & 0 \end{pmatrix}. \tag{16}$$

$h \in [1/4, 1/3]$ and $h \in [1/3, 1/2]$:

$$\begin{pmatrix} 0 & (1) & \frac{1-3h}{h} & \frac{4h-1}{h} \\ 1 & 0 & 0 & 1 \\ 1 & 0 & 0 & 1 \\ \frac{4h-1}{h} & \frac{1-3h}{h} & (1) & 0 \end{pmatrix}, \begin{pmatrix} \left(\frac{3h-1}{h}\right) & \left(\frac{1-2h}{h}\right) & 0 & 1 \\ 1 & 0 & 0 & 1 \\ 1 & 0 & 0 & 1 \\ 1 & 0 & \left(\frac{1-2h}{h}\right) & \left(\frac{3h-1}{h}\right) \end{pmatrix}. \tag{17}$$

$h \in [1/2, 1]$ which is Markov:

$$\begin{pmatrix} (1) & 0 & 0 & 1 \\ 0 & (1) & (1) & 0 \\ 0 & (1) & (1) & 0 \\ 1 & 0 & 0 & (1) \end{pmatrix}. \tag{18}$$

A.2.2 Third order

The third order parameter dependent transition matrices for $h \in [0, 1/14]$ and $h \in [1/14, 1/10]$:

$$\begin{pmatrix} 0 & 0 & (1) & 1 & 0 & 0 \\ 1 & 0 & 0 & 1 & 0 & 0 \\ 0 & \frac{8h}{1-6h} & \frac{1-14h}{1-6h} & 1 & 0 & 0 \\ 0 & 0 & 1 & \frac{1-14h}{1-6h} & \frac{8h}{1-6h} & 0 \\ 0 & 0 & 1 & 0 & 0 & 1 \\ 0 & 0 & 1 & (1) & 0 & 0 \end{pmatrix}, \begin{pmatrix} 0 & 0 & (1) & 1 & 0 & 0 \\ 1 & 0 & 0 & 1 & 0 & 0 \\ 0 & 1 & 0 & \frac{2-20h}{1-6h} & \frac{14h-1}{1-6h} & 0 \\ 0 & \frac{14h-1}{1-6h} & \frac{2-20h}{1-6h} & 0 & 1 & 0 \\ 0 & 0 & 1 & 0 & 0 & 1 \\ 0 & 0 & 1 & (1) & 0 & 0 \end{pmatrix}, \tag{19}$$

$h \in [1/10, 1/8]$ and $h \in [1/8, 1/7]$:

$$\begin{pmatrix} 0 & 0 & (1) & 1 & 0 & 0 \\ 1 & 0 & 0 & \frac{1}{2h} - 4 & 5 - \frac{1}{2h} & 0 \\ 0 & 1 & 0 & 0 & 1 & 0 \\ 0 & 1 & 0 & 0 & 1 & 0 \\ 0 & 5 - \frac{1}{2h} & \frac{1}{2h} - 4 & 0 & 0 & 1 \\ 0 & 0 & 1 & (1) & 0 & 0 \end{pmatrix}, \begin{pmatrix} 0 & 0 & (1) & \frac{1}{h} - 7 & 8 - \frac{1}{h} & 0 \\ 1 & 0 & 0 & 0 & 1 & 0 \\ 0 & 1 & 0 & 0 & 1 & 0 \\ 0 & 1 & 0 & 0 & 1 & 0 \\ 0 & 1 & 0 & 0 & 0 & 1 \\ 0 & 8 - \frac{1}{h} & \frac{1}{h} - 7 & (1) & 0 & 0 \end{pmatrix}, \tag{20}$$

$h \in [1/7, 1/6]$ and $h \in [1/6, 1/5]$:

$$\begin{pmatrix} 0 & \left(\frac{7h-1}{h}\right) & \left(\frac{1-6h}{h}\right) & 0 & 1 & 0 \\ 1 & 0 & 0 & 0 & 1 & 0 \\ 0 & 1 & 0 & 0 & 1 & 0 \\ 0 & 1 & 0 & 0 & 1 & 0 \\ 0 & 1 & 0 & 0 & 0 & 1 \\ 0 & 1 & 0 & \left(\frac{1-6h}{h}\right) & \left(\frac{7h-1}{h}\right) & 0 \end{pmatrix}, \begin{pmatrix} 0 & \left(\frac{1-5h}{h}\right) & \left(\frac{6h-1}{h}\right) & 0 & 1 & 0 \\ 1 & 0 & 0 & 0 & 1 & 0 \\ 1 & 0 & 0 & 0 & 0 & 1 \\ 1 & 0 & 0 & 0 & 0 & 1 \\ 0 & 1 & 0 & 0 & 0 & 1 \\ 0 & 1 & 0 & \left(\frac{6h-1}{h}\right) & \left(\frac{1-5h}{h}\right) & 0 \end{pmatrix}, \tag{21}$$

$h \in [1/5, 1/4]$ and $h \in [1/4, 3/10]$:

$$\begin{pmatrix} 0 & 0 & (1) & 5-\frac{1}{h} & \frac{1}{h}-4 & 0 \\ 1 & 0 & 0 & 0 & 1 & 0 \\ 1 & 0 & 0 & 0 & 0 & 1 \\ 1 & 0 & 0 & 0 & 0 & 1 \\ 0 & 1 & 0 & 0 & 0 & 1 \\ 0 & \frac{1}{h}-4 & 5-\frac{1}{h} & (1) & 0 & 0 \end{pmatrix}, \begin{pmatrix} 0 & 0 & (1) & 1 & 0 & 0 \\ 0 & 0 & (1) & 0 & 1 & 0 \\ 1 & 0 & 0 & 0 & \frac{8h-2}{1-2h} & \frac{3-10h}{1-2h} \\ \frac{3-10h}{1-2h} & \frac{8h-2}{1-2h} & 0 & 0 & 0 & 1 \\ 0 & 1 & 0 & (1) & 0 & 0 \\ 0 & 0 & 1 & (1) & 0 & 0 \end{pmatrix}, \tag{22}$$

$h \in [3/10, 1/3]$ and $h \in [1/3, 5/14]$:

$$\begin{pmatrix} 0 & 0 & (1) & 1 & 0 & 0 \\ 0 & 0 & (1) & 0 & 1 & 0 \\ \frac{4-12h}{1-2h} & \frac{10h-3}{1-2h} & 0 & 0 & 1 & 0 \\ 0 & 1 & 0 & 0 & \frac{10h-3}{1-2h} & \frac{4-12h}{1-2h} \\ 0 & 1 & 0 & (1) & 0 & 0 \\ 0 & 0 & 1 & (1) & 0 & 0 \end{pmatrix}, \begin{pmatrix} 0 & (1) & 0 & 0 & 1 & 0 \\ 0 & 0 & (1) & 0 & 1 & 0 \\ \frac{12h-4}{1-2h} & \frac{5-14h}{1-2h} & 0 & 0 & 1 & 0 \\ 0 & 1 & 0 & 0 & \frac{5-14h}{1-2h} & \frac{12h-4}{1-2h} \\ 0 & 1 & 0 & (1) & 0 & 0 \\ 0 & 1 & 0 & 0 & (1) & 0 \end{pmatrix}, \tag{23}$$

$h \in [5/14, 3/8]$ and $h \in [3/8, 4/10]$:

$$\begin{pmatrix} 0 & (1) & 0 & 0 & 1 & 0 \\ 0 & 0 & (1) & 0 & 1 & 0 \\ 1 & 0 & 0 & 0 & \frac{6-16h}{1-2h} & \frac{14h-5}{1-2h} \\ \frac{14h-5}{1-2h} & \frac{6-16h}{1-2h} & 0 & 0 & 0 & 1 \\ 0 & 1 & 0 & (1) & 0 & 0 \\ 0 & 1 & 0 & 0 & (1) & 0 \end{pmatrix}, \begin{pmatrix} 0 & (1) & 0 & 0 & 1 & 0 \\ 0 & 0 & (1) & 0 & \frac{4-10h}{1-2h} & \frac{8h-3}{1-2h} \\ 1 & 0 & 0 & 0 & 0 & 1 \\ 1 & 0 & 0 & 0 & 0 & 1 \\ \frac{8h-3}{1-2h} & \frac{4-10h}{1-2h} & 0 & (1) & 0 & 0 \\ 0 & 1 & 0 & 0 & (1) & 0 \end{pmatrix}, \tag{24}$$

$h \in [4/10, 3/7]$ and $h \in [3/7, 1/2]$:

$$\begin{pmatrix} 0 & (1) & 0 & 0 & \frac{3-7h}{3h-1} & \frac{10h-4}{3h-1} \\ 0 & 0 & (1) & 0 & 0 & 1 \\ 1 & 0 & 0 & 0 & 0 & 1 \\ 1 & 0 & 0 & 0 & 0 & 1 \\ 1 & 0 & 0 & (1) & 0 & 0 \\ \frac{10h-4}{3h-1} & \frac{3-7h}{3h-1} & 0 & 0 & (1) & 0 \end{pmatrix}, \begin{pmatrix} \left(\frac{7h-3}{3h-1}\right) & \left(\frac{2-4h}{3h-1}\right) & 0 & 0 & 0 & 1 \\ 0 & 0 & (1) & 0 & 0 & 1 \\ 1 & 0 & 0 & 0 & 0 & 1 \\ 1 & 0 & 0 & 0 & 0 & 1 \\ 1 & 0 & 0 & (1) & 0 & 0 \\ 1 & 0 & 0 & 0 & \left(\frac{2-4h}{3h-1}\right) & \left(\frac{7h-3}{3h-1}\right) \end{pmatrix}. \tag{25}$$

For $h \in [1/2, 1]$ we saw above that the transition matrix is already Markov at the second order approximation, therefore there is no need for a third order approximation.

Publication list

- G. Knight and R. Klages. Linear and fractal diffusion coefficients in a family of one-dimensional chaotic maps. *Nonlinearity* **24** 227 2011.
- G. Knight and R. Klages. Capturing correlations in chaotic diffusion by approximation methods. *Phys. Rev. E.* **84** 041135 2011.
- G. Knight, O. Georgiou, C. P. Dettmann, and R. Klages. Where to place a hole to achieve a maximal diffusion coefficient. *ArXiv e-prints 1112.3922v1* Submitted to Chaos 2011

References

E. G. Altmann and A. Endler. Noise-enhanced trapping in chaotic scattering. *Phys. Rev. Lett.*, 105:244102, 2010. 31, 99

E. G. Altmann and T. Tél. Poincaré recurrences and transient chaos in systems with leaks. *Phys. Rev. E*, 79:016204, Jan 2009. 31, 100

V.I. Arnold and A. Avez. *Ergodic problems of classical mechanics*. W.A. Benjamin, New York, 1968. 30, 68

R. Artuso. Diffusive dynamics and periodic orbits of dynamical systems. *Phys. Lett. A*, 160:528–530, 1991. 28, 130

R Artuso. *Classical and quantum zeta functions and periodic orbits theory, in G. Casati, I. Guarneri and U. Smilansky (eds), New Directions in Quantum Chaos*. Proceedings of the International School of Physics 'Enrico Fermi', Course CXLIII. IOP Press, Amsterdam, 2000. 124

R. Artuso and G. Cristadoro. Periodic orbit theory of strongly anomalous transport. *J. Phys. A: Math. Gen.*, 37:85–103, 2004. 139

R. Artuso and G. Cristadoro. Anomalous deterministic transport. *Chaos*, 15: 015116/1–7, 2005. 139

R. Artuso and R. Strepparava. Recycling diffusion in sawtooth and cat maps. *Physics Letters A*, 236(5):469–475, 1997. 28, 130

V. Baladi. *Dynamical zeta functions, in B. Branner and P. Hjorth (eds), Real and complex dynamical systems*. NATO ASI series: Mathematical and physical sciences. Kluwer Academic Publishers, 1995. 123

V. Baladi. Periodic orbits and dynamical spectra (survey). *Ergodic Theory and Dynamical Systems*, 18(02):255–292, 1998. 123, 129

V. Baladi. *Kneading Determinants and transfer operators in Higher Dimensions, in M. L. Lapidus and M. van Frankenhuijsen (eds), Fractal Geometry and Applications: A Jubilee of Benoit Mandelbrot.* Proceedings of Symposia in Pure Mathematics, 72, part. 2, pp. 407-417. Amer. Math. Soc., 2004. 139

V. Baladi and G. Keller. Zeta functions and transfer operators for piecewise monotone transformations. *Communications in Mathematical Physics*, 127: 459–477, 1990. 123, 128

V. Baladi and D. Ruelle. An extension of the theorem of Milnor and Thurston on the zeta functions of interval maps. *Ergodic Theory and Dynamical Systems*, 14:621–632, 1994. 32, 123, 132, 133

P. Bálint and I. Toth. Exponential decay of correlations in multi-dimensional dispersing billiards. *Annales Henri Poincaré*, 9:1309–1369, 2008. 90

J. Bardeen and C. Herring. *Diffusion in Alloys and the Kirkendall Effect in Imperfections in nearly perfect crystals, W. Shockley (ed).* Wiley, 1952. 27, 76

P. Barthelemy, J. Bertolotti, and D. S. Wiersma. A Levy flight for light. *Nature*, 453(7194):495–498, 2008. 143

H. van Beijeren. Transport properties of stochastic Lorentz models. *Rev. Mod. Phys.*, 54:195–234, 1982. 142

H. van Beijeren and K. W. Kehr. Correlation factor, velocity autocorrelation function and frequency-dependent tracer diffusion coefficient. *Journal of Physics C: Solid State Physics*, 19(9):1319, 1986. 27

R.B. Bird, W.E. Stewart, and E.N. Lightfoot. *Transport phenomena.* Wiley International edition. J. Wiley, 2007. 19

L. Boltzmann. *Lectures on Gas Theory.* Univ. of California Press, Berkeley, 1964. 18

R. Brown. *The miscellaneous botanical works: containing I, geographico-botanical and II, structural and physiological memoirs.* Hardwicke, 1866. 23

L. A. Bunimovich and C. P. Dettmann. Open circular billiards and the riemann hypothesis. *Phys. Rev. Lett.*, 94:100201, Mar 2005. 100

L. A. Bunimovich and C. P. Dettmann. Peeping at chaos: Nondestructive monitoring of chaotic systems by measuring long-time escape rates. *EPL (Europhysics Letters)*, 80(4):40001, 2007. 100

L. A. Bunimovich and A. Yurchenko. Where to place a hole to achieve a maximal escape rate. *Israel Journal of Mathematics*, 182:229–252, 2011. 31, 32, 99, 101, 117, 119

D. Burnett. The distribution of molecular velocities and the mean motion in a non-uniform gas. *Proceedings of the London Mathematical Society*, 40(1 - 4): 382–435, 1935. 142

J.R. Cary and J.D. Meiss. Rigorously diffusive deterministic map. *Phys. Rev. A*, 24:2664–2668, 1981. 29, 75

R. Chen and S. T. Dunham. Correlation factors for interstitial-mediated self-diffusion in the diamond lattice: Kinetic lattice monte carlo approach. *Phys. Rev. B*, 83:134124, 2011. 27

N.I. Chernov and C.P. Dettmann. The existence of burnett coefficients in the periodic lorentz gas. *Physica A: Statistical Mechanics and its Applications*, 279 (1 - 4):37 – 44, 2000. 142

G. Cristadoro. Fractal diffusion coefficient from dynamical zeta functions. *Journal of Physics A: Mathematical and General*, 39:L151–L157, 2006. 32, 36, 75, 100, 101, 123, 124, 132

P. Cvitanovic and A Pikovsky. Cycle expansion for power spectrum. *Chaos in Communications*, 2038:290–298, 1993. 123, 124

P. Cvitanović, P. Gaspard, and Th. Schreiber. Investigation of the Lorentz gas in terms of periodic orbits. *Chaos*, 2:85–90, 1992. 28, 130

P. Cvitanović, R. Artuso, R. Mainieri, G. Tanner, and G. Vattay. *Chaos: Classical and quantum*. Niels Bohr Institute, Copenhagen, 2010. webbook under chaosbook.org. 19, 24, 28, 35, 75, 100, 101, 108, 109, 115, 123, 124, 141, 142

I. Dana, N.W. Murray, and I.C. Percival. Resonances and diffusion in periodic Hamiltonian maps. *Phys. Rev. Lett.*, 65:1693–1697, 1989. 28, 29, 31, 37, 68, 75, 100, 139, 142

G. de Rham. On some curves defined by functional equations. In Edgar G, editor, *Classics on fractals*, Studies in Nonlinearity. Westview Press, Colorado, 2003. 29, 43

M. F. Demers and L.S. Young. Escape rates and conditionally invariant measures. *Nonlinearity*, 19(2):377, 2006. 31, 100

C. P. Dettmann. *Recent advances in open billiards with some open problems, in Z. Elhadj and J. C. Sprott (eds), Frontiers in the Study of Chaotic Dynamical Systems with Open Problems*. World Scientific Series on Nonlinear Science, B, Vol. 16. World Scientific Pub. Co. Inc., 2011. 31, 100

C. P. Dettmann and O. Georgiou. Transmission and reflection in the stadium billiard: Time-dependent asymmetric transport. *Phys. Rev. E*, 83:036212, Mar 2011. 100

C. P. Dettmann and E. D. Leonel. Escape and transport for an open bouncer: Stretched exponential decays. *Physica D: Nonlinear Phenomena*, 241(4):403 – 408, 2012. 100

C. P. Dettmann and G. P. Morriss. Stability ordering of cycle expansions. *Phys. Rev. Lett.*, 78:4201–4204, Jun 1997. 35, 115

R.L. Devaney. *An introduction to chaotic dynamical systems*. Addison-Wesley, Reading, second edition, 1989. 24, 32, 51, 122, 132

J.R. Dorfman. *An introduction to chaos in nonequilibrium statistical mechanics*. Cambridge University Press, Cambridge, 1999. 19, 35, 36, 38, 40, 75, 77, 78, 79, 80, 85, 90, 100, 101, 104, 105, 117, 123, 126

B. Eckhardt. Periodic orbits and diffusion in standard maps. *Physics Letters A*, 172(6):411 – 415, 1993. 75

A. Einstein. On the movement of small particles suspended in a stationary liquid demanded by the molecular-kinetic theory of heat. *Annalen der Physik (Leipzig)*, 17:549–560, 1905. 23, 40

K.J. Falconer. *Fractal geometry: mathematical foundations and applications*. Wiley, 2003. 28

N. Friedman, A. Kaplan, D. Carasso, and N. Davidson. Observation of chaotic and regular dynamics in atom-optics billiards. *Phys. Rev. Lett.*, 86:1518–1521, 2001. 121

H. Fujisaka and S. Grossmann. Chaos-induced diffusion in nonlinear discrete dynamics. *Z. Physik B*, 48:261–275, 1982. 27, 32, 75, 77, 100, 101, 102, 105, 114, 136, 141

R. Fürth. Die brownsche bewegung bei bercksichtigung einer persistenz der bewegungsrichtung. mit anwendungen auf die bewegung lebender infusorien. *Zeitschrift für Physik A Hadrons and Nuclei*, 2:244–256, 1920. 27, 76, 85

P. Gaspard. Diffusion, effusion, and chaotic scattering. *J. Stat. Phys.*, 68:673–747, 1992. 28, 31, 78

P. Gaspard. *Chaos, scattering and statistical mechanics*. Cambridge University Press, Cambridge, 1998. 19, 35, 36, 75, 77, 85, 90, 100, 117, 118, 121, 142

P. Gaspard and J.R. Dorfman. Chaotic scattering theory, thermodynamic formalism, and transport coefficients. *Phys. Rev. E*, 52:3525–3552, 1995. 77, 90

P. Gaspard and R. Klages. Chaotic and fractal properties of deterministic diffusion-reaction processes. *Chaos*, 8:409–423, 1998. 35, 36, 38, 53, 78, 85, 100, 101, 105, 106, 118, 120

P. Gaspard and G. Nicolis. Transport properties, Lyapunov exponents, and entropy per unit time. *Phys. Rev. Lett.*, 65:1693–1696, 1990. 28, 31, 77, 90, 100, 117

T. Geisel and J. Nierwetberg. Onset of diffusion and universal scaling in chaotic systems. *Phys. Rev. Lett.*, 48:7–10, 1982. 27, 35, 38, 75, 77, 100, 101, 124

T. Geisel and S. Thomae. Anomalous diffusion in intermittent chaotic systems. *Phys. Rev. Lett.*, 52:1936–1939, 1984. 27

T. Geisel, J. Nierwetberg, and A. Zacherl. Accelerated diffusion in Josephson junctions and related chaotic systems. *Phys. Rev. Lett.*, 54:616–619, 1985. 27

J.W. Gibbs. *Elementary principles of statistical mechanics*. Dover, New York, 1960. 18

T. Gilbert and D. P. Sanders. Persistence effects in deterministic diffusion. *Phys. Rev. E*, 80(4):041121, Oct 2009. 76, 77, 85, 86, 98

T. Gilbert and D. P. Sanders. Diffusion coefficients for multi-step persistent random walks on lattices. *Journal of Physics A: Mathematical and Theoretical*, 43(3):035001, 2010. 77, 85, 90

T. Gilbert, H. C. Nguyen, and D. P. Sanders. Diffusive properties of persistent walks on cubic lattices with application to periodic lorentz gases. *Journal of Physics A: Mathematical and Theoretical*, 44(6):065001, 2011. 77, 85

J. Gleick. *Chaos - Making a new science*. Penguin, New York, 1988. 24

M.S. Green. Markoff random processes and the statistical mechanics of time-dependent phenomena ii: Irreversible processes in fluids. *J. of Chem. Phys.*, 22:398–413, 1954. 40

J. Groeneveld and R. Klages. Negative and nonlinear response in an exactly solved dynamical model of particle transport. *Journal of Statistical Physics*, 109:821–861, 2002. 35, 36, 75, 78, 101, 132

S. Grossmann and H. Fujisaka. Diffusion in discrete nonlinear dynamical systems. *Phys. Rev. A*, 26:1779–1782, 1982. 27, 35, 38, 124

S. Grossmann and S. Thomae. Shape dependence of correlation times in chaos-induced diffusion. *Phys. Lett. A*, 97:263–267, 1983. 27

T. Harayama and P. Gaspard. Diffusion of particles bouncing on a one-dimensional periodically corrugated floor. *Phys. Rev. E*, 64:036215/1–16, 2001. 30, 75, 100, 121, 139, 142

T. Harayama, R. Klages, and P. Gaspard. Deterministic diffusion in flower-shaped billiards. *Phys. Rev. E*, 66:026211/1–7, 2002. 30, 75, 76, 85, 101, 121, 139, 142

J.W. Haus and K. W. Kehr. Diffusion in regular and disordered lattices. *Phys. Rep.*, 150:264–406, 1987. 27, 76, 85

O.G. Jepps and L. Rondoni. Thermodynamics and complexity of simple transport phenomena. *J. Phys. A: Math. Gen.*, 39:1311–1338, 2006. 75

M. Kaisermayr, J. Combet, B. Sepiol, and G. Vogl. Correlation factors in intermetallic alloys determined using neutron scattering: Ni3Sb, NiGa and CoGa. *Defect and Diffusion Forum*, 194–199:461–466, 2001. 27

J. Kärger and D.M. Ruthven. *Diffusion in zeolites*. Wiley, 1992. 27

A. Katok and B. Hasselblatt. *Introduction to the modern theory of dynamical systems*, volume 54 of *Encyclopedia of Mathematics and its Applications*. Cambridge University Press, Cambridge, 1995. 24, 32, 51, 122, 132

G. Keller and C. Liverani. Rare events, escape rates and quasistationarity: Some exact formulae. *Journal of Statistical Physics*, 135:519–534, 2009. 31, 32, 99, 101, 117, 119

G. Keller, P. J. Howard, and R. Klages. Continuity properties of transport coefficients in simple maps. *Nonlinearity*, 21(8):1719, 2008. 29

A.I.A. Khinchin. *Mathematical foundations of statistical mechanics*. Dover series in mathematics and physics. Dover Publications, 1949. 19

R. Klages. *Deterministic diffusion in one-dimensional chaotic dynamical systems*. Wissenschaft & Technik-Verlag, Berlin, 1996. 29, 30, 32, 35, 36, 38, 43, 47, 56, 57, 59, 73, 75, 78, 84, 91, 100, 101, 102, 105, 106, 114, 117, 118, 136, 141

R. Klages. Suppression and enhancement of deterministic diffusion in disordered dynamical systems. *Phys. Rev. E*, 65:055203(R)/1–4, 2002a. 142

R. Klages. Transitions from deterministic to stochastic diffusion. *Europhys. Lett.*, 57:796–802, 2002b. 142

R. Klages. *Microscopic chaos, fractals and transport in nonequilibrium statistical mechanics*, volume 24 of *Advanced Series in Nonlinear Dynamics*. World Scientific, Singapore, 2007. 19, 22, 30, 31, 35, 36, 37, 40, 72, 73, 75, 76, 77, 78, 79, 84, 85, 98, 100, 101, 104, 105, 106, 108, 109, 117, 118, 120, 121, 139, 141, 142

R. Klages and C. Dellago. Density-dependent diffusion in the periodic Lorentz gas. *J. Stat. Phys.*, 101:145–159, 2000. 30, 37, 72

R. Klages and J.R. Dorfman. Simple maps with fractal diffusion coefficients. *Phys. Rev. Lett.*, 74:387–390, 1995. 28, 35, 36, 56, 57, 75, 77, 78, 84, 91, 92, 100, 117, 118, 120, 124

R. Klages and J.R. Dorfman. Dynamical crossover in deterministic diffusion. *Phys. Rev. E*, 55(2):R1247–R1250, 1997. 32, 47, 59, 102, 105, 114, 136, 141

R. Klages and J.R. Dorfman. Simple deterministic dynamical systems with fractal diffusion coefficients. *Phys. Rev. E*, 59:5361–5383, 1999. 35, 36, 56, 57, 73, 75, 77, 78, 84, 91, 92

R. Klages and P. Howard. *Introduction to Dynamical Systems*. Lecture Notes for MAS424/MTHM021. Queen Mary University of London, 2008. 24, 26

R. Klages and T. Klauß. Fractal fractal dimensions of deterministic transport coefficients. *J.Phys.A: Math. Gen.*, 36:5747–5764, 2003. 28, 53

R. Klages and G. Knight. Reply to the comment of T.Gilbert and D.P.Sanders on 'Capturing correlations in chaotic diffusion by approximation methods'. *ArXiv e-prints 1112.3927*, 2011. 31, 76

R. Klages and N. Korabel. Understanding deterministic diffusion by correlated random walks. *J. Phys. A: Math. Gen.*, 35:4823–4836, 2002. 40, 76, 79, 80

R. Klages, I.F. Barna, and L. Mátyás. Spiral modes in the diffusion of a single granular particle on a vibrating surface. *Phys. Lett. A*, 333:79–84, 2004. 35

R. Klages, G. Radons, and I.M. Sokolov (eds). *Anomalous transport: foundations and applications*. Wiley-VCH, 2008. 28, 139, 143

G. Knight and R. Klages. Capturing correlations in chaotic diffusion by approximation methods. *Phys. Rev. E*, 84:041135/1–11, 2011a. 77, 101, 105, 106, 138, 139

G. Knight and R. Klages. Linear and fractal diffusion coefficients in a family of one-dimensional chaotic maps. *Nonlinearity*, 24(1):227, 2011b. 13, 37, 75, 76, 78, 79, 80, 84, 97, 101, 105, 106, 114, 117, 120

G. Knight, O. Georgiou, C. P. Dettmann, and R. Klages. Where to place a hole to achieve a maximal diffusion coefficient. *ArXiv e-prints 1112.3922v1*, December 2011. 102

N. Korabel and R. Klages. Fractality of deterministic diffusion in the nonhyperbolic climbing sine map. *Physica D*, 187:66–88, 2004. 35, 62, 75, 76, 85, 108, 109

Z. Koza. Fractal dimension of transport coefficients in a deterministic dynamical system. *J. Phys. A: Math. Gen.*, 37:10859–10877, 2004. 28

R. Kubo. Statistical-mechanical theory of irreversible processes i: General theory and simple applications to magnetic and conduction problems. *J. Phys. Soc. Jap.*, 12:570–586, 1957. 40

A. Lasota and M.C. Mackey. *Chaos, fractals, and noise*, volume 97 of *Applied Mathematical Sciences*. Springer, Berlin, 2nd edition, 1994. 41

H.A. Lorentz. The motion of electrons in metallic bodies. *Proc. Roy. Acad. Amst.*, 7:438–453, 1905. 30

E.N. Lorenz. Deterministic nonperiodic flow. *J. Atmos. Sci.*, 20:130–141, 1963. 24

J. Machta and R. Zwanzig. Diffusion in a periodic Lorentz gas. *Phys. Rev. Lett.*, 50:1959–1962, 1983. 75

B.B. Mandelbrot. *The fractal geometry of nature*. W.H. Freeman and Company, San Francisco, 1982. 28

L. Mátyás and R. Klages. Irregular diffusion in the bouncing ball billiard. *Physica D*, 187:165–183, 2004. 75, 76, 85

J.C. Maxwell. Illustrations of the dynamical theory of gases. In S.G. Brush, editor, *Kinetic Theory*, volume 1, pages 148–171, Oxford, 1965a. Pergamon Press. 18

J.C. Maxwell. On the dynamical theory of gases. In S.G. Brush, editor, *Kinetic Theory*, volume 2, pages 23–87, Oxford, 1965b. Pergamon Press. 18

V. Milner, J. L. Hanssen, W. C. Campbell, and M. G. Raizen. Optical billiards for atoms. *Phys. Rev. Lett.*, 86:1514–1517, Feb 2001. 121

J. Milnor and W. Thurston. On iterated maps of the interval. In James Alexander, editor, *Dynamical Systems*, volume 1342 of *Lecture Notes in Mathematics*, pages 465–563. Springer Berlin / Heidelberg, 1988. 32, 122

Y. Okamura, E. Blaisten-Barojas, S. Fujita, and S. V. Godoy. Theory of atomic diffusion in cubic crystals with impurities based on the correlated-walks theory. *Phys. Rev. B*, 22:1638–1644, Aug 1980. 87

E. Ott. *Chaos in Dynamical Systems*. Cambridge University Press, Cambridge, 1993. 24

W. Parry and M. Pollicott. *Zeta functions and the periodic orbit structure of hyperbolic dynamics*. Astérisque, 187-188. Société mathématique de France, 1990. 129

K. Pearson. The problem of the random walk. *Nature*, 72:294, 342, 1905. 22

I. Percival and F. Vivaldi. A linear code for the sawtooth and cat maps. *Physica D: Nonlinear Phenomena*, 27(3):373 – 386, 1987a. 30, 75

I. Percival and F. Vivaldi. Arithmetical properties of strongly chaotic motions. *Physica D: Nonlinear Phenomena*, 25(1-3):105 – 130, 1987b. 30, 75

K. Petersen. *Ergodic Theory*, volume 2 of *Cambridge studies in advanced mathematics*. Cambridge University Press, Cambridge, 1983. 63

H. Poincaré. *Les méthodes nouvelles de la mécanique céleste*. Gauthier-Villars, 1899. 24

A.B. Rechester and R.B. White. Calculation of turbulent diffusion for the Chirikov-Taylor model. *Phys. Rev. Lett.*, 44:1586–1589, 1980. 75, 97, 100, 139, 142

F. Reif. *Fundamentals of statistical and thermal physics*. McGraw-Hill series in fundamentals of physics. Waveland Press, 2008. 20, 22

D. Ruelle. Zeta-functions for expanding maps and anosov flows. *Inventiones Mathematicae*, 34:231–242, 1976. 128

D. Ruelle. *Statistical mechanics and dynamical systems*. Duke University mathematics series. Mathematics Dept., Duke University, 1977. 19

D. Ruelle. *Chance and chaos*. Penguin science. Penguin Books, 1993. 24

D. Ruelle. *Dynamical zeta functions for piecewise monotone maps of the interval*. CRM monograph series. American Mathematical Society, 1994. 129

D. Ruelle. *Thermodynamic formalism: the mathematical structures of equilibrium statistical mechanics*. Cambridge mathematical library. Cambridge University Press, 2004. 19, 126

M. M. Sano. Parametric dependence of the pollicott-ruelle resonances for sawtooth maps. *Phys. Rev. E*, 66(4):046211, Oct 2002. 30, 70, 75

M. Schell, S. Fraser, and R. Kapral. Diffusive dynamics in systems with translational symmetry: A one-dimensional-map model. *Phys. Rev. A*, 26:504–521, 1982. 27, 32, 35, 38, 75, 77, 100, 101, 102, 105, 114, 124, 136, 141

M. Seri, M. Lenci, Mi. D. Esposti, and G. Cristadoro. Recurrence and higher ergodic properties for quenched random Lorentz tubes in dimension bigger than two. *Journal of Statistical Physics*, 144:124–138, 2011. 143

J.W. Strutt. The problem of the random walk. *Nature*, 72:318, 1905. 22

T. Takagi. A simple example of the continuous function without derivative. *Proc. Phys. Math. Soc. Japan Ser. II*, 1:176–177, 1903. 43, 53

S. Tasaki and P. Gaspard. Fractal distribution and Fick's law in a reversible chaotic system. In M. Yamaguti, editor, *Towards the Harnessing of Chaos*, pages 273–288. Elsevier, Amsterdam, 1994. 29

S. Tasaki, I. Antoniou, and Z. Suchanecki. Deterministic diffusion, de Rham equation and fractal eigenvectors. *Phys. Lett. A*, 179:97–102, 1993a. 29

S. Tasaki, Z. Suchanecki, and I. Antoniou. Ergodic properties of piecewise linear maps on fractal repellers. *Phys. Lett. A*, 179:103–110, 1993b. 29

G. I. Taylor. Diffusion by continuous movements. *Proceedings of the London Mathematical Society*, s2-20(1):196–212, 1922. 27, 76, 85

G.I. Taylor. Diffusion by continuous movements. *Proc. London Math Soc.*, 20: 196–212, 1921. 40

W.N. Vance. Unstable periodic orbits and transport properties of nonequilibrium steady states. *Phys. Rev. Lett.*, 69:1356–1359, 1992. 28

R. Venegeroles. Leading Pollicott-Ruelle resonances and transport in area-preserving maps. *Phys. Rev. Lett.*, 99(1):014101, Jul 2007. 75, 97, 98

R. Venegeroles and A. Saa. Non-Gaussian features of chaotic Hamiltonian transport. *Journal of Statistical Mechanics: Theory and Experiment*, 2008(01): P01005, 2008. 29

N. Wax. *Selected papers on noise and stochastic processes*. Dover, New York, 1954. 22, 23

G.H. Weiss. *Aspects and applications of the random walk*. North-Holland, Amsterdam, 1994. 22, 23, 27, 76, 85

S. Wiggins. *Chaotic transport in dynamical systems*, volume 2 of *Interdisciplinary Applied Mathematics*. Springer, New York, 1992. 27